UNITED STATES
DEPARTMENT OF THE INTERIOR
GEOLOGICAL SURVEY

MODELING HIGHLY TRANSIENT FLOW, MASS, AND HEAT TRANSPORT IN THE CHATTAHOOCHEE RIVER NEAR ATLANTA, GEORGIA

By Harvey E. Jobson and Thomas N. Keefer

Open-File Report 79-270

UNITED STATES
DEPARTMENT OF THE INTERIOR
GEOLOGICAL SURVEY

MODELING HIGHLY TRANSIENT FLOW, MASS, AND HEAT TRANSPORT IN THE CHATTAHOOCHEE RIVER NEAR ATLANTA, GEORGIA

By Harvey E. Jobson and Thomas N. Keefer

Open-File Report 79-270

NSTL Station, Mississippi

January 1979

UNITED STATES DEPARTMENT OF THE INTERIOR

CECIL D. ANDRUS, Secretary

GEOLOGICAL SURVEY

H. William Menard, Director

CONTENTS

ILLUSTRATIONS

TABLES

SYMBOLS

A = cross-sectional area of the channel;

$ALON$ = longitude of the river (84.2°W);

AZS = azimuth of the sun;

BW = bank width;

C = concentration of dye;

C_N = Courant number;

C_p = specific heat of water at constant pressure;

C_υ = heat storage capacity of the bed;

D_x = longitudinal dispersion coefficient;

E = rate of evaporation;

e_a = vapor pressure of air;

EBH = effective barrier height;

$ELEV$ = elevation of the sun in degrees;

e_o = saturation vapor pressure of air evaluated at a temperature equal to that of the water surface;

EW_i = water-surface elevation at grid point i;

g = acceleration of gravity;

HA = hour angle of the sun;

H_i = sum of last two terms in equation 10 evaluated at grid point i and at time $j\Delta t$;

HR = time of day, in hours;

$H(t)$ = increase in heat content of the slab between time 0 and t;

I = rainfall rate;

K = kinematic surface exchange coefficient;

L = latent heat of vaporization;

ℓ = latitude of the river (N34.0°);

n = Manning's roughness coefficient;

N_H = dimensionless surface exchange number;

P = wetted perimeter of the channel;

Q = discharge;

q = lateral inflow per unit length;

Q_T = tributary flow rate;

R_H = hydraulic radius;

RS = part of incoming solar radiation absorbed by the water;

RSM = part of the incoming solar radiation which would be absorbed by the water under shade-free conditions;

S_f = friction slope;

T = cross-sectional average water temperature;

t = time;

Ta = air temperature;

Te = excess water temperature above ambient;

To = final temperature of the water as it leaves the system;

Ti = initial temperature of the water as it enters the system;

T_i^j = temperature at grid point i and at time $j\Delta t$;

Tq = temperature of tributary inflow;

T_w = wet-bulb air temperature;

TZM = meridian of the time zone;

U = cross-sectional average velocity;

U_i^j = velocity at grid point i and at time $j\Delta t$;

U_* = shear velocity;

V = windspeed;

W = top width of the channel;

x = longitudinal distance along the channel;

XN = normal distance from the tops of the trees to the shade point;

y = depth of flow;

y_b = distance above the insulated bottom of the slab;

y_{mo} = measured depth at steady low flow;

Z = thickness of bottom slab;

z = elevation of the bed above some datum;

β = acute angle between the azimuth of the sun and the azimuth of the river subreach;

γ = psychrometric constant;

δ = declination of the sun;

ΔS = change in tributary storage to occur during a time step;

Δt = time step in finite-difference solution;

ΔT_B = temperature rise within the slab;

Δx = distance step in finite-difference solution;

ε = emissivity of water;

η_o = Manning's roughness at steady low flow;

η_1 = rate of change of Manning roughness with stage;

θ = space derivative weighting factor;

κ = thermal diffusivity;

ρ = density of water;

σ = Stefan-Boltzman constant for blackbody radiation;

τ = traveltime of a water particle through the system;

Φ_B = flux of thermal energy from the bed to the water;

Φ_b = heat flux caused by longwave radiation emitted by the water;

Φ_e = heat utilized by evaporation;

Φ_h = heat conducted from the water as sensible heat;

Φ_N = net heat flux caused by incoming radiation from the sun and the sky;

Φ_q = heat flux added to the river by tributary inflow;

Φ_R = heat added to the water by rainfall directly on the surface;

Φ_T = flux of thermal energy from the air to the water; and

ψ = empirical wind function.

CONVERSION TABLE

Factors for converting metric units to inch-pound units are shown to four significant figures.

Multiply metric unit	By	To obtain inch-pound unit
meters (m)	3.281	feet (ft)
kilometers (km)	0.6214	miles (mi)
millimeters (mm)	0.03937	inch (in)
meters per second (m/s)	35.31	feet per second (ft/s)
cubic meters per second (m^3/s)	0.02832	cubic feet per second (ft^3/s)
pascal (Pa)	10.00	millibars (mb)
watts per square meter ($Watts/m^2$)	0.3172	British thermal units per square foot per hour ($Btu/ft^2 \cdot h$)

MODELING HIGHLY TRANSIENT FLOW, MASS, AND HEAT TRANSPORT IN THE CHATTAHOOCHEE RIVER NEAR ATLANTA, GEORGIA

by Harvey E. Jobson and Thomas N. Keefer

ABSTRACT

A coupled flow-temperature model has been developed and verified for a 27.9-km reach of the Chattahoochee River between Buford Dam and Norcross, Ga. Flow in this reach of the Chattahoochee is continuous but highly regulated by Buford Dam, a flood-control and hydroelectric facility located near Buford, Ga. Calibration and verification utilized two sets of data collected under highly unsteady discharge conditions. Existing solution techniques, with certain minor improvements, were applied to verify the existing technology of flow and transport modeling.

The linear, implicit finite-difference flow model was calibrated by use of a depth profile obtained at steady low flow and unsteady flow data obtained in March 1976. During the calibration period, the model was generally able to reproduce observed stages to within 0.15 m and discharges at less than 100 m^3/s, to within 5 percent. Peak discharges of about 200 m^3/s were underpredicted by about 20 percent. During the verification period, October 1975, the flow model reproduced observed stage changes to within about 0.15 m, and its timing and overall performance was considered to be very good.

Dye was added to the upstream end of the river reach at a constant rate while the river flow was highly unsteady. The numerical solution of either the conservative or nonconservative form of the mass-transport equation did an excellent job of simulating the observed concentrations of dye in the river.

The temperature model was capable of predicting temperature changes through this reach of as large as 5.8°C with a RMS (root-mean-square) error of 0.32°C in October 1975 and 0.20°C in March 1976.

Hydropulsation has a significant effect on the water temperature below Buford Dam. These effects are very complicated because they are quite dependent on the timing of the release with respect to both the time of day and past releases.

INTRODUCTION

In 1964 the Department of the Interior was designated as the lead agency for coordinating federal activities in water-data acquisition. Responsibility for these activities was assigned to the U.S. Geological Survey. Federal and nonfederal committees were formed to advise the Survey about water-data needs. In the early 1970's the nonfederal committee recommended that a series of interdisciplinary river-quality assessment studies be performed to (1) define the kinds and amounts of data required to adequately assess various types of river-quality problems, and (2) to develop and document methods for assessing planning alternatives in terms of potential impacts on river quality.

Partly because it is in a developed basin with current problems, the Chattahoochee River basin was selected as one site for a river-quality assessment study. The Chattahoochee is one of the largest rivers in the southeastern United States. Its headwaters are in the Blue Ridge province of north Georgia. It flows across the Piedmont and onto the Coastal Plain near Columbus, Ga. The Chattahoochee River joins the Flint River at the Georgia-Florida State line to form the Apalachicola River which drains into the Gulf of Mexico. The Chattahoochee's length from headwaters to the confluence with the Flint River is about 710 km, and its drainage area is about 23,000 km^2. On April 1, 1975, a river quality assessment project began addressing problems related to (1) thermal loading and heat dissipation, (2) wastes from concentrated urban-industrial areas, (3) effects on river quality of hydropower pulsation, and (4) sediment sources, transport characteristics, and deposition for the Chattahoochee River basin below Buford Dam and above West Point Dam.

One element of the Chattahoochee River assessment study was to develop and verify coupled flow-temperature models of a 27.9-km reach between Buford and Norcross, Ga., with special emphasis on evaluating the effects of hydropulsation on the flow and temperature regimes. The purpose of this report is to present these models with verification and to identify and specify the procedures necessary for their successful application.

Buford Dam, located approximately 65 km northeast of Atlanta, Ga., creates Lake Sidney Lanier. Its hydroelectric units are used for peaking purposes, so the flow in the Chattahoochee River below the dam is highly unsteady. For example, the U.S. Army Corps of Engineers maintain a minimum flow of 15.4 m^3/s through the dam but typically releases two pulses of water with peak discharges of about 215 m^3/s during week days. Just downstream of the dam, the total stage rise associated with the pulses usually occur in a time span of 10 to 20 minutes.

A linear, implicit finite-difference flow model is coupled with two implicit finite-difference transport models to describe the flow as well as the transport of heat and dye in the reach of the Chattahoochee River below Buford Dam. The study reach is illustrated in figure 1. It extends from the powerhouse at Buford Dam to the Highway 141 Bridge near Norcross. The river flows through rolling hills for most of this distance. The overall slope is 0.00036. The first 3.2 km are steep and rocky with a slope of 0.0011, and supercritical flow is present at several places during low flow. A bedrock control, below Highway 20, ponds the water in about a 6.4-km reach at low flow. The channel ranges from 45 to 65 m wide with a roughly rectangular cross section (see fig. 2). A characteristic cross section has large fallen trees protruding 6 to 15 m into the stream at the banks. The trees have fallen in because of bank sloughing which results from the large and rapid stage variations. Along the tips of the fallen trees, the water is somewhat deeper than in the center of the channel. The fallen trees apparently act in much the same way as jetties or groins. The channel bed is primarily coarse sand (1 mm) on bedrock. At low flow, sand dunes, 1.8 to 3 m in length and about 0.3 m high, cover the bed. A typical Manning roughness coefficient is 0.042.

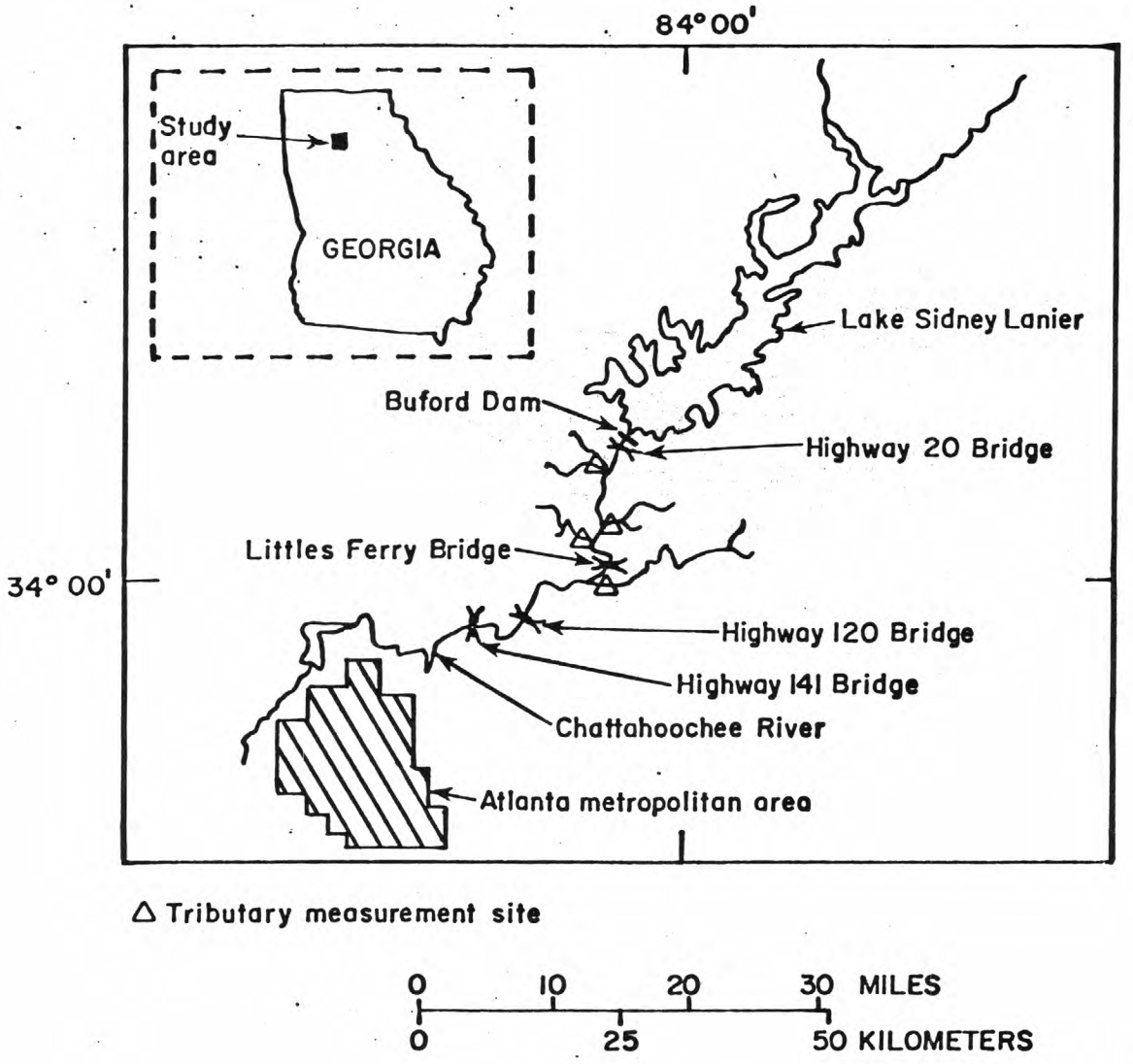

Figure 1.--Chattahoochee River showing the data collection points and tributary measurement sites (open triangles).

Figure 2.--View of Chattahoochee River near Settles Bridge (river km 553.0) at low flow.

In the following sections, the flow, mass and temperature models are described, and the available data, as well as the calibration and verification of each model, are presented. Two data sets, each containing continuous flow, stream temperature, and meteorologic data were obtained. One set was for the period of October 20 through October 26, 1975, and the other for March 21 through March 24, 1976. In addition, a conservative tracer (rhodamine-WT dye) was injected continuously at a constant rate during the March run, and samples were collected at 10-minute intervals near the center and at the end of the reach. These data are used to verify the transport model, and in addition, they served as an excellent check for the flow model. After the calibration and verification results have been presented, each model is discussed with special emphasis being placed on identifying the problems associated with analyzing transport in highly unsteady flows and the potential accuracy of such an analysis. Finally, the effect of the hydropulsation on the flow, transport and temperature regimes is dealt with in some detail.

MODEL DEVELOPMENT

Flow Model

Techniques available for modeling unsteady open-channel flow have advanced rapidly in the past 10 to 15 years, but almost all models are based on the same basic equations. These are continuity equations describing the conservation of mass

$$U \frac{\partial A}{\partial x} + A \frac{\partial U}{\partial x} + \frac{\partial A}{\partial t} - q = 0 \qquad (1)$$

and the conservation of momentum

$$\frac{\partial U}{\partial t} + U \frac{\partial U}{\partial x} + g \left(\frac{\partial y}{\partial x} - \frac{\partial z}{\partial x} + S_f \right) = 0 \qquad (2)$$

in which U = cross-sectional average velocity, A = cross-sectional area, x = longitudinal distance, t = time, q = lateral inflow per unit length, g = acceleration of gravity, y = depth of flow, z = elevation of the bed above some datum, and S_f = friction slope. The friction slope may be evaluated from either the Chezy or the Manning equation. The Manning equation

$$S_f = \frac{n^2 Q^2}{A^2 R_H^{4/3}} \qquad (3)$$

will be used in this paper where n = Manning's roughness coefficient, Q = discharge, and R_H = hydraulic radius. Equation 3 is not dimensionless but is expressed in SI units. To convert to the inch-pound system of units, a numerical value of 2.22 must be placed in the denominator.

Equations 1 and 2 are nonlinear in velocity, and no practical analytic solutions are available for unsteady flow. Early efforts to develop computer based numerical solutions centered around the method of characteristics (Lai, 1967, Yevjevich and Barnes, 1970, Wylie, 1970). More recent efforts have centered around direct finite-difference solutions. Explicit techniques, an example of which was pioneered by Garrison, Granju and Price (1969), are bounded by rigid stability criteria and tend to be expensive. Probably the earliest truly practical solution technique was the nonlinear, implicit finite-difference scheme of Amein and Fang (1970) which is unconditionally stable for any time step and allows an accurate and economical solution for most flow problems.

The solution technique chosen here, called linear, implicit, is a subset of the Amein and Fang technique which eliminates the need for iteration when advancing from time step to time step. In figure 3, which illustrates the finite-difference grid, the solid black circles represent points where all variables in equations 1 and 2 are known, and the open circles represent points at which variables are unknown. The subscript j designates the time grid point, and the subscript i designates the space grid point. Time and space derivatives are represented by the following respective finite-difference approximations:

$$\frac{\partial f}{\partial t} = \frac{1}{2\Delta t}\left[f_{i+1}^{j+1} - f_{i+1}^{j} + f_{i}^{j+1} - f_{i}^{j}\right] \tag{4}$$

and

$$\frac{\partial f}{\partial x} = \frac{1}{\Delta x}\left[f_{i+1}^{j+1} - f_{i}^{j+1}\right] \tag{5}$$

in which Δt = time step, Δx = distance step, and f is the variable whose derivative is sought, that is, U, A, or y. The approximation of the space derivative at the unknown time level $(j + 1)$ gives this scheme the name "fully forward" implicit. According to Fread (1974), this scheme is the most stable of the four-point difference techniques. It must, however, be operated with a reasonably small grid size to maintain accuracy.

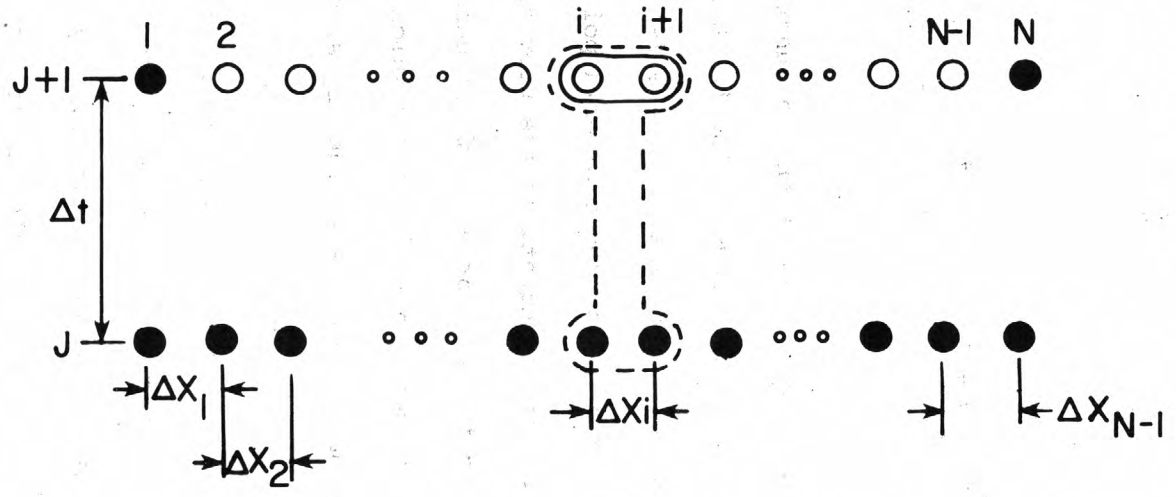

Figure 3.--Computation stencil for the linear, implicit finite-difference solution of the flow equation.

When the difference approximation, equations 4 and 5, are applied to equations 1 and 2, a system of equations of the following form is obtained:

$$(B_1)_i^j U_i^{j+1} + (B_2)_i^j y_i^{j+1} + (B_3)_i^j U_{i+1}^{j+1} + (B_4)_i^j y_{i+1}^{j+1} = E_i^j \quad (6)$$

and

$$(C_1)_i^j U_i^{j+1} + (C_2)_i^j y_i^{j+1} + (C_3)_i^j U_{i+1}^{j+1} + (C_4)_i^j y_{i+1}^{j+1} = D_i^j \quad (7)$$

in which B, C, D, and E are coefficients which are functions of Δx, Δt, U, y, and Manning n at the known time level. The friction slope at the new time step was approximated by use of a Taylor series expansion about the old time step value. For a given number of grid points, N, there are N-2 such equations. Two additional equations are provided by the upstream and downstream boundary conditions. For most of the cases reported here, the upstream boundary condition was a rating curve which related discharge to depth, the relationship having been determined by stream gaging techniques. This would not normally be good practice under highly unsteady conditions. The reasons for its applicability here are discussed later. A few runs were made using only the measured stage as an upstream boundary condition, and the results were almost identical. The downstream boundary condition was specified as $y(t)$, where y_N^{j+1}, the depth at the new time step, was approximated by a constant factor times y_{N-1}^{j}. The value of the constant factor was determined by experimentation with a step-backwater program. This type of boundary condition produces some backwater and drawdown effects but is more stable than a rating curve and more realistic than assuming a constant depth.

It is sometimes referred to as a zero-gradient boundary condition. Measured downstream depth could have been incorporated as the downstream boundary condition but was not for lack of time. The resulting system of equations was solved at each time step by Von Rosenberg's (1969) technique for pentadiagonal matrices.

The lateral inflow term in equation 1, q, was used to handle tributary flow and withdrawals along the Chattahoochee. Field observations at low and high flows indicated that while the mean tributary discharge was small, several of the tributary valleys have a considerable storage capacity. Figure 4 shows an upstream view of Suwanee Creek during a high stage in the Chattahoochee. When the Chattahoochee River was rising, it was not unusual to observe reverse flow conditions in the tributary channels where they joined the main stem. So while the discharge in the tributaries at points well away from the Chattahoochee was nearly constant, the actual interchange of water between the river and the tributaries was quite variable due to constantly changing stage in the main stream. The actual interchange of water between the tributaries and the river was simulated by routing the tributary flow through a hypothetical tank, or pond, attached to the main stem. The storage in the pond was computed as a function of the water-surface elevation in the Chattahoochee, and the lateral inflow component to the river, q, was determined by the continuity equation

$$q = Q_T - \frac{\Delta S}{\Delta t} \tag{8}$$

in which Q_T = tributary flow rate, and ΔS = change in tributary storage to occur during time step Δt. This simple modification produced more realistic recessions on the hydrographs by releasing additional tributary flow during the falling stage of the main stem.

Figure 4.--Suwanee Creek (view upstream) during a high stage in the Chattahoochee River.

Mass and Heat Transport Models

Applying the principle of conservation of thermal energy to a one-dimensional open channel, the conservative form of the governing transport equation becomes

$$\frac{\partial(AT)}{\partial t} + \frac{\partial(UAT)}{\partial x} = \frac{\partial(D_x A \partial T)}{\partial x^2} + \frac{\Phi_T W}{C_p \rho} + \frac{\Phi_B P}{C_p \rho} \qquad (9)$$

in which T = cross-sectional average water temperature, D_x = longitudinal dispersion coefficient, Φ_T = flux of thermal energy from the air to the water, W = top width of the channel, C_p = specific heat of water at constant pressure, ρ = density of water, Φ_B = flux of thermal energy from the bed to the water, P = wetted perimeter of the channel, and the other symbols are as previously defined.

Assuming water to be incompressible and the product $D_x A$ to be independent of x, equation 9 can be simplified to

$$\frac{\partial T}{\partial t} + U \frac{\partial T}{\partial x} = D_x \frac{\partial^2 T}{\partial x^2} + \frac{\Phi_T W}{C_p \rho A} + \frac{\Phi_B P}{C_p \rho A} \qquad (10)$$

which is called the nonconservative form of the transport equation. If the velocity field satisfies the continuity of flow equation, the exact solutions of equations 9 and 10 are identical. When numerical techniques are used, however, equation 9 will provide a more conservative solution (Roache, 1972).

When the transported substance is dye rather than thermal energy, the values of Φ_T and Φ_B are zero, and T can be replaced by C which represents the concentration of dye. Both equations 9 and 10 were solved when modeling the movement of dye, but only equation 10 was used in the temperature model.

The next to the last term in equations 9 and 10 represents the rate of change of water temperature due to exchange of energy between the atmosphere and water. The ratio A/W is the effective water depth, sometimes called the hydraulic depth. The rate of exchange of energy between the atmosphere and water has been discussed many times, but one of the first and most complete analyses of the processes involved has been given by Anderson (1954). For the purpose of this study, the net exchange was expressed as the sum

$$\Phi_T = \Phi_N - \Phi_b - \Phi_e - \Phi_h + \Phi_R + \Phi_q \qquad (11)$$

in which Φ_N = net heat flux caused by incoming radiation from the sun and the sky; Φ_b = heat flux caused by longwave radiation emitted by the water; Φ_e = heat utilized by evaporation; Φ_h = heat conducted from the water as sensible heat; Φ_R = heat added by rain falling directly on the surface; and Φ_q = heat flux added to the river by tributary inflow. The values of Φ_T, Φ_N, and Φ_R are positive and the values of Φ_b, Φ_e, and Φ_h are negative if the water is gaining thermal energy as a result of the respective processes.

The net flux caused by incoming radiation from the sun and the sky, Φ_N, is composed of four components, the incoming atmospheric and solar radiation and the reflected components of each. The incoming components were measured directly, but the reflected parts had to be estimated. The traditional assumption that 3 percent of the atmospheric radiation is reflected (Anderson, 1954) was made.

The source of all solar radiation is the sun, and if some object is between the water surface and the sun, much of this radiation will be intercepted. The banks of the Chattahoochee River between Buford and Norcross are almost completely tree lined (figs. 2 and 5). The incoming solar radiation, however, was measured by use of a pyranometer placed in an unobstructed area. The part of the measured solar radiation actually absorbed by the water is a complex function of the elevation and azimuth of the sun as well as the azimuth of the river reach, the height and density of the trees, and the width of the river.

A two-step procedure was used to estimate the part of the measured solar radiation, *RS*, actually absorbed by the water. The first step was to determine the part of the available solar radiation which would have been absorbed providing no shading had occurred. Anderson (1954) has presented a formula for the computation of this shade free absorption

$$RSM = 1.0 - 1.18\ ELEV^{-0.77} \tag{12}$$

in which *RSM* = part of the incoming solar radiation which would be absorbed under shade free conditions, and *ELEV* = elevation of the sun in degrees. The sun's elevation was computed from

$$ELEV = \sin \delta \sin \ell + \cos \delta \cos \ell \cos HA \tag{13}$$

in which δ = declination of the sun, ℓ = latitude of the river (N34.0°), and *HA* = hour angle of the sun which was computed from

$$HA = (180 + ALON - TZM) - 15\ HR \tag{14}$$

in which *ALON* = longitude of the river (84.2°W), *TZM* = meridian of the time zone, and *HR* = time of day in hours. The equation of time was ignored and the declination of the sun, obtained from a solar ephemeris, was assumed constant during each run.

Figure 5.--Aerial view of Chattahoochee River showing shading conditions.

The second step was to reduce the value of *RSM* appropriately to account for the shading of the water due to trees and other obstructions on the banks. The shaded part of the water surface was assumed to absorb solar radiation at 20 percent of the measured rate, and the clear part of the water surface was assumed to absorb at *RSM* times the measured rate. The value of *RS*, therefore, was determined as 0.2 times the part of the water surface shaded plus *RSM* times the part of the water surface exposed to the sun. The part of the water surface in any subreach to be shaded at any time of day was determined from the geometric relation between the elevation and azimuth of the sun, the azimuth of the river subreach, the effective barrier height, *EBH*, the water-surface width, *W*, and the bank width, *BW*. The physical relationship between these terms is illustrated in figure 6. The river cross section was assumed to be symmetric about the centerline, which is a reasonable assumption for the study reach. The normal distance from the tree tops to the shade point, *XN*, was determined from the expression

$$XN = \frac{EBH}{(\tan ELEV)\ (\cos \beta)} \qquad (15)$$

in which β = the acute angle between the azimuth of the sun and the azimuth of the river subreach. The azimuth of the sun, *AZS*, was computed from

$$AZS = \text{arc cos } (\sin \delta - \sin ELEV \sin \ell)/(\cos ELEV \cos \ell) \qquad (16)$$

Using the above expressions, the part of the measured solar radiation to be absorbed by the water, *RS*, was computed once for each subreach and each time step during the day.

Analytic expressions must be used to relate all other terms in equation 11 to the water temperature and the meteorologic variables. The expression used to determine each term will be summarized.

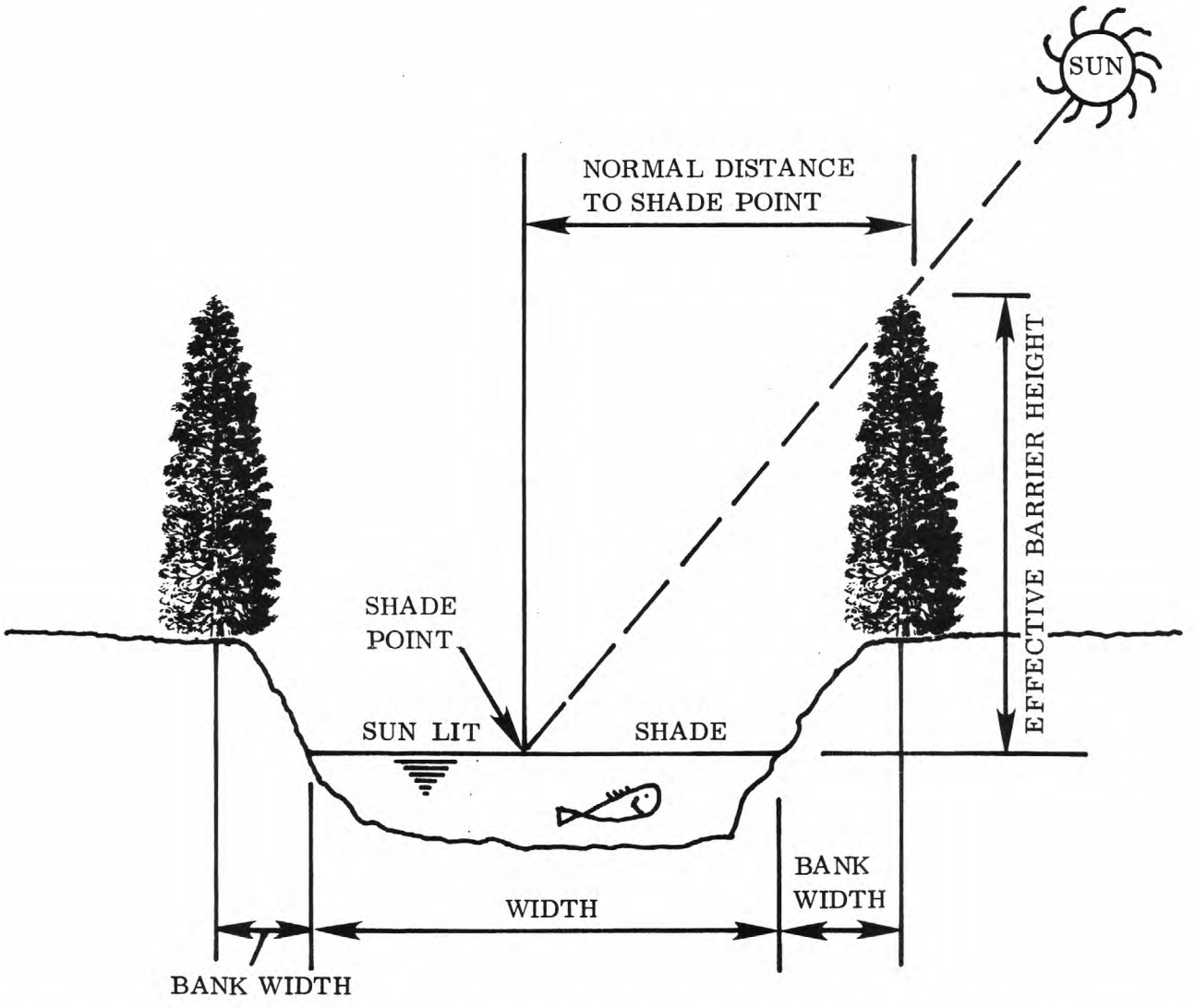

Figure 6.--Schematic of river cross section used to determine the part of the water surface to be shaded by bank vegetation.

Longwave radiation emitted by the water surface was computed using the Stefan-Boltzman law for blackbody radiation

$$\Phi_b = \varepsilon\sigma\,(T + 273.16)^4 \qquad (17)$$

in which ε = emissivity of water (0.97), σ = Stefan-Boltzman constant for blackbody radiation (5.67E-8 W/[m^2C^4]), and 273.16 converts to the Kelvin scale when T is given in degrees Celsius.

The energy added by rainfall was determined by

$$\Phi_R = C_p\rho I\,(T_w - T) \qquad (18)$$

in which I = rainfall rate, and T_w = wet-bulb air temperature. Equation 18 does not account for the water flowing into the river as sheet flow or from small ditches during or after a rain. In some cases this nontributary inflow is believed to be a significant, but unaccounted for, item in the energy budget.

It is assumed that the rate of evaporation can be estimated by a formula of the Dalton type

$$E = \psi\ (e_o - e_a) \tag{19}$$

in which E = rate of evaporation in units of length per time, ψ = an empirical coefficient or wind function, e_o = saturation vapor pressure of air evaluated at a temperature equal to that of the water surface, and e_a = vapor pressure of the air above the water, which is commonly measured at a height equal to the height of the measured wind velocity. The wind function was estimated from

$$\psi = 3.01 + 1.13V \tag{20}$$

in which ψ = wind function that gives the evaporation rate in millimeters per day when the vapor pressure deficit is expressed in kilopascals, and the windspeed, V, is expressed in meters per second. Equation 20 was derived from thermal data collected on the San Diego Aqueduct in southern California (Jobson, 1977) and to the authors' knowledge, it is the only wind function ever derived from an energy balance of an open channel. Empirical wind functions derived from lake or pan data are numerous (Ryan and Stolzenbach, 1972; Tennessee Valley Authority, 1972; Brutsaert and Yeh, 1970). The thermal energy utilized by evaporation was expressed as

$$\Phi_e = \rho L\psi\ (e_o - e_a) \tag{21}$$

in which L = latent heat of vaporization.

Heat exchange by conduction has received relatively little attention because its magnitude is usually small in comparison to the evaporative heat exchange. Assuming that the eddy diffusivities of heat and mass are identical, which leads directly to the Bowen ratio concept, the conduction term can be expressed as

$$\Phi_h = \gamma \rho L \psi (T - T_a) \tag{22}$$

in which γ = psychrometric constant (0.598 based on an assumed atmospheric pressure of 98.0 kPa); and T_a = air temperature which should be measured at the same elevation as the vapor pressure.

The last term in equations 9 and 10 represents the thermal flux at the bed of the river. Past attempts to model the bed conduction term have estimated the heat flux as the product of the thermal conductivity and the temperature gradient within the bed. This transient temperature gradient was either estimated (Messenger, 1963) or determined from a few measurements within the bed (Brown, 1969; Pluhowski, 1970). Measurements of bed temperatures are difficult and seldom available. In addition, bed conditions are seldom uniform. Even though the bed conduction term has been shown to be significant (Brown, 1969, Pluhowski, 1970), at least for shallow depths, it is usually ignored because of the above difficulties.

The earth under a river can be approximated as an infinitely thick conducting medium, the thermal properties of which can be estimated, at least approximately. The thermal conductivity of flowing water is much greater, because of turbulence, than that of the soil, so the surface temperature of the bed can be assumed to follow the water temperature very closely.

Mathematical expressions for the temperature distribution and heat fluxes within a semi-infinite medium which result from an arbitrary temporal variation in surface temperature are relatively simple (Carslaw and Jaeger, 1959). Unfortunately, these expressions converge slowly, and their use in a thermal model would be expensive. On the other hand, if the earth below the river were considered to be a slab, insulated on the bottom and of an arbitrary thickness, Z, the equations are still fairly simple but converge much faster. If the temporal variations in surface temperature are cyclical, the heat fluxes determined by the semi-infinite and finite thickness slab equations become indistinguishable as the slab thickness increases. In fact, assuming a diurnal water temperature swing of 10°C and thermal properties for saturated sand, the surface heat fluxes for a slab only 25 cm thick are within 6 percent of the values for a semi-infinite medium.

The heat exchange between the water and the bed was, therefore, estimated by considering the bed to be a homogenous slab, insulated on the lower face and with a surface temperature on top equal to that of the overlying water. The heat flux into or out of the bed was then determined as a function of the past history of the water temperature. Only the thermal diffusivity and heat-storage capacity of the soil needed to be known. A slab thickness of 100 cm was assumed to be sufficiently thick to give the desired accuracy.

The temperature distribution within a slab, initially at constant temperature, for which the surface is subjected to a unit increase in temperature at time zero is given by (Carslaw and Jaeger, 1959)

$$\Delta T_B = 1 - \frac{4}{\pi} \sum_{n=0}^{\infty} \frac{(-1)^n}{2n+1} \exp\left[-\kappa(2n+1)^2\pi^2 t/4Z^2\right] \cos\left[(2n+1)\pi y_b/2Z\right] \quad (23)$$

in which ΔT_B = the temperature rise within the slab, κ = the thermal diffusivity, Z = thickness of the slab, and y_b = the distance above the insulated bottom of the slab. The increase in the heat content of the slab can be evaluated at any time by multiplying equation 23 by the heat-storage capacity, then integrating over the total thickness

$$H(t) = C_v Z\left\{1 - \frac{8}{\pi^2} \sum_{n=0}^{\infty} \frac{(-1)^n}{(2n+1)^2} \exp\left[-\kappa(2n+1)^2\pi^2 t/4Z^2\right] \sin\left[(2n+1)\pi/2\right]\right\} \quad (24)$$

in which $H(t)$ = the increase in heat content of the slab between time 0 and t resulting from the unit increase in surface temperature at time zero; and C_v = the heat-storage capacity of the slab which is the product of the density and specific heat. Of course, this heat must have been provided from the overlying water.

Equations 9 and 10 are solved by use of a finite-difference approximation that advances in time by discrete steps of duration Δt. The heat flux to the water $\Delta H(j)$ during any time step $j\Delta t$ to $(j+1)\Delta t$ which results from a unit increase in temperature at time zero, can be computed as

$$\Delta H(j) = H(j\Delta t) - H[(j+1)\Delta t] \quad (25)$$

The $\Delta H(j)$'s describe the time variation of the response of the system to a unit change in water temperature.

Equation 24 is linear with respect to temperature, and since water temperature fluctuations can be represented by a series of step changes, the superposition principle is used to determine the heat flux from the bed to the water for any temperature history by use of the equation

$$\Phi_B(j\Delta t) = \sum_{k=-s}^{j} \Delta T(k\Delta t)\Delta H(j-k) \tag{26}$$

in which $\Phi_B(j\Delta t)$ is the heat flux to the water from the bed during the time $j\Delta t$ to $(j+1)\Delta t$; $\Delta T(k\Delta t)$ is the change in water temperature which occurred at $k\Delta t$ $(k \leq j)$; ΔH is given by equation 25; and the water temperature is assumed to have been constant for times before $t = -s\Delta t$. Equation 26 is solved for each grid point and each time step in the temperature model. The river temperature was assumed to have been constant before the model started ($\Delta T = 0$ for $k<0$), and the bed conduction term was limited to a 24-hour memory ($s = 288 - j$).

The heat content of the tributary inflows was modeled in equation 10 by treating it as a surface exchange term. The equivalent surface exchange was determined from

$$\Phi_q = \frac{(T_q - T)C_p\rho q}{W\Delta x} \tag{27}$$

in which Φ_q = heat flux added to the river by the tributary inflow; T_q = temperature of the tributary inflow; and q = tributary flow rate at the river. The value of Φ_q is added to the value of Φ_T for use in the model. The value of q represents the actual interchange of water between the tributary and the river as computed from equation 9. If the flow was from the river to the tributary, the value of T_q was set equal to the river temperature, otherwise it was set equal to the temperature of the water in the tributary storage. The temperature of the water in tributary storage was updated each time step by considering the steady tributary flow, Q_T, and storage volume. No surface exchange was allowed for the water held in tributary storage.

The dispersion coefficient used when solving equation 10 was determined from

$$\frac{D_x}{R_H U_*} = 250 \qquad (28)$$

in which U_* = shear velocity, and 250 is the approximate average of the indicated ratio for the data summarized by Fischer (1973). Roache (1972) gives a method of determining the effective numerical dispersion coefficient for a differencing scheme such as that of Stone and Brian (1963). Under the combination of grid spacing and time steps used for the variable grid model of the Chattahoochee (eq. 9), the effective numerical dispersion coefficient often exceeded the value given by equation 28. Although the model coding allowed for its inclusion, the value of D_x was assumed equal to zero when solving equation 9.

Equations 9 and 10 are Eulerian equations, meaning that they represent a description of the variation of temperature with respect to a fixed coordinate system. Another description, the Lagrangian, considers the variation of the temperature of a given fluid particle or fluid lump as the particle moves through the system. In the Lagrangian framework, one conceptually follows an individual fluid particle while keeping track of the factors which tend to change its temperature. Applying the thermal continuity equation to a unit mass of fluid, one obtains

$$\frac{dT}{dt} = D_x\left(\frac{\partial^2 T}{\partial x^2}\right) + \frac{\Phi_T W}{AC_p\rho} + \frac{\Phi_B P}{AC_p\rho} \tag{29}$$

Integrating equation 29 during the traveltime,

$$T_o - T_i = \int_0^\tau \left(D_x \frac{\partial^2 T}{\partial x^2} + \frac{\Phi_T W}{AC_p\rho} + \frac{\Phi_B P}{AC_p\rho} \right) dt \tag{30}$$

in which T_i = initial temperature of the water particle as it enters; T_o = final temperature of the water particle as it leaves; and τ = traveltime of the particle through the system. Expanding the right hand side of equation 30 yields

$$T_o - T_i = \int_0^\tau \left(D_x \frac{\partial^2 T}{\partial x^2}\right) dt + \int_0^\tau (\Phi_N - \Phi_b + \Phi_R + \Phi_q) \frac{W}{AC_p\rho}\, dt + \int_0^\tau \left(\frac{\Phi_B P}{AC_p\rho}\right) dt$$

$$- \int_0^\tau \psi[L(e_o - e_a) + \gamma L(T - T_a)] \frac{W}{AC_p}\, dt \tag{31}$$

Equation 31 cannot be solved before equation 10 because the value of the temperature as a function of distance and time must be known to perform the integration. Equation 31 was solved for each time step in the model, however, because it is of great value in the process of analyzing the results of the model. Its main value lies in evaluating the contribution of each physical process to the total temperature change of a particle of water passing through the system.

Solution of the one-dimensional transport equation is a much less formidable task than solving the flow equations. Most numerical efforts have dealt with ways to minimize numerical dispersion of steep concentration fronts. To the writers' knowledge, numerical dispersion caused by sudden flow changes, such as those that occur on the Chattahoochee, have not previously been analyzed, however.

In order to find a stable, accurate, solution technique, which would minimize numerical dispersion with large distance steps and widely varying velocities, preliminary experiments were conducted with three types of solutions. An explicit scheme was found to be highly dispersive and its stability is strictly limited to values of Δt and Δx which satisfy

$$\frac{U\Delta t}{\Delta x} \leq 1 \tag{32}$$

The quantity on the left is called the transport Courant number. A finite-element technique with linear basis functions was derived which is more stable and contains less numerical dispersion than the explicit technique, but it still requires the transport Courant number to be less than two. Later research revealed that this centered, implicit, 6-point scheme is very similar to the method presented by Price, Cavendish, and Varga (1968).

The technique finally selected for use in this study was a slight variation of the implicit scheme of Stone and Brian (1963). This centered 6-point scheme considers all points in the time derivative as shown in figure 7. The weighting coefficients on the points used to estimate the time derivative, θ, are cyclic functions of time, which according to Stone and Brian reduce the numerical dispersion of propagating high frequency harmonics more effectively. With the time derivative weighting factor, θ, greater than 0.5, the method is unconditionally stable, however, it is still desireable to keep the transport Courant number less than 2 when considering high frequency transients.

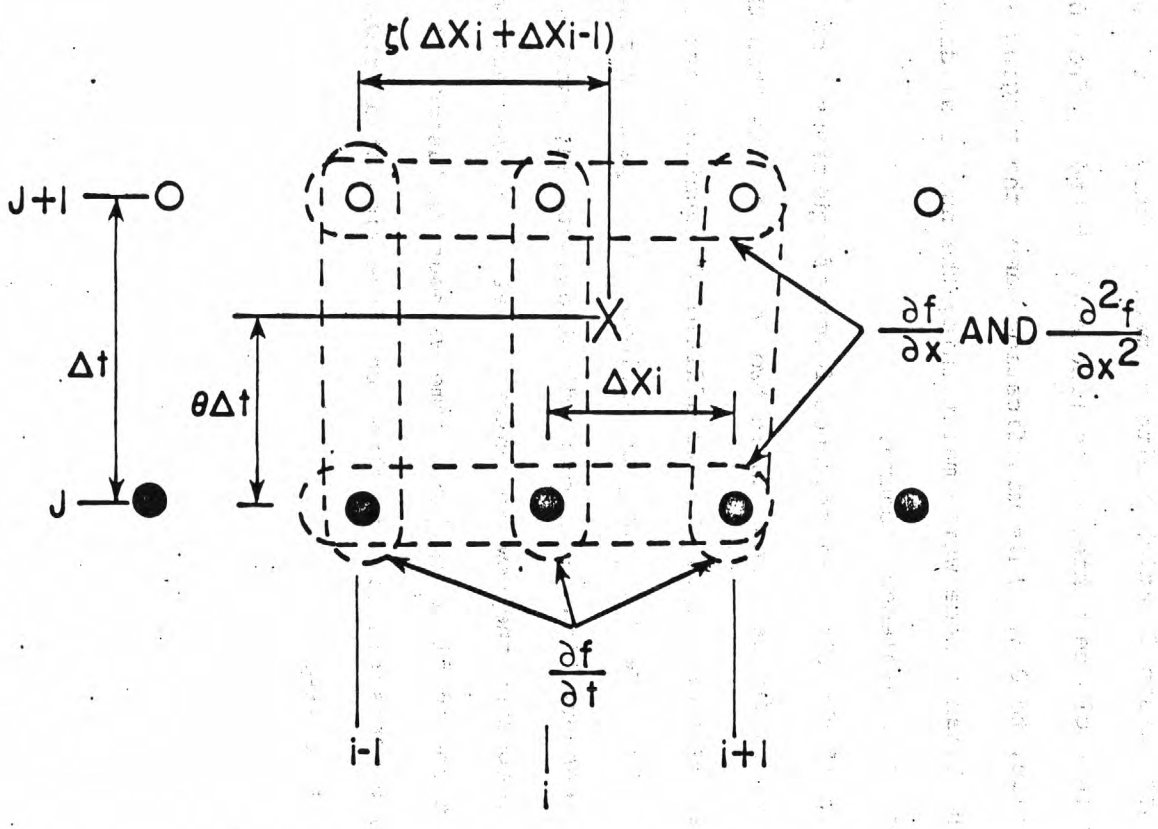

Figure 7.--Computation stencil for the finite-difference solution of the transport equation.

The weighting coefficients on the known and unknown concentration values for the space derivatives derived by Stone and Brian (1963) are identical to those for a linear basis function finite-element technique. The authors modified the values of the centering coefficients, θ and ζ, from 0.5 used by Stone and Brian, to 0.6. This modification damps the ringing and overshoot of the Stone and Brian scheme while maintaining the numerical dispersion advantage of the finite-element scheme.

Application of the finite-difference forms of equations 9 or 10 to the stencil shown in figure 7 results in two less equations than there are unknowns at the new time step. The two additional equations are provided by the upstream and downstream boundary conditions. The upstream condition was simply a known concentration. A zero gradient downstream boundary condition was assumed by computing the new concentration at the downstream boundary from an explicit upwind differencing scheme without diffusion. The solution for the remaining concentrations involved the inversion of a tridiagonal matrix for each time step.

At the beginning of the project, a solution code for equations 10 and 31, which had been developed for use on the San Diego Aqueduct (Jobson, 1976), was available. This model contained three simplifications from the modified Stone and Brian technique however. The coefficient, θ, was not time variable, the value of ζ was 0.5, and only equally spaced grid points were allowed. Because of the highly unsteady flow in the Chattahoochee, there was some doubt regarding the accuracy of this simplified solution technique to the nonconservative form of the transport equation. To address this concern the transport of dye was modeled by equation 9, which was solved by the modified Stone and Brian technique, and equations 10 and 31, which were solved by the simplified technique. It was found that the dye concentrations predicted by the two models were essentially equal so the temperature model was not recoded. The solution to equation 9 will be referred to as the conservative model since it solves the conservative form of the transport equation and the simplified solution to equation 10 will be referred to as the nonconservative model.

The finite-difference formulation for the nonconservative model (eq 10) was

$$\left[\frac{1}{6\Delta t} + \frac{\theta U_i}{2\Delta x} - \frac{D_x}{2\Delta x^2}\right] T_{i+1}^{j+1} + \left[\frac{4}{6\Delta t} + \frac{\theta}{2\Delta x}\,(U_{i-1} - U_i) + \frac{D_x}{\Delta x^2}\right] T_i^{j+1}$$

$$+ \left[\frac{1}{6\Delta t} - \frac{\theta U_{i-1}}{2\Delta x} - \frac{D_x}{2\Delta x^2}\right] T_{i-1}^{j+1} = \left[\frac{1}{6\Delta t} + \frac{(1-\theta)U_i}{2\Delta x} + \frac{D_x}{2\Delta x^2}\right] T_{i+1}^{j}$$

$$+ \left[\frac{4}{6\Delta t} - \frac{(1-\theta)(U_{i-1} - U_i)}{2\Delta x} + \frac{D_x}{\Delta x^2}\right] T_i^j + \left[\frac{1}{6\Delta t} + \frac{(1-\theta)U_{i-1}}{2\Delta x}\right.$$

$$\left. + \frac{D_x}{2\Delta x^2}\right] T_{i-1}^j + H_i \ldots \qquad (33)$$

in which θ = space derivative weighting factor (0.60), T_i^j = temperature at grid point i and time, $j\Delta t$, U_i^j = velocity at grid point i and time $j\Delta t$, and H_i = the sum of the last two terms in equation 10 evaluated at grid point i and time $j\Delta t$.

Little has been written about the numerical simulation of the source-sink terms, H_i, in equations 9 or 10 but certain precautions are necessary. In equation 33 the surface exchange term is evaluated at the old time step. One consideration is the maximum size of the time step which can be used with this procedure without seriously compromising accuracy. To illustrate the requirements consider a Lagrangian excess temperature model with no bed conduction or dispersion. The governing differential equation simplifies to

$$\frac{dTe}{dt} = - \frac{KW}{A} Te \tag{34}$$

in which Te = the excess water temperature, above ambient, and K = the kinematic surface exchange coefficient. For steady uniform flow with constant meteorological conditions, the coefficient on the right of equation 34 is constant and an exact solution is easily obtained. Evaluating the surface exchange at the old time step, the finite-difference approximation becomes

$$Te^{j+1} = Te^{j} \left(1 - \frac{KW\Delta t}{A}\right) \tag{35}$$

The dimensionless surface exchange number, N_H, as given by

$$N_H = \frac{KW\Delta t}{A} \tag{36}$$

governs the accuracy of the numerical solution. A few simple calculations will demonstrate that the numerical solution is very accurate for values of $N_H < 0.2$ while the numerical solution overshoots and becomes oscillatory for values of $N_H > 1$. The surface exchange term, H_j, in equation 10 is nearly a linear function of temperature for temperature differences encountered during any one time step in the model. The surface exchange number, is, therefore, a meaningful criteria for limiting time step size.

As shown by Jobson (1973) the value of the kinematic surface exchange coefficient will almost never exceed 8 m/d while the minimum hydraulic depth in the Chattahoochee is always greater than 0.3 m. By use of equation 36, it is easily seen that the numerical scheme should accurately model the surface exchange for values of Δt less than 10 minutes. A 5-minute time step was used throughout for both the flow and the transport models.

Consideration should also be given to the distribution of the surface exchange term between grid points. With a steady uniform condition and no surface exchange except at grid point k, the water temperature must remain constant both upstream and downstream of grid k and increase by the amount $H_k \Delta x/U_k$ between grid point $k - 1$ and k. Simplifying equation 33 for steady conditions by observing that the old and new temperatures must be the same, one obtains

$$\left[\frac{U_{i-1}}{2} - \frac{D_x}{\Delta x} \right] T_{i+1} + \left[\frac{(U_{i-1} - U_i)}{2} + \frac{2D_x}{\Delta x} \right] T_i - \left[\frac{U_{i-1}}{2} + \frac{D_x}{\Delta x} \right] T_{i-1} = AH_i \Delta x \tag{37}$$

in which AH_i represents the distributed part of the surface exchange to be applied at grid point i. Under the assumed conditions, it is easily seen that $AH_i = 0$ for $k - 2 \geq i \geq k + 1$. That is, in order to get realistic results from equation 33, a point source of heat must be distributed between two grid points. Applying equation 37 between grid points $k - 2$ and k and simplifying, the amount to be applied at grid $k - 1$ is obtained

$$\left(\frac{U_{k-1}}{2} - \frac{D_x}{\Delta x} \right) \frac{H_k}{U_k} = AH_{k-1} \tag{38}$$

applying the same equation between grid points $k - 1$ and $k + 1$, the amount to be applied at grid point k is obtained

$$\left(\frac{U_{k-1}}{2} + \frac{D_x}{\Delta x} \right) \frac{H_k}{U_k} = AH_k \tag{39}$$

Summing equations 38 and 39, it is seen that the sum of the distributed surface exchanges is equal to the total point source. If a point source is not distributed as indicated in equations 38 and 39, the numerical solution will contain errors upstream of the source similar to what is sometimes referred to as ringing.

In order to preserve thermal continuity under unsteady, nonuniform conditions, the physical surface exchange terms were distributed between two grid points using

$$AH_i = H_i \left[0.5 - \frac{D_x}{\Delta x U_{i-1}} \right] + H_{i+1} \left[0.5 + \frac{D_x}{\Delta x U_i} \right] \quad (40)$$

This procedure was found to work well in both the conservative and nonconservative models.

Coupling

The flow and transport models were run independently. At each time step five items of information for each of the 48 grid points in the flow model were stored on magnetic disk for use by the transport model. These items include the top width, velocity, cross-sectional area, tributary inflow (at the river), and the tributary flow into the storage volume (beside the river). This arrangement saved a significant amount of computer cost because the transport models were not run until the flow model was calibrated. After final calibration, the flow model was not rerun. Likewise, the transport model could be run as many times as necessary without rerunning the flow model.

In using the conservative transport model (eq 9), the coupling was direct since this solution allowed for unequal distance steps, and the grid spacing in the flow and the transport model were identical.

The nonconservative transport model (eq. 10), which also contained the solution code for equation 31, required equal grid spacing. In order to make the output of the flow model compatible with the solution to equation 10, the flow data were interpolated to an equal grid spacing by use of a processor program. The logic of the processor program assumed that the velocity and cross-sectional area of the "true" river varied linearly with distance between the flow model grid points. The cross-sectional area at grid i in the equally spaced model was determined by integrating the "true" area from the point $x_i - \Delta x/2$ to $x_i + \Delta x/2$ and dividing by Δx. This procedure assured that the total instantaneous volume of water within a subreach was the same for both models. The velocity at any grid in the equally spaced model was assumed to be equal to the value at that point in the "true" river.

Top widths for the temperature model were determined from the cross-sectional areas provided by the flow model. For each available cross section, the measured relation between width and area was fitted with a third degree polynomial of the form

$$W = a_o + a_1 A + a_2 A^2 + a_3 A^3 \qquad (41)$$

in which a_o, a_1, a_2, and a_3 are fitted coefficients, and A is the given area.

MODEL CALIBRATION AND VERIFICATION

Flow Model

The most sophisticated mathematical procedures are of little value without adequate data to verify them. Data needed for a flow model include internal reach data, which describe the physical characteristics of the river (geometry, channel elevation, and roughness), and boundary condition data such as flow or stage at each end of the reach and flow in each tributary.

For modeling purposes the internal characteristics of the river are discretized at a number of grid points which represent the longitudinal variations of channel geometry, elevation, and roughness. The required number of grid points is a function of the objectives of the study as well as the frequency of temporal variations in the boundary conditions. In this case it was desireable to model extreme flow changes (discharge varying by a factor of 14) which occur in very short time periods (about 10 minutes). Assuming these flow changes are equivalent to a periodic function with a 20-minute period, a 10-minute sampling period should be statistically adequate (Bendat and Piersol, 1966). This provides two samples per cycle of the highest frequency change. A 5-minute time step was used throughout this study.

The magnitude of the time step generally dictates the spacing of the internal grid points. Stability and accuracy are related to the Courant number

$$C_N = \frac{(U + \sqrt{gy})\Delta t}{\Delta x} \quad (42)$$

Explicit models and the method of characteristics become unstable at $C_N > 1$. Even in highly unsteady flow as in the Chattahoochee, implicit models operate satisfactorily for values of C_N as large as 15, but accuracy decreases as the value of C_N departs from unity. The average velocity in the Chattahoochee varied from 0.33 m/s at steady low flow to 0.79 m/s at high flow while the average depth varied from about 1.1 to 2.2 m. The distance step required for maximum accuracy therefore varied from about 1.1 km at low flow to about 1.6 km at high flow. The actual spacing of the cross-sectional data depended somewhat on field conditions, but the average spacing was 0.7 km (table 1).

All hydraulic data were obtained by project personnel of the Chattahoochee River Quality Assessment Project and a complete description of the data and methods used in its acquisition is in progress (R. E. Faye, U.S. Geological Survey, written commun., 1978). Briefly, the cross-sectional data were obtained at high flow by use of a sonic depth sounder and a boat. Absolute bed elevations were obtained by referencing the water-surface elevation, at the time the cross section was taken, to references which had previously been set on the bank. The field crew also estimated the flow resistance (Manning n) at the time of the field survey.

Table 1.--Internal reach data for the Chattahoochee River between Buford and Norcross, Georgia

Section number	Comments	River kilometer	Bottom elevation (m)	Coefficients in equation 43		Measured hydraulic depth at low flow (m)	Manning's roughness	
				T_a (m)	T_b (m^{-1})		η_o	η_1 (m^{-1})
1	Buford Gage	560.20	277.53	76.2	0	0.82	0.060	0.0
2		560.00	277.22	62.2	0.67	.52	.086	.0
3	Interpolated Section	559.76	276.79	54.9	0	[1].55	.054	.0
4	Interpolated Section	559.46	276.19	54.9	0	[1].55	.056	.0
5		559.12	275.47	49.4	1.35	.58	.051	.0
6		558.56	274.67	36.6	.45	[1].76	.038	.0
7		557.67	274.18	43.9	.39	1.05	.026	.0
8		556.93	273.85	39.0	.81	1.36	.025	.0
9	Highway 20	556.51	273.55	64.0	.44	1.65	.030	- .003
10	Interpolated Section	556.30	273.52	48.8	.46	[1]1.68	.041	- .003
11	James Creek	556.06	273.00	36.6	.63	2.19	.030	- .003
12		555.26	274.06	46.3	.99	1.11	.021	.0
13		555.01	274.03	36.6	.66	1.12	.021	.0
14		554.72	274.00	34.1	.88	1.14	.018	.0

Table 1.--Continued

Section number	Comments	River kilometer	Bottom elevation (m)	Coefficients in equation 43		Measured hydraulic depth at low flow (m)	Manning's roughness	
				T_a (m)	T_b (m^{-1})		η_o	η_1 (m^{-1})
15		553.87	273.87	41.5	0.49	1.24	0.018	0.0
16	Settles Bridge	552.97	274.48	63.4	.88	0.57	.030	.0
17		552.34	274.20	48.8	.68	.74	.030	.0
18		551.26	273.98	41.5	3.71	.84	.024	- .007
19	Interpolated Section	550.80	273.55	41.5	.66	[1]1.04	.046	- .007
20	Level Creek	550.41	272.98	42.7	.58	1.22	.080	- .015
21	Interpolated Section	549.86	272.64	46.3	.56	[1]1.23	.092	- .012
22	Dick Creek	549.38	272.27	51.2	.64	1.23	.110	.0
23		548.56	271.72	42.7	.21	1.34	.088	.0
24		547.47	271.53	43.9	.23	.80	.058	.0
25	Littles Ferry	546.95	270.61	39.6	1.02	1.63	.026	.0
26		546.50	270.74	48.8	.97	1.49	.016	.0
27	Interpolated Section	546.02	271.39	47.2	.98	[1].82	.019	.0
28		545.54	271.34	46.0	1.75	.77	.023	.0
29		544.97	271.10	51.8	.51	.91	.023	.0

Table 1.--Continued

Section number	Comments	River kilometer	Bottom elevation (m)	Coefficients in equation 43		Measured hydraulic depth at low flow (m)	Manning's roughness	
				T_a (m)	T_b (m^{-1})		η_o	η_1 (m^{-1})
30	Interpolated Section	544.60	271.08	48.8	0.52	0.88	0.026	0.0
31	Suwanee Creek	544.26	271.05	47.2	.58	.88	.026	.0
32	Gwinnett Co. Intake	544.04	271.03	47.2	.58	[1].88	.029	.0
33	Interpolated Section	543.81	271.09	50.3	.49	[1].76	.027	.0
34		543.59	271.12	57.9	.46	.70	.026	.0
35		543.09	270.79	51.8	.58	.96	.035	.0
36		542.24	270.69	45.1	.0	.84	.041	.0
37		541.24	269.82	40.2	.80	1.12	.051	.0
38		540.16	269.41	40.2	1.15	.95	.061	.0
39	Highway 120	539.55	268.59	51.8	.51	1.01	.050	.0
40		538.78	268.53	42.7	.23	.87	.033	.0
41		537.92	268.04	36.9	1.01	.94	.040	.0
42		536.96	267.68	56.1	.0	1.07	.040	.0
43		536.12	267.46	51.8	.0	1.19	.040	.0
44		535.61	267.31	41.8	.93	1.29	.041	.0

Table 1.--Continued

Section number	Comments	River kilometer	Bottom elevation (m)	Coefficients in equation 43		Measured hydraulic depth at low flow (m)	Manning's roughness	
				T_a (m)	T_b (m^{-1})		η_o	η_1 (m^{-1})
45		535.01	267.10	53.3	0.59	1.46	0.046	0.0
46		534.14	267.10	54.9	.33	1.40	.045	.0
47		533.35	267.46	54.9	.73	0.91	.046	.0
48	Highway 141	532.32	266.98	64.0	.91	1.25	.051	.0
		Length = 27.88 km				Average = 1.05 m	Average = 0.042	

[1]Interpolated value.

The cross-sectional data were processed as follows. First the sonic sounder charts were digitized to form coordinate pairs which described the shape and elevation of the cross section. A program was then developed which produced tabular values of area and top width versus maximum depth and fitted these tabular values with an expression of the form

$$A = T_a y_m + 1/3(T_b y_m^3) \tag{43}$$

in which y_m = maximum water depth in the cross section, T_a = bottom width of the channel, and T_b is the shape factor which determines the rate of increase of width with elevation.

The coefficients for equation 43 are shown in table 1 along with the location of the cross section and other pertinent information. The bottom elevation, in table 1, is the bed elevation of a cross section with a shape defined by equation 43 which was judged to best represent actual measured cross section. In general this was the mean elevation of the channel bottom at low flow.

In addition to the above internal reach data, which is more or less the standard field data collected for flow modeling purposes, the hydraulic depth at each cross section was measured on July 17, 1976, under conditions of steady low flow. These depths, shown in table 1, were obtained by averaging 3- to 10-point measurements obtained at uniform spacing across the river.

Boundary condition information consisted of a continuous record of stage at the upstream end of the reach as well as discharge at the four tributaries and at one withdrawal point. A stage discharge rating curve was also available at the upstream end of the reach. This stage-discharge relation was used along with the recorded stage to drive the model. Normally this would be poor practice but was justified here. Unique rating curves apply only to steady flow under constant influence of downstream backwater, if present. Under unsteady flow conditions, a different value of stage will be obtained for the same discharge depending on whether the discharge is increasing or decreasing and how fast. The Chattahoochee River below Buford is hydraulically somewhat unique. First, the flow is totally governed by releases from the Buford powerplant. These releases occur in fixed increments. Long periods (3 to 5 hours) of steady flow separated by rapid changes (10 to 15 minutes) are the rule. The reach of river from the dam to the Highway 20 bridge is very steep, with supercritical flow at several locations. Virtually no upstream reflection of waves is possible and backwater effects are nonexistent. Thus, when a flow change is made at Buford Dam, the flow at the gage located less than 0.4 km downstream stabilizes rapidly. During periods of unsteady flow, when the hysteresis loop rating should be considered, the time period of the loop is shorter than or equal to the time steps or the resolution of the model. Thus, no great inaccuracy is involved in using the rating curve as a boundary condition. Several runs were made using the stage directly as a boundary condition with no significant change in results.

Field reconnaissance and topographic maps indicated that a rock outcrop about 10 km below the Highway 141 Bridge controlled the depth in the lower end of the reach. The downstream boundary conditions were simulated, therefore, by assuming that the water between the bridge and this control was ponded to an average depth of about 2 m at low flow. The Manning's roughness coefficient over the control was assumed to be 0.016. Measured stage could have easily been used as a downstream boundary condition, but results were considered good enough without this refinement.

In addition to the boundary data, at least partial records of stage and discharge were available at the Highway 20 Bridge, Littles Ferry Bridge, Highway 120 Bridge, and the Highway 141 Bridge.

Discharges on tributary streams were virtually constant for both periods, so a constant flow was assumed. The observed values are shown in table 2.

The calibration of the flow model centered on the March data and involved a two-step process. The first step was to calibrate the model at steady low flow and the second step involved additional calibration necessary to match the dynamic response of the system.

Table 2.--Discharge values for the tributaries and withdrawal points on the Chattahoochee River during the October 20-25, 1975, and the March 21-24, 1976, modeling periods

Tributary	October flow (m^3/s)	March flow (m^3/s)
James Creek	0.5	1.1
Level Creek	.3	0.6
Dick Creek	.3	.7
Suwanee Creek	1.8	4.0
Gwinnett Co. Intake	- .2	- .2

The steady low flow calibration was accomplished as follows. The measured depth was added to the bottom elevation (table 1) and an "observed" water-surface profile was plotted. For steady flow the energy equation can be integrated between any two cross sections to give

$$\frac{U_i^2}{2g} + EW_i = \frac{U_{(i^2+1)}}{2g} + EW_i + 1 + \frac{n_i^2 U_i U^2_{(i+1)} \Delta x}{R_{Hi}^{2/3} R_{H(i+1)}^{2/3}} \qquad (44)$$

in which EW_i = water-surface elevation at grid point i, and n_i = Manning's roughness coefficient applicable to the subreach between grid points i and $i + 1$. Equation 44 was easily solved for the unknown roughness coefficient, n_i, applicable to each subreach since all other terms were known. In a few cases errors in the water-surface elevation were detected. These showed up as subreaches where the water appeared to run uphill or where the computed n value was unrealistically small or large (less than 0.005 or greater than 0.1). When this situation occurred for a subreach, the value of n was set equal to a realistic value, such as the value estimated in the field, and a corrected water-surface elevation for the grid point was computed. The bed elevation at the grid point was then established as the water-surface elevation minus the measured depth.

The roughness coefficients computed by use of equation 44 are applicable to the subreach between grid points, and the dynamic model requires roughness coefficients applicable to a subreach centered on the grid point. Some judgment was necessary, therefore, in averaging the roughness coefficients computed from equation 44 to obtain values, which were used in the dynamic model. Using the roughness values, tabulated in table 1, the dynamic flow model was run to equilibrium at steady low flow and the surface profile computed. This computed profile can be compared to the "observed" profile in figure 8. The above procedure assured that the flow model gave realistic depths, volumes, and surface areas, at least at steady low flow.

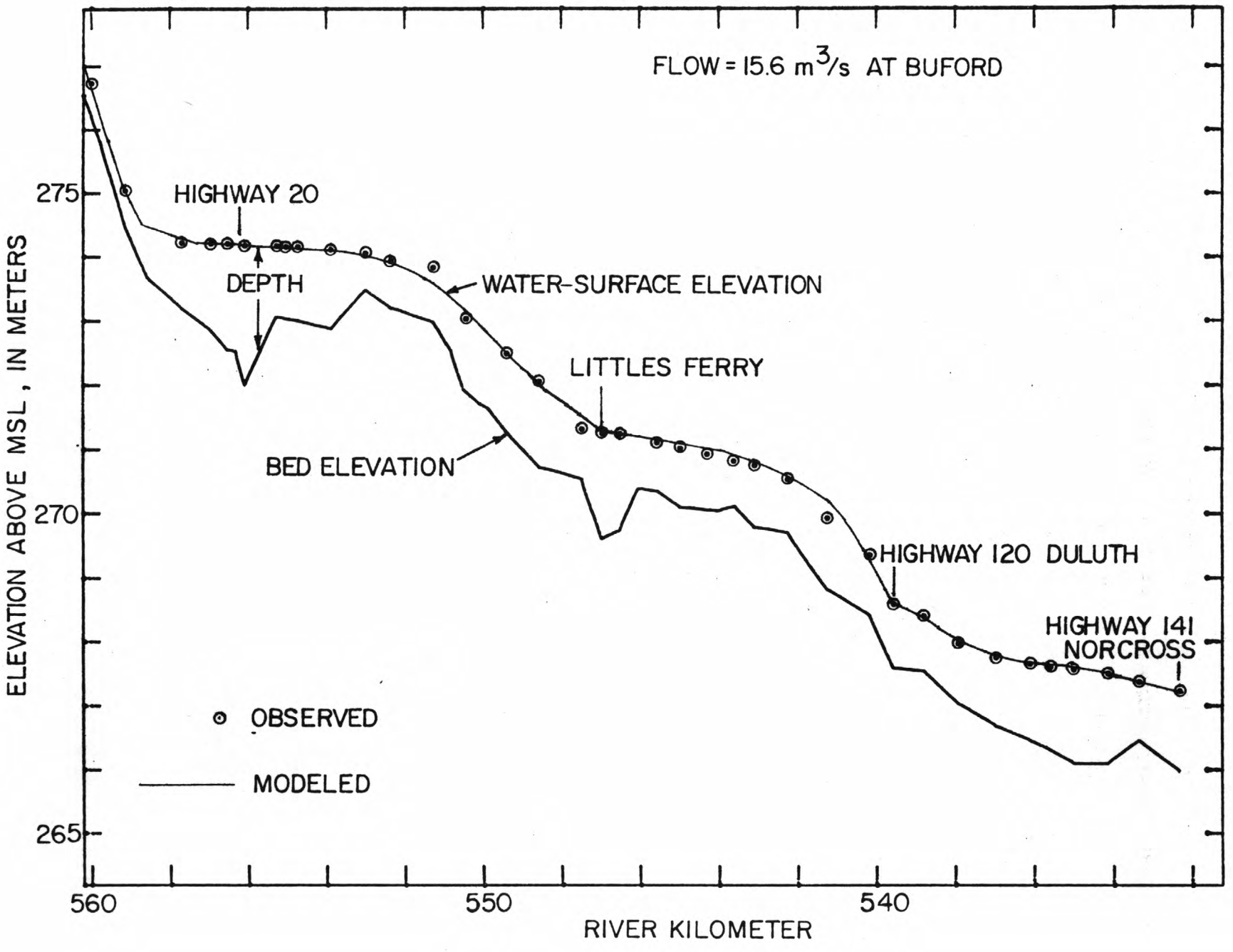

Figure 8.--Steady flow depth profile for the Chattahoochee River between Buford Dam and Norcross.

The ability to match the depths at all cross sections under steady low flow conditions does not guarantee that the model will reproduce unsteady flow. In order to match the dynamic response of the system, it was found necessary to vary some of the roughness coefficients with depth. These variations were necessary to make the modeled and observed rises in stage during the hydropulses agree. The roughness was assumed to vary with depth as

$$n(y) = \eta_o + \eta_1 \ (y - y_{mo}) \tag{45}$$

in which $n(y)$ = roughness coefficient at depth y, η_o = steady low-flow roughness (table 1), η_1 = rate of change of roughness with stage, also shown in table 1, and y_{mo} = measured hydraulic depth at low flow. The grid points at which the roughness was to be varied with depth and an approximate value of η_1 was determined from a sensitivity analysis using a simple backwater program for different flows. Once the model was calibrated at steady low flow, dynamic calibration using the March data only required seven of the roughness values be varied with depth. The variation with depth was not extreme. At section 18 the roughness decreased by 85 percent as the flow increased to its maximum, but variations in the roughness at other sections were less than 50 percent.

One set of adjustments was made to the flow model as a result of observations of the behavior of the transport model. The low-flow traveltime in the upper reach was increased slightly by arbitrarily increasing the low-flow cross-sectional areas, above the values indicated in table 1 at section numbers 7 through 15 in the pool above the control at section 16, by an average of about 36 percent. This adjustment was believed to be justified because of the rather poor quality of the low-flow depth information in this reach. The adjustment had very little effect on the modeled stage or discharge values but improved the low flow timing of the transport model at Littles Ferry.

The results of the final calibration are illustrated in figure 9 in which the observed and modeled stages at Buford Dam and the four bridges are plotted for the 3 1/2-day calibration period. The small rise in the observed stage at Highway 141 on March 21 was caused by a light rain which occurred before 0600 that day. No tributary flow measurements were available during this day, so constant values were assumed in the model. Visually, the stage predictions are good. The cross correlation of observed and modeled stages indicate peak correlation coefficients of 0.997, 0.997, 0.999, and 0.988 at lags in minutes of +20 for Highway 20, -5 for Littles Ferry, -30 for Highway 120, and -10 for Highway 141, respectively. A positive lag indicates the model lagged behind the observed. At zero lag the correlation coefficients were 0.989, 0.996, 0.979, and 0.987, respectively.

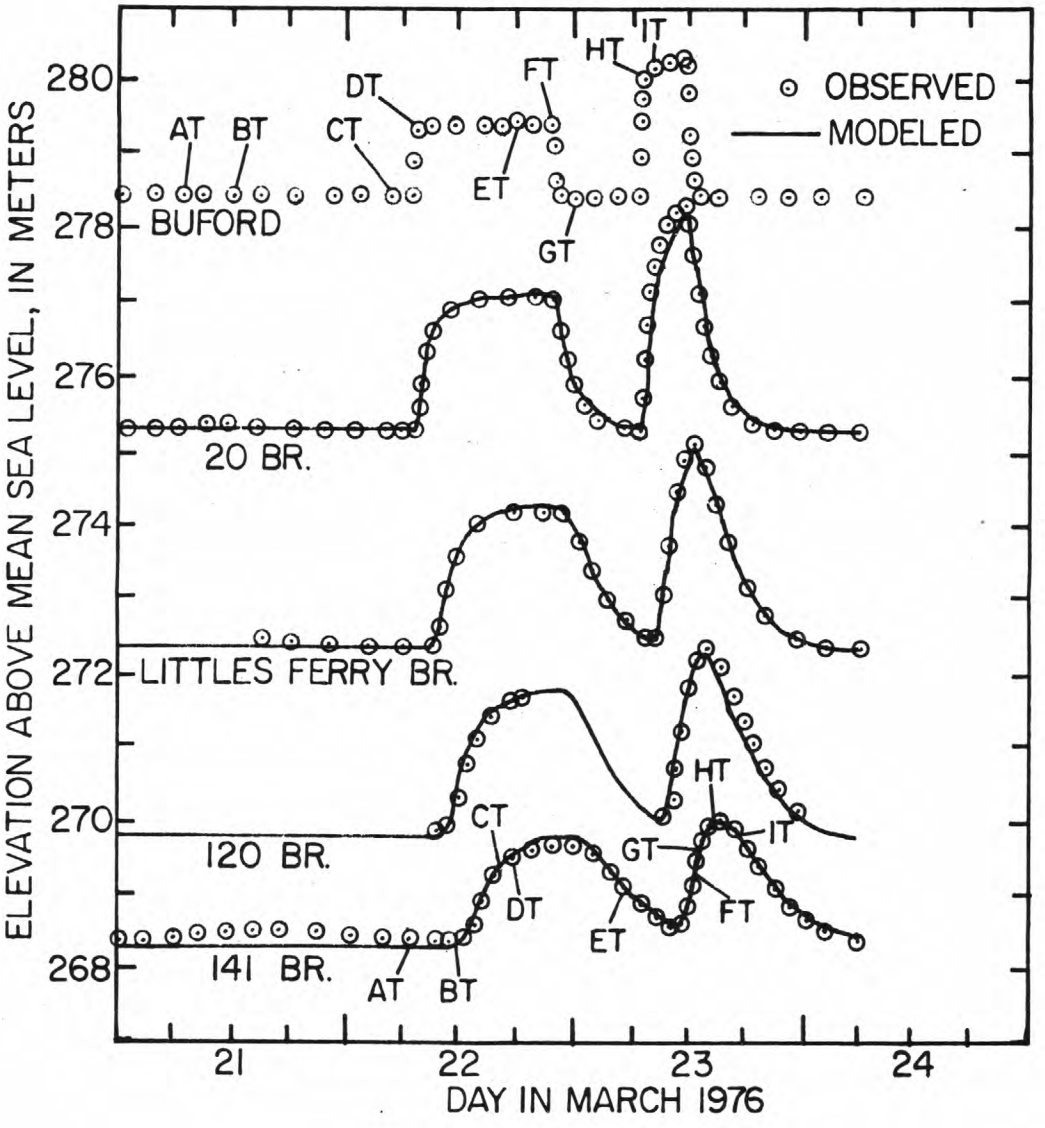

Figure 9.--Calibration of the Chattahoochee River flow model with the March 1976 stage data. The symbols AT through IT represent the time of arrival of specific water particles at the respective locations.

During the March run, field crews attempted to continuously measure discharge at the bridges. A detailed description of the manner in which these measurements were obtained is in progress (R. E. Faye, written commun., 1978), but briefly it involved the periodic measurement of velocity and depth at particular transverse stations, plotting the data at each station against time, and interpolating the data to a particular time in order to estimate the instantaneous discharge. A complete traverse of the river required about 1 hour. Figures 10 through 13 are presented so that a comparison of the modeled and measured discharges can be made. A rating curve was also available at the Highway 141 Bridge, so that an "observed" discharge could also be determined by use of the table and the observed stage. The agreement of the modeled and measured discharges is excellent for flows as large as 110 m^3/s. The differences are less than 5 percent. At higher flows, the model consistently predicts lower than observed discharges. The peak modeled discharge on March 23 at Littles Ferry and Highway 141 was 20 percent lower than the measured value. Because discharge measurements under highly unsteady flow conditions are of questionable accuracy, the 20 percent difference in results was not considered serious. Overall, the model results were considered to be very good. The consistency with which the transport model reproduced the dye concentrations bears out the accuracy of the flow model.

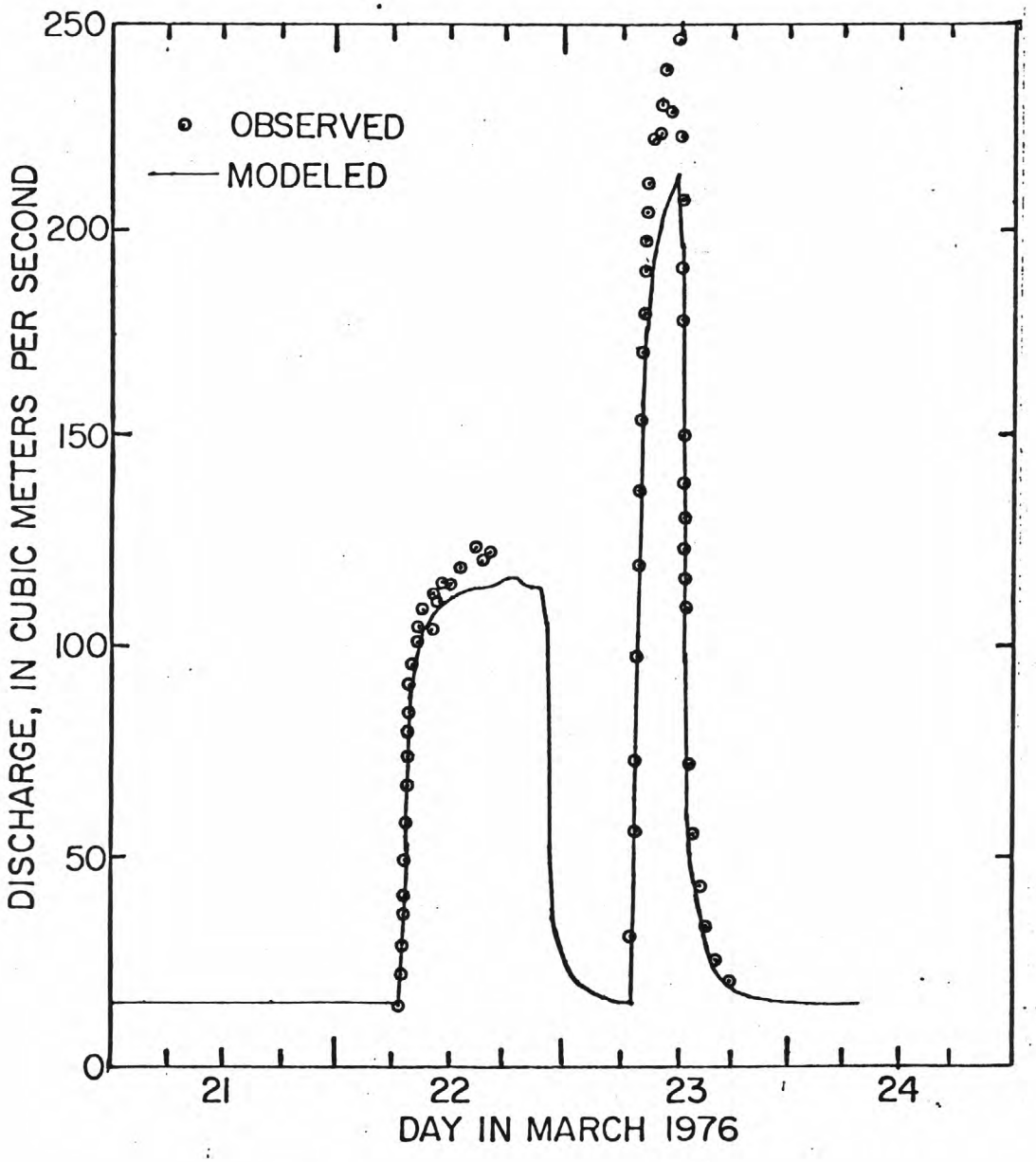

Figure 10.--Comparison of modeled and observed discharge in the Chattahoochee River at the Highway 20 Bridge during the March 1976 calibration period.

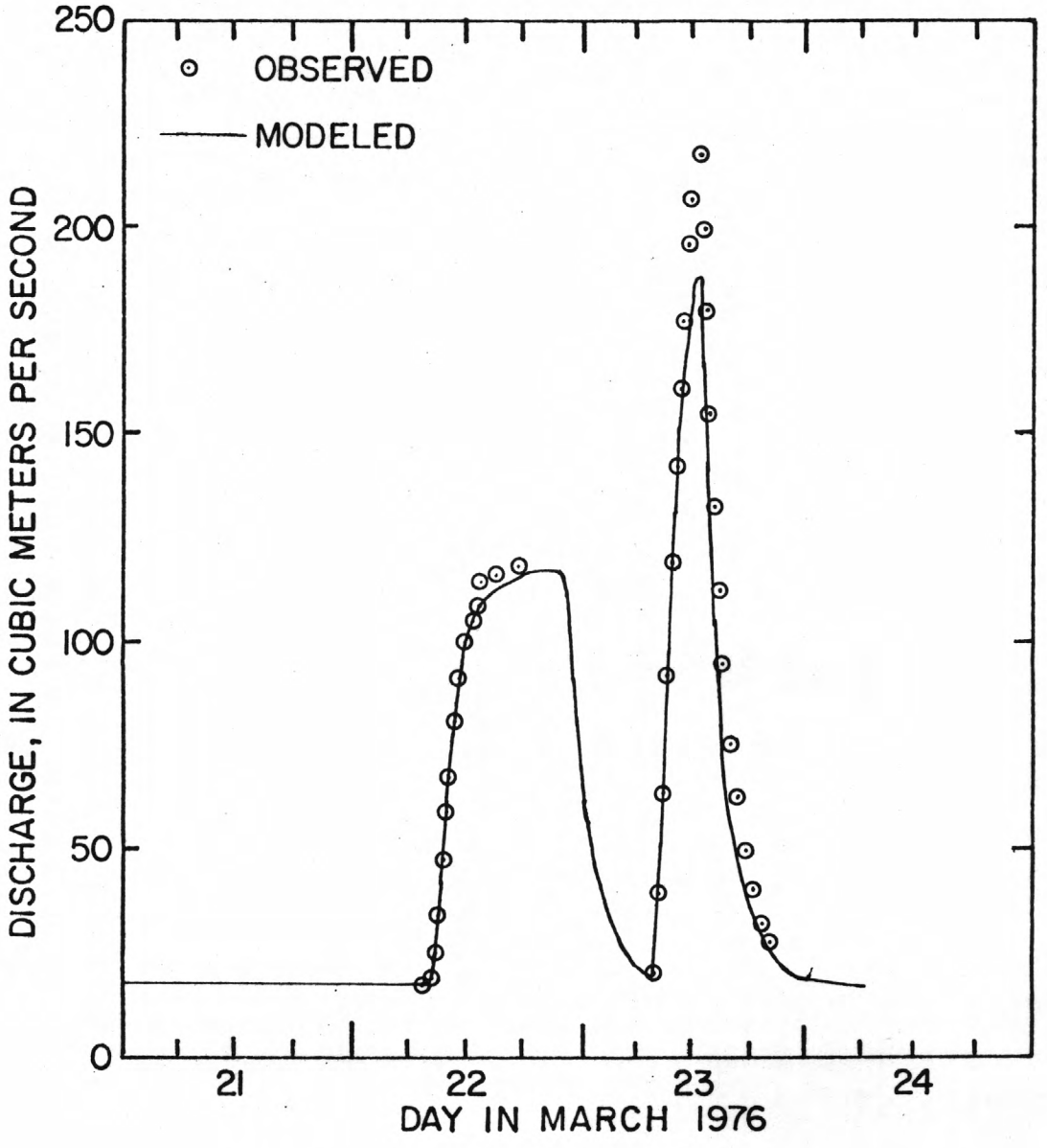

Figure 11.--Comparison of modeled and observed discharge in the Chattahoochee River at the Littles Ferry Bridge during the March 1976 calibration period.

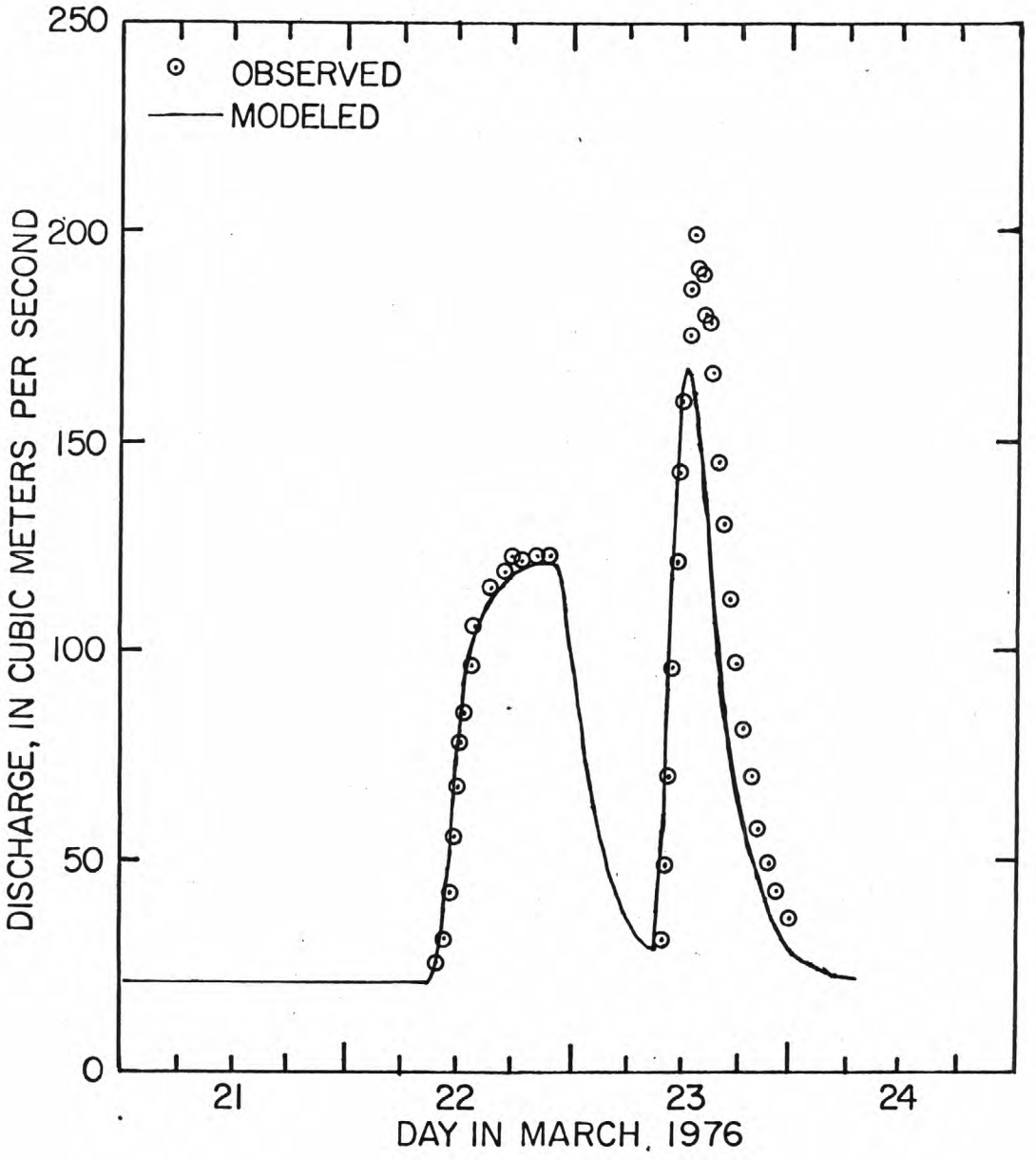

Figure 12.--Comparison of modeled and observed discharge in the Chattahoochee River at the Highway 120 Bridge during the March 1976 calibration period.

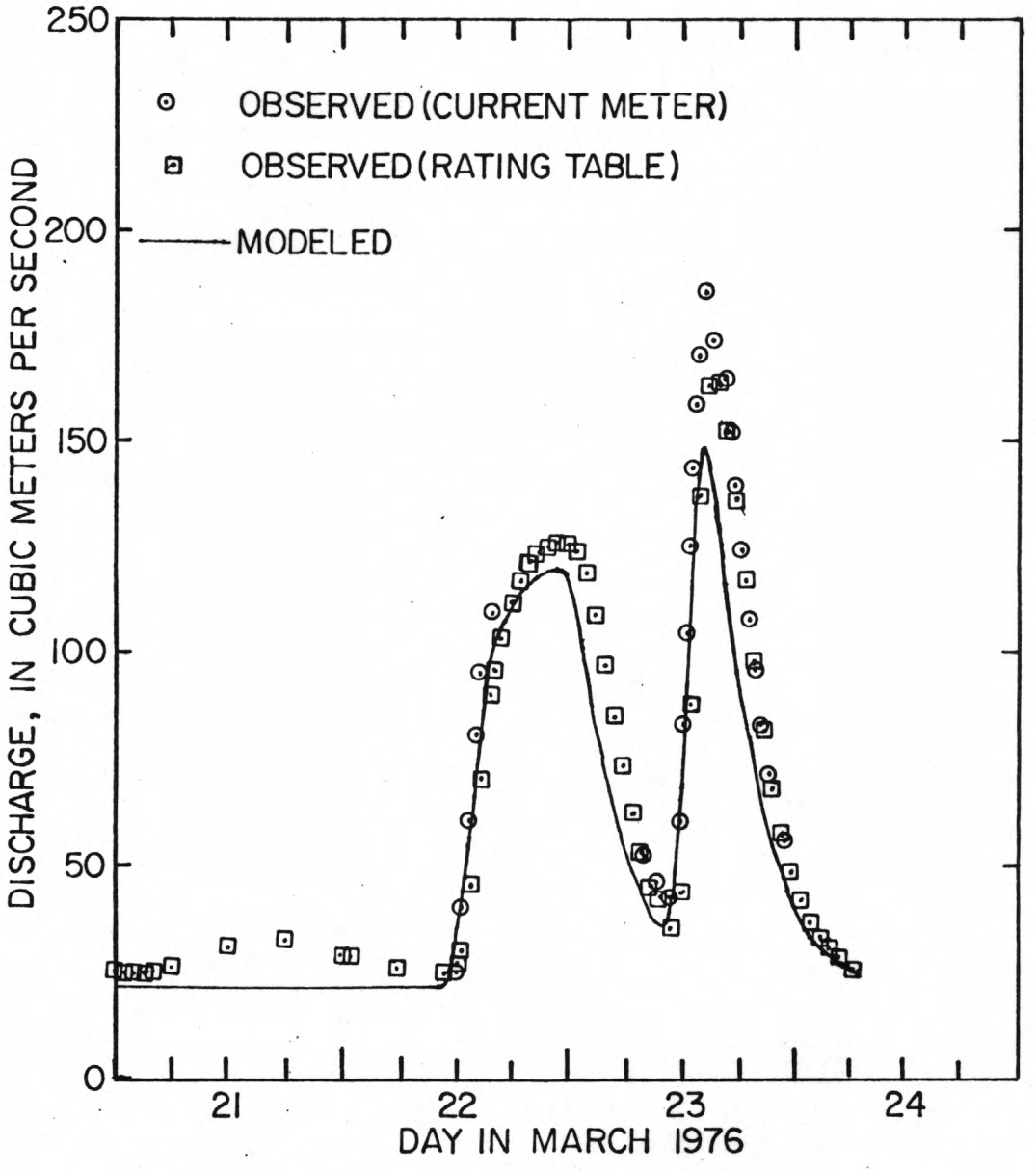

Figure 13.--Comparison of modeled and observed discharge in the Chattahoochee River at the Highway 141 Bridge during the March 1976 calibration period.

The model was verified by use of the data collected during October 1975. A comparison of the predicted and modeled stages can be obtained from figure 14. The predicted stage values are within 0.15 m of the observed values in most cases, and timing is accurate to within about 30 minutes. Cross correlation of the measured and modeled stage data indicate correlation coefficients of 0.995 and 0.988 when measured values were lagged by +25 and +40 minutes at Georgia Highways 20 and 141 respectively. Zero lag correlation coefficients were 0.971 and 0.974, respectively. The model does appear to underestimate the stage at Littles Ferry and Highway 20. The match could be improved by decreasing the roughness, η_o, at sections 16 and 17 to 0.021 from 0.030, setting the value of η_1 to +0.0033 for sections 25, 29, 36, and 37, and setting the value of η_1 to +0.0066 and +0.0056 at sections 38 and 39, respectively. The predicted and observed stages obtained with these updated resistance coefficients are shown in figure 15 which illustrates that the visual effect of these corrections is small. Use of the updated coefficients with the March data underpredicted the high stage at Littles Ferry by about 0.5 m, otherwise, the results were similar.

Only a few discharge measurements were available for the October run. These were made on October 23 and 24 and are illustrated in figure 16. The measured peak discharge at Littles Ferry on October 23 was 12 percent higher than the modeled value obtained with the updated roughness coefficients. As with the spring run, the agreement between the modeled and observed discharge on the rising limb of the hydrograph is good.

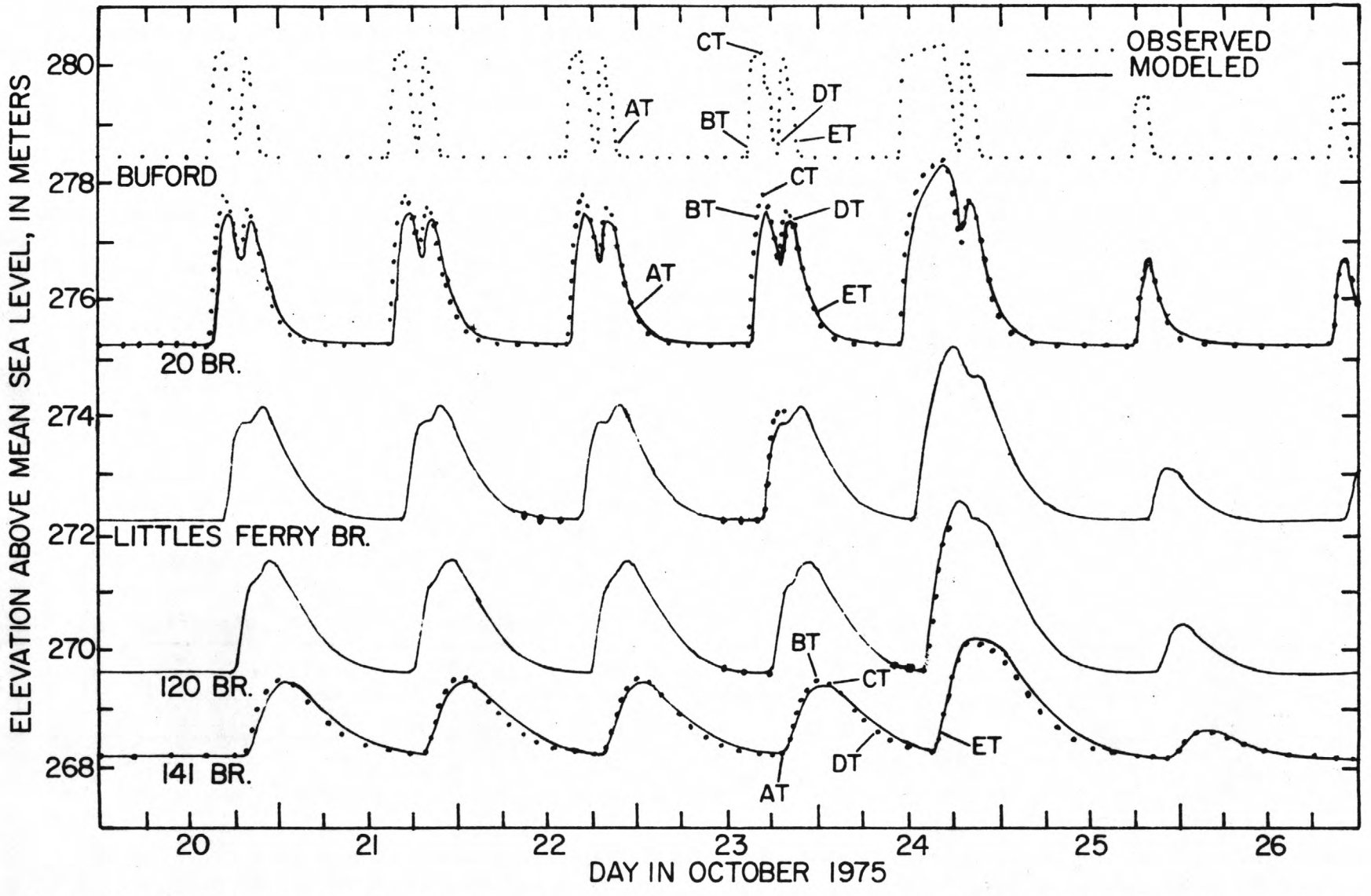

Figure 14.--Verification of the Chattahoochee River flow model using the October 1975 stage data. The symbols represent the time of arrival of specific water particles at the respective locations.

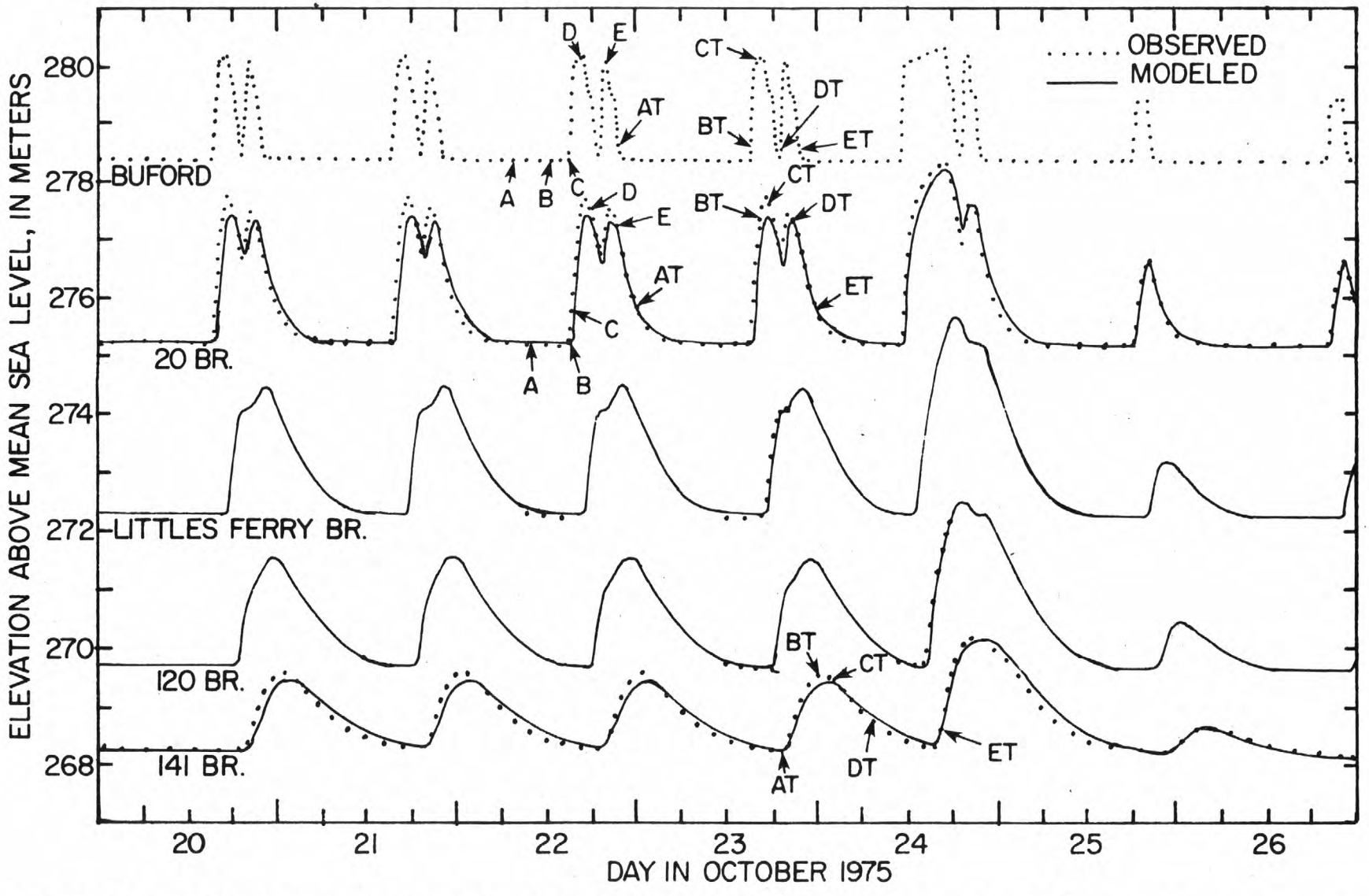

Figure 15.--Calibration of the Chattahoochee River flow model using the October 1975 stage data. The symbols represent the time of arrival of specific water particles at the respective locations.

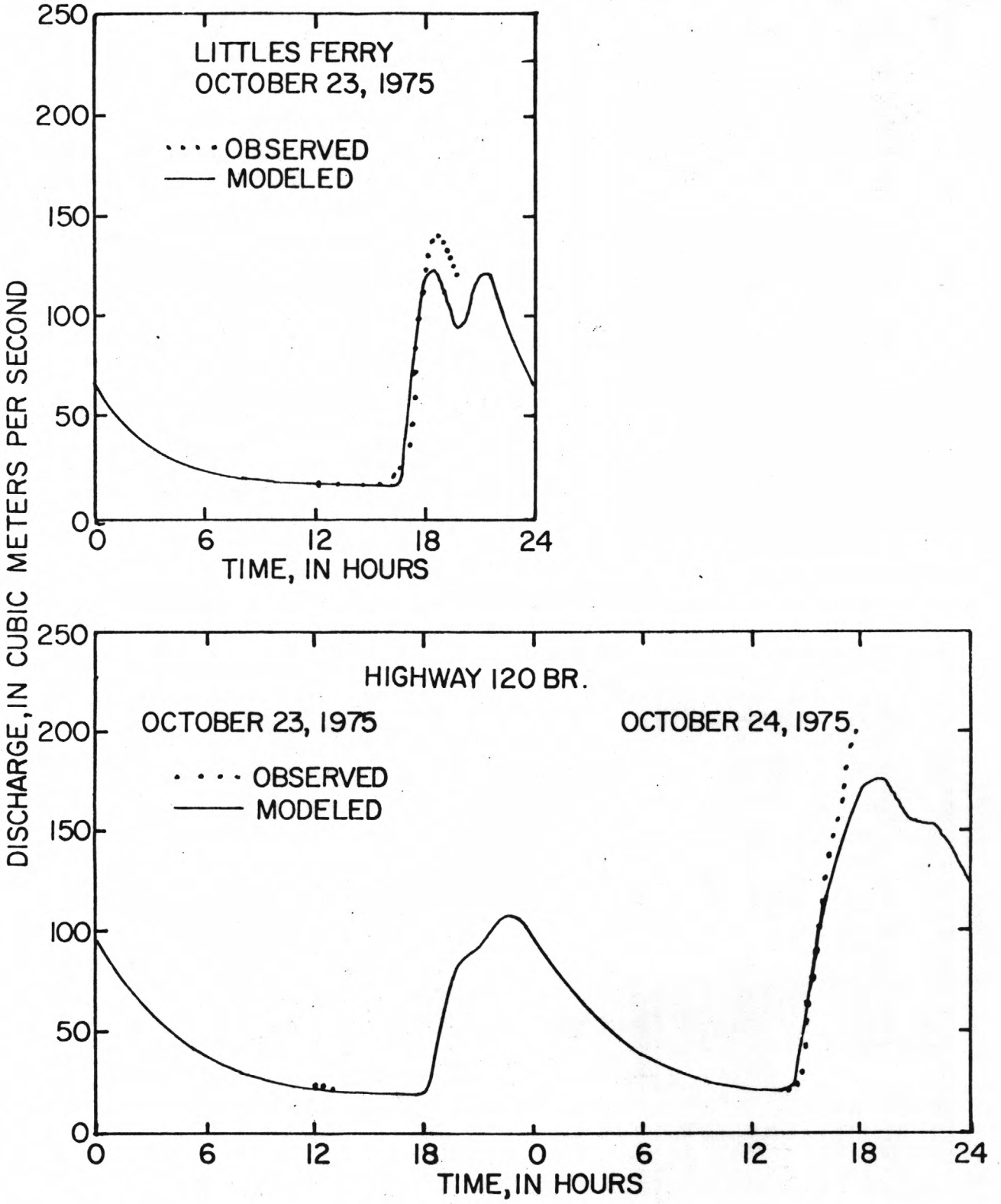

Figure 16.--Comparison of the modeled and observed discharges in the Chattahoochee River during the October calibration run.

It was assumed that a slight change in roughness occurred between October 1975 and March 1976, so the roughness coefficients given in table 1 were used when generating a flow field for the spring transport model, and the updated coefficients, given above, were used in generating the flow field for the fall transport model.

Mass Transport of a Conservative Substance

It is generally recognized that neither equation 9 or 10 accurately represent the longitudinal mixing (dispersion) of a slug injection until considerable mixing has occurred. In fact, the criteria given by Fischer (1973) suggest that the equations will not accurately represent the dispersion of a slug injection in the Chattahoochee within the first 7.3 km at high flow or with the first 8.6 km at low flow. On the other hand, it has been shown that dispersion plays an almost insignificant role for the case of a steady injection rate (Sayre and Chang, 1968). In consideration of the above, an independent verification of the transport model was deemed desirable.

To generate data against which the transport model could be verified, rhodamine-WT dye was injected into the river just below Buford Dam starting at 1100 hours, March 21, 1976. The injection rate was held constant for a 3-day period by use of a small positive-displacement pump. Figure 17 contains a photograph of the injection site. The dye was pumped from the barrels through a tube, hung on a cable, to the center of the channel. The dye fell about 3 m before striking the water surface. Three hours after injection began, sampling began at Littles Ferry Bridge and 6 hours later it began at the Highway 141 Bridge. Dip samples were collected in 25 mL bottles clipped to an angle iron (see fig. 18). Samples were taken from the thalweg of the river every 10 minutes, and at 6-hour intervals samples were collected at 6-m intervals across the river. During times of steady flow, the maximum variation in concentration across the width of the river was about 5 percent. Unfortunately, during unsteady conditions, the traverse results were relatively meaningless because of the time required to obtain the samples.

Dye concentrations at Littles Ferry and Highway 141 Bridges were then simulated by both the conservative (eq. 9) and nonconservative (eq. 10) transport models. The results are presented in figures 19, 20, 21, and 22 along with the measured concentration values. The model results in figures 19 and 20 were obtained by use of the conservative model (solution to eq. 9 with unequally spaced grid points) and the results in figures 21 and 22 were obtained by use of the nonconservative model (solution to eq. 10 with equally spaced grid points).

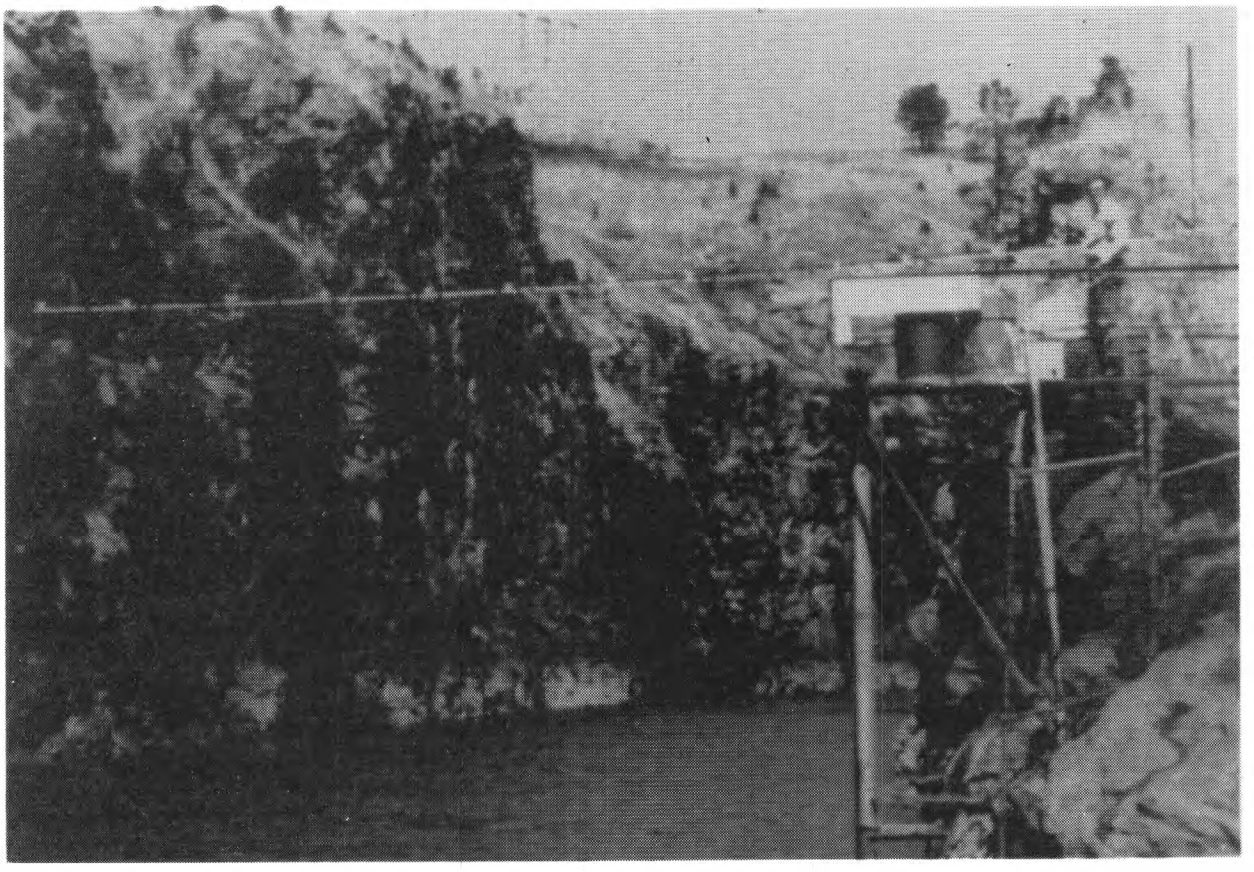

Figure 17.--Dye injection site for the March 1976 dye study, 200 meters downstream of Buford Dam.

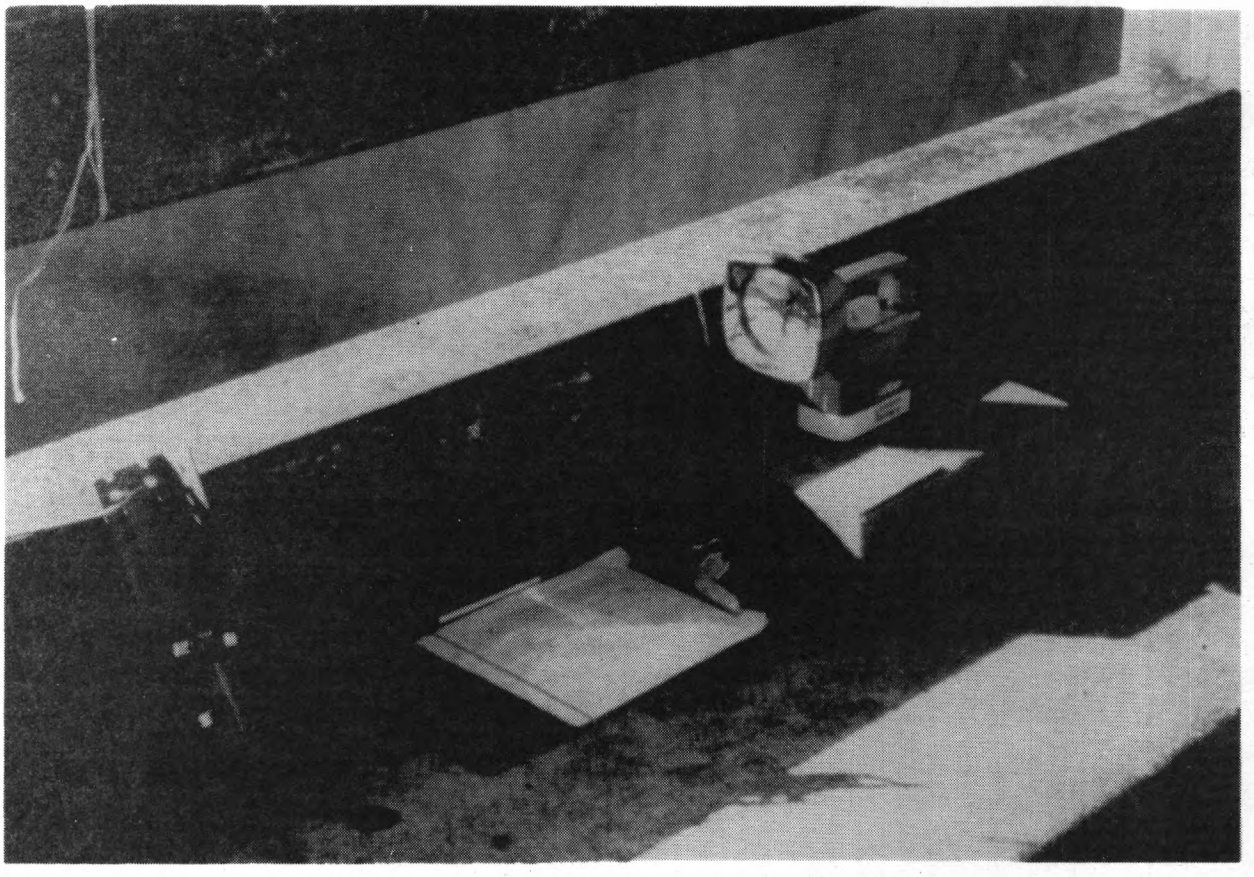

Figure 18.--Sample bottle for dye study.

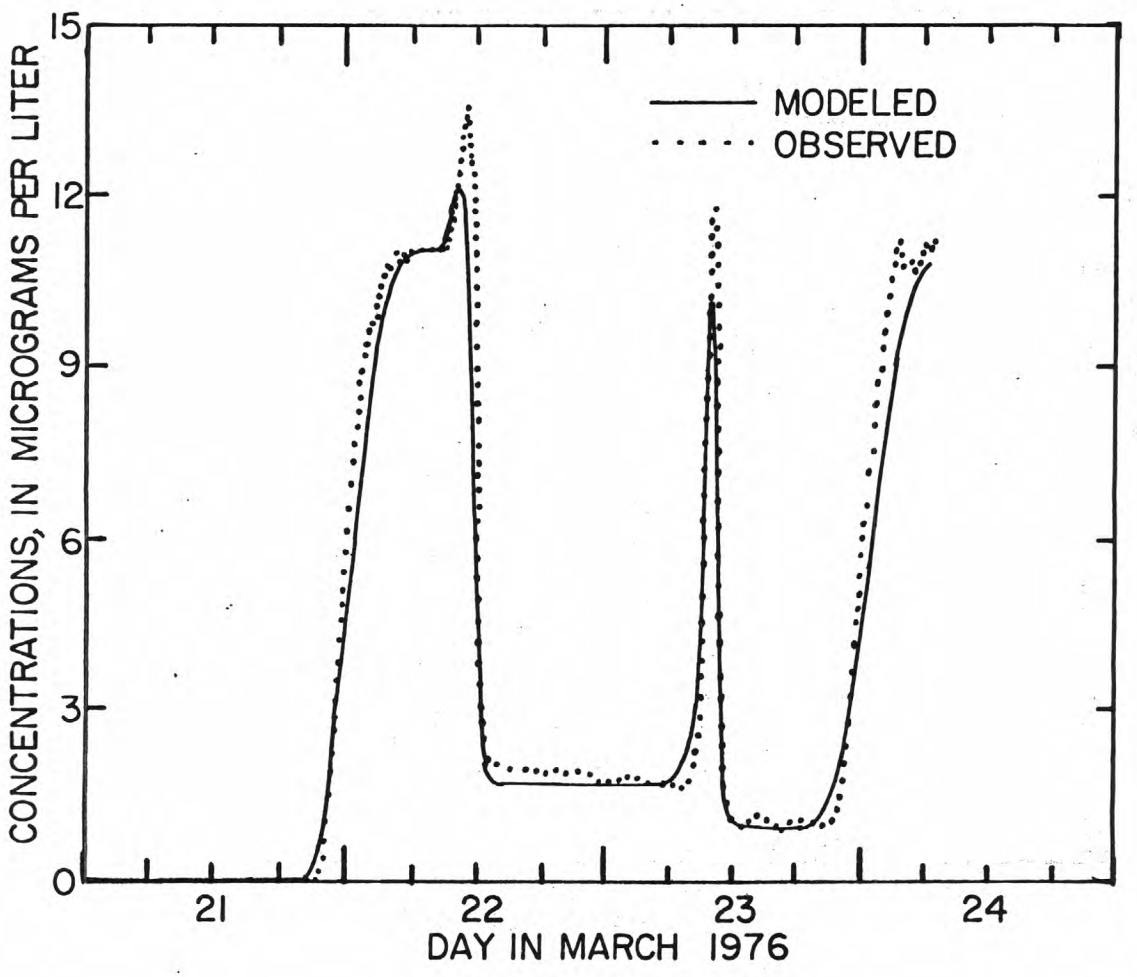

Figure 19.--Modeled and observed dye concentrations at Littles Ferry Bridge as computed using the conservative transport model with unequal grid spacing.

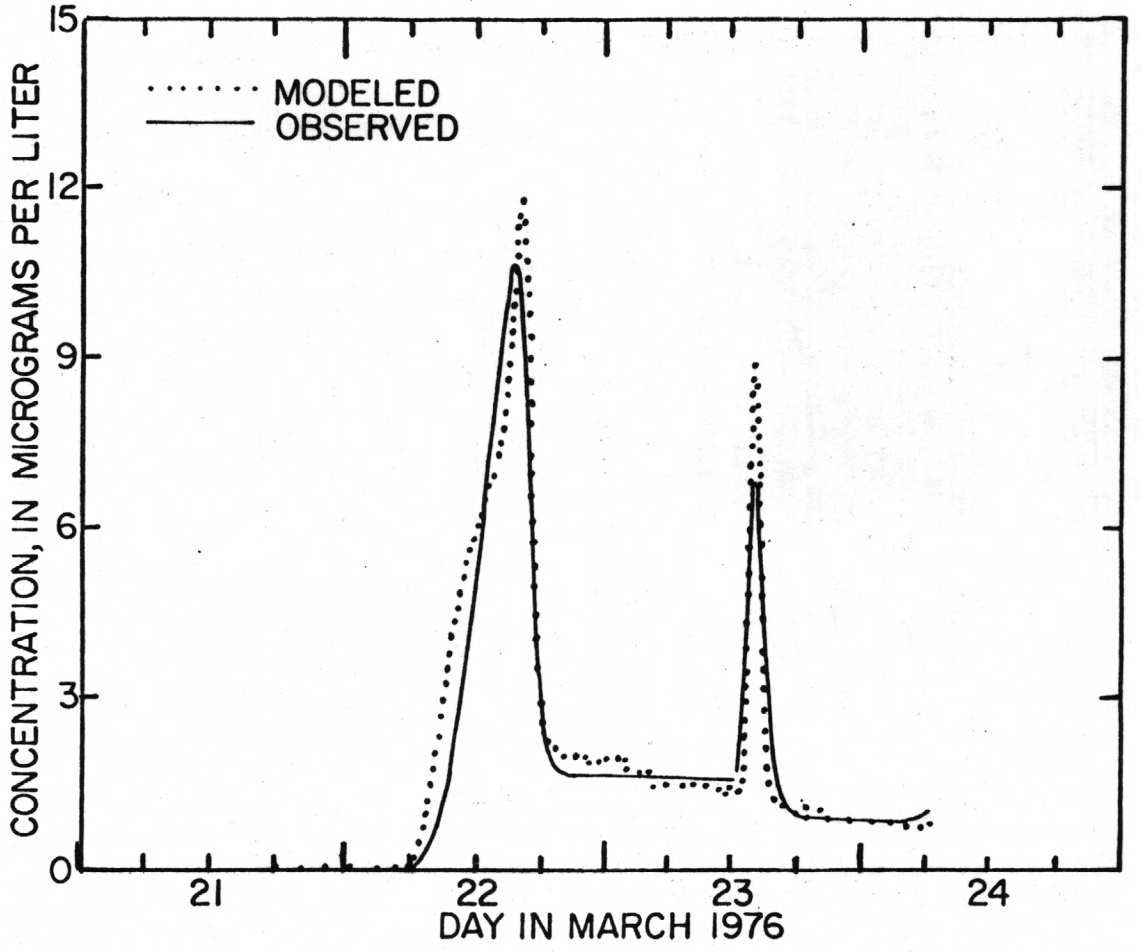

Figure 20.--Modeled and observed dye concentrations at Highway 141 as computed using the conservative transport model with unequal grid spacing.

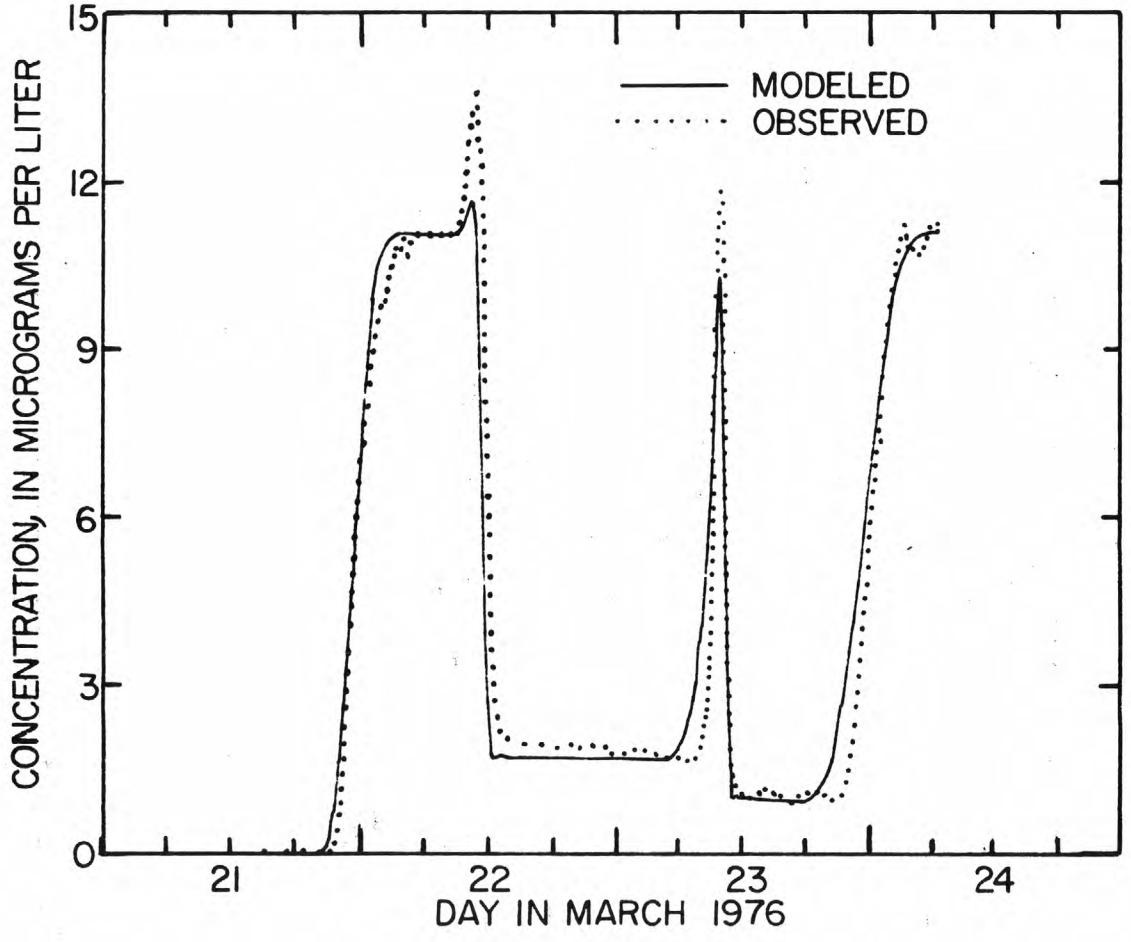

Figure 21.--Modeled and observed dye concentrations at Littles Ferry Bridge as computed using the nonconservative transport model with equal grid spacing.

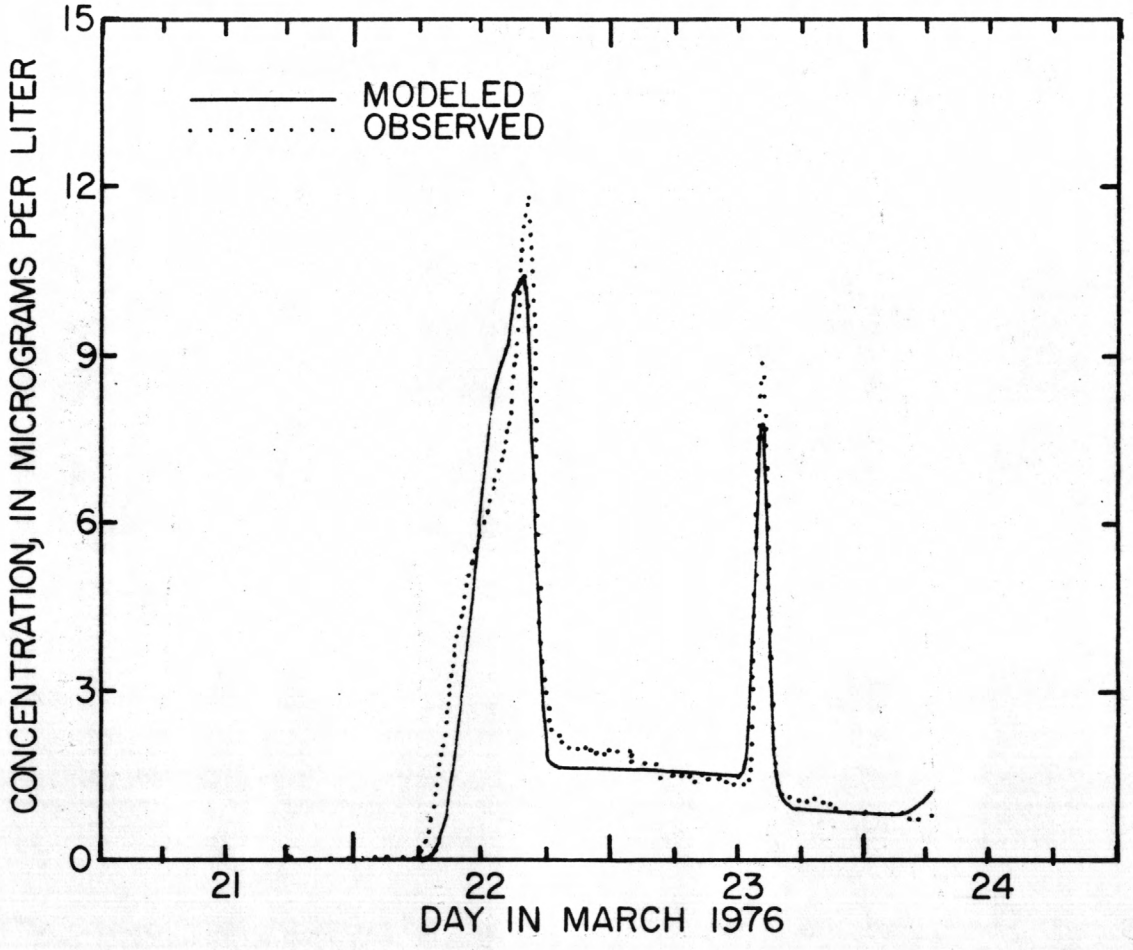

Figure 22.--Modeled and observed dye concentrations at Highway 141 as computed using the nonconservative transport model with equal grid spacing.

The model results presented in figures 19 and 20 are considered to be excellent. Cross correlation of the measured and modeled concentrations indicated correlation coefficients of 0.992 and 0.952 when the measured values were lagged by 15 and 0 minutes, respectively, at the Littles Ferry and Highway 141 Bridges. At Littles Ferry the zero lag correlation coefficient was 0.986.

The results presented in figures 21 and 22 are also considered to be excellent. Comparison of figures 19 and 21 shows that the conservative model maintains slightly better timing of results at Littles Ferry but that its solution is slightly more dispersive even though it was run with the dispersion coefficient set equal to zero. The conservative model also provides a better simulation of the anomalous rise in concentration beginning about 1000 hours on March 22. On the other hand a comparison of figures 20 and 22 indicates that the nonconservative model gave slightly better timing results at Highway 141. On the whole, however, the results of both models appear excellent and their differences appear to be trivial. Because the nonconservative model appeared to satisfactorily represent the transport under the highly unsteady conditions in the Chattahoochee and because the existing conservative model did not allow for surface exchange or the solution to equation 31, the temperature model was not recoded to solve the conservative form of the transport equation.

The Temperature Model

Four types of data are needed for use with a temperature model. These are: hydraulic data which describe the flow, physical data which define the geometric relation between the river and its surroundings, meteorologic data which help define the heat flux at the air-water interface, and temperature data at the upstream boundary and at all tributaries.

Hydraulic data input to the temperature model included flow velocity and area as well as the tributary flow (both the steady and variable component) at each grid point and time step. These data were passed to the temperature model directly from the flow model.

Physical data included the azimuth, effective barrier height, bank width, and the relation between top width and flow area for each grid point. Top widths were determined for each cross section by use of equation 41. Spot checks indicated the relations defined by equation 41 were accurate to within 1.5 percent most of the time for within bank flow, which is all that is of concern here. The azimuth of each subreach, the effective barrier height, and the coefficients for use in equation 41 are shown in table 3. The azimuth values, centered at the grid point, were determined by use of a 1:24,000 scale topographic map, and the effective barrier heights, figure 6, were estimated in the field at the time the longitudinal depth profile was measured. The banks of the Chattahoochee are very steep and the trees often lean out over the river as shown in figure 5. A constant bank width of 0.3 m was assumed. In so far as the shading computations were concerned, the river top width was assumed to have a value representative of steady low flow at each grid point.

Table 3.--Physical data relevant to the Chattahoochee River between Buford and Norcross.

Temperature model grid	Coefficients in equation 41*				Azimuth	Effective barrier height (m)
	a_0	a_1	a_2	a_3		
1	61.10	39.79	-19.459	2.921	227.3	12
2	60.29	-13.68	13.130	-2.027	214.4	12
3	17.15	80.59	-47.530	8.878	185.7	18
4	35.34	62.55	-48.568	11.658	212.7	12
5	36.28	30.05	-8.855	.948	194.4	12
6	5.29	68.89	-12.038	-5.080	209.9	11
7	12.15	85.74	-36.101	4.886	208.4	18
8	22.23	60.64	-35.677	6.918	180.2	18
9	20.19	72.47	-34.403	5.035	208.7	18
10	40.48	45.86	-14.771	1.754	212.4	18
11	56.86	7.68	-1.768	.323	192.1	18
12	17.19	137.49	-138.739	42.648	191.3	18
13	40.26	41.25	-26.820	5.800	186.2	18
14	16.29	134.83	-89.536	17.956	198.9	18
15	26.75	63.42	-36.898	6.639	130.8	18
16	36.81	52.39	-35.384	7.307	154.8	18
17	11.39	74.16	-36.025	5.532	113.7	20
18	17.12	93.75	-68.102	15.606	201.5	15
19	35.26	61.05	-43.448	9.683	241.0	18
20	20.45	75.95	-41.749	7.144	217.2	11
21	34.32	42.99	-23.634	4.442	237.3	6

Table 3.--Continued

Temperature model grid	Coefficients in equation 41*				Azimuth	Effective barrier height (m)
	a_0	a_1	a_2	a_3		
22	40.13	41.08	-27.701	6.164	258.7	12
23	50.82	16.91	-7.528	1.880	254.2	12
24	22.02	78.01	-49.816	10.118	270.6	14
25	10.43	190.32	-281.511	145.283	281.7	18
26	16.54	96.45	-60.425	11.483	246.5	15
27	20.31	85.66	-80.764	23.757	224.3	15
28	14.40	45.43	-22.654	5.028	199.5	12
29	34.30	31.69	-16.888	3.272	195.9	18
30	10.66	150.71	-157.014	48.941	186.3	18
31	25.37	71.79	-61.229	16.904	207.6	18
32	34.72	65.76	-51.248	12.714	234.3	15
33	20.90	102.24	-114.297	41.513	259.9	18
34	18.73	112.03	-77.910	16.383	339.0	18
35	25.77	48.90	-15.380	1.729	359.5	18

*Top widths are given in meters when the area is given in hundreds of square meters.

The thermal properties of the river bed might also be classified as physical data. The bed of the Chattahoochee River is mostly covered with small sand dunes so the thermal diffusivity and heat storage capacity were assumed to be 0.77 mm^2/s and 0.68 cal/cm^3 °C, respectively. Braslavskii and Vikulina (1963) suggest these values are applicable for saturated sand.

Stream temperatures in the Chattahoochee River and its tributaries were monitored by personnel of the Chattahoochee River Quality Assessment Project. These data and the details of their collection will be reported elsewhere (R. E. Faye, written commun., 1978). The location of the data collection points, however, are shown in figure 1.

During the October run the temperature recorder at the upstream end of the reach malfunctioned, so the upstream boundary of the temperature model was set at the Highway 20 Bridge, which is 3.7 km downstream of the boundary of the flow model. Water temperatures at Highway 20 were available on 15-minute intervals, starting at 1300 hours on October 21, 1975, and continuing for the duration of the run. Before 1300 hours on the 21st, the upstream temperatures were estimated. Hourly temperatures were available for all tributaries and at the Highway 141 Bridge for the entire Fall run. Intermittant temperature data were available at the Littles Ferry and Highway 120 Bridges.

Much more complete temperature data were collected during the March run. Beginning at 0000 hours on March 21 and continuing to 0700 hours on March 24, 1976, 5-minute data were recorded at the upstream boundary as well as at Highway 20, Littles Ferry, Highway 120, and Highway 141. Because of a recorder malfunction, approximately 24 hours of data were missing at Highway 120, however. Five-minute data were also recorded on Suwanee Creek from 0000 hours on March 21 until 1800 hours on March 23, 1976. Only a few temperature measurements, obtained at random times, were available for the other tributaries. Using available temperatures, regression equations were derived for each tributary which predicted the instantaneous tributary temperature from the Suwanee Creek temperature. After 1800 hours on March 23, all tributary temperatures, including the Suwanee Creek temperature, were estimated from the air temperature using a regression expression which had been derived from the random data. Before 1800 hours on March 23, the predicted temperatures in Level, James, and Dick Creeks were probably accurate to within ± 2°C and after this time about ± 3°C.

All temperature data were first placed on cards and then plotted to check for keypunching or instrument errors. Once the data were verified in this manner, the hourly or 15-minute data were expanded to a 5-minute time base by straight line interpolation. The expanded data sets were stored on magnetic disk for use with the temperature model.

The initial temperature distribution in the river was assumed to vary linearly with distance between points of observation.

Meteorologic data needed to drive the temperature model include windspeed, incoming solar radiation, incoming atmospheric radiation, air temperature, wet-bulb air temperature, and rainfall intensity. All meteorologic data were obtained at the R. M. Clayton Sewage Treatment Plant in Atlanta, Ga. This site was selected primarily because of its security, its nearness to the study headquarters, its proximity to the river, and because it offered good exposure to the sun and wind. Figure 23 contains a view of the building upon which the meteorologic instrumentation was mounted. Some of the instrumentation can be seen on top of the building tower in the center of the pictures. The R. M. Clayton plant is about 55 km southwest of Buford Dam and about 35 km southwest of the Highway 141 Bridge.

A propeller-type anemometer was used to sense the windspeed. The starting speed of the propeller was about 0.45 m/s with full tracking at about 1.4 m/s. The wind direction was also recorded but not used in the model. The general exposure of the anemometer is shown in figures 23 and 24. A closeup of the anemometer with the Chattahoochee River in the background is shown in figure 25.

The total incoming solar radiation was determined by use of an Eppley[1/] precision spectral pyranometer. The instrument is sensitive to radiation with a wavelength between 0.3 and 3 μm. The pyranometer is the instrument on the left in figure 26. The incoming atmospheric radiation was determined by use of two Eppley pyrgeometers which are sensitive to radiation in the range of 4 to 50 μm. These instruments are shown to the right of figure 26.

[1/] The use of brand names in this report is for identification purposes only and does not imply endorsement by the U.S. Geological Survey.

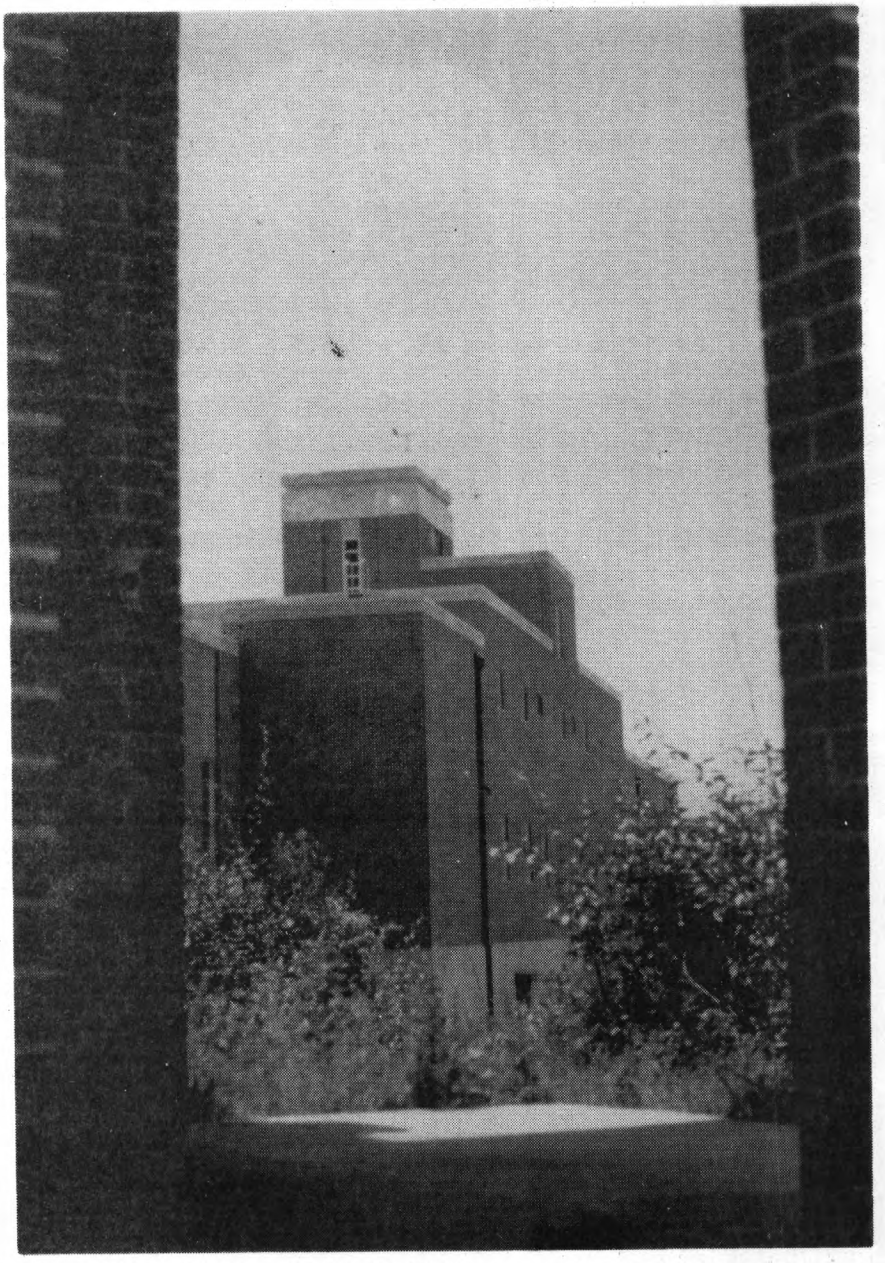

Figure 23.--View of the building at the R. M. Clayton Sewage Treatment Plant which supported the meteorologic instrumentation.

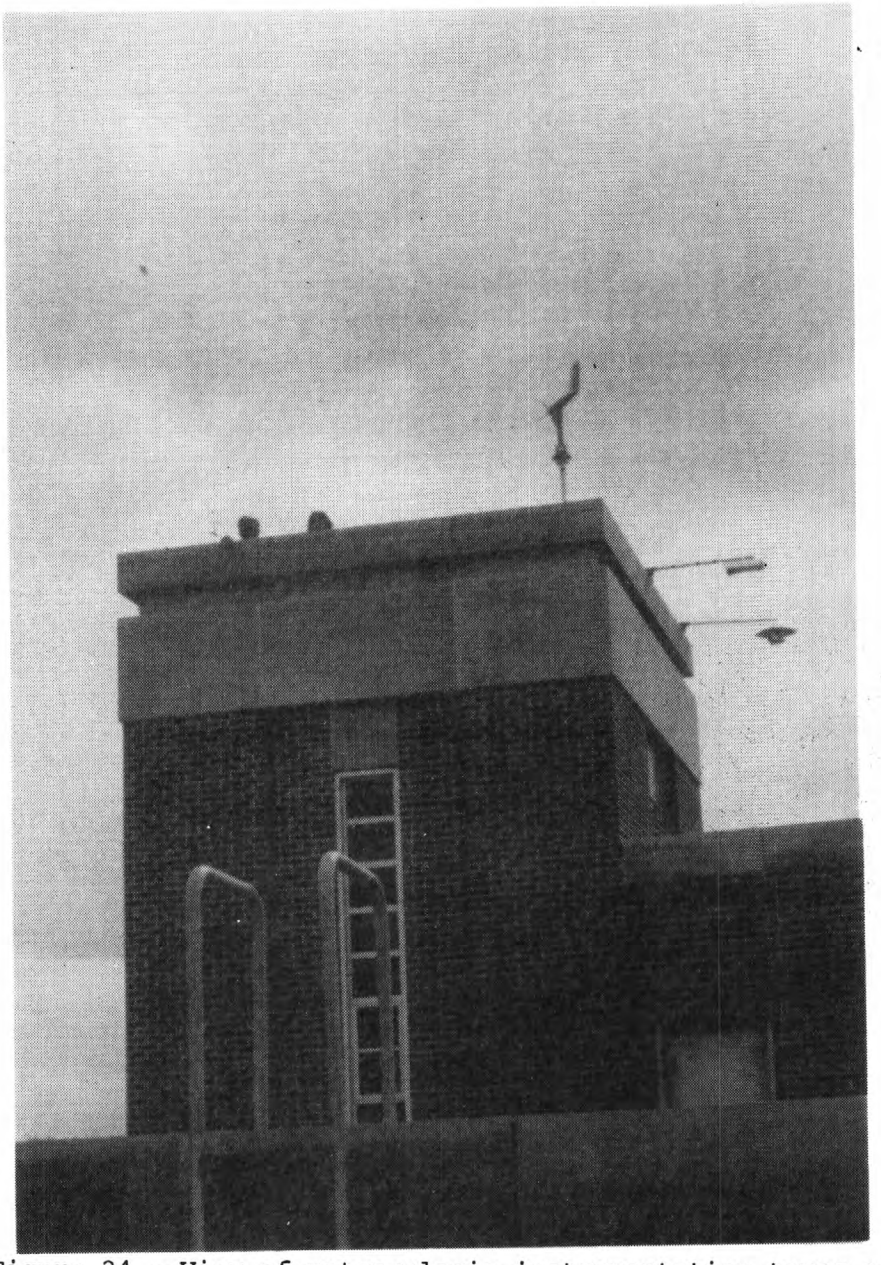

Figure 24.--View of meteorologic instrumentation tower of the R. M. Clayton Sewage Treatment Plant showing the anemometer and two psychrometers.

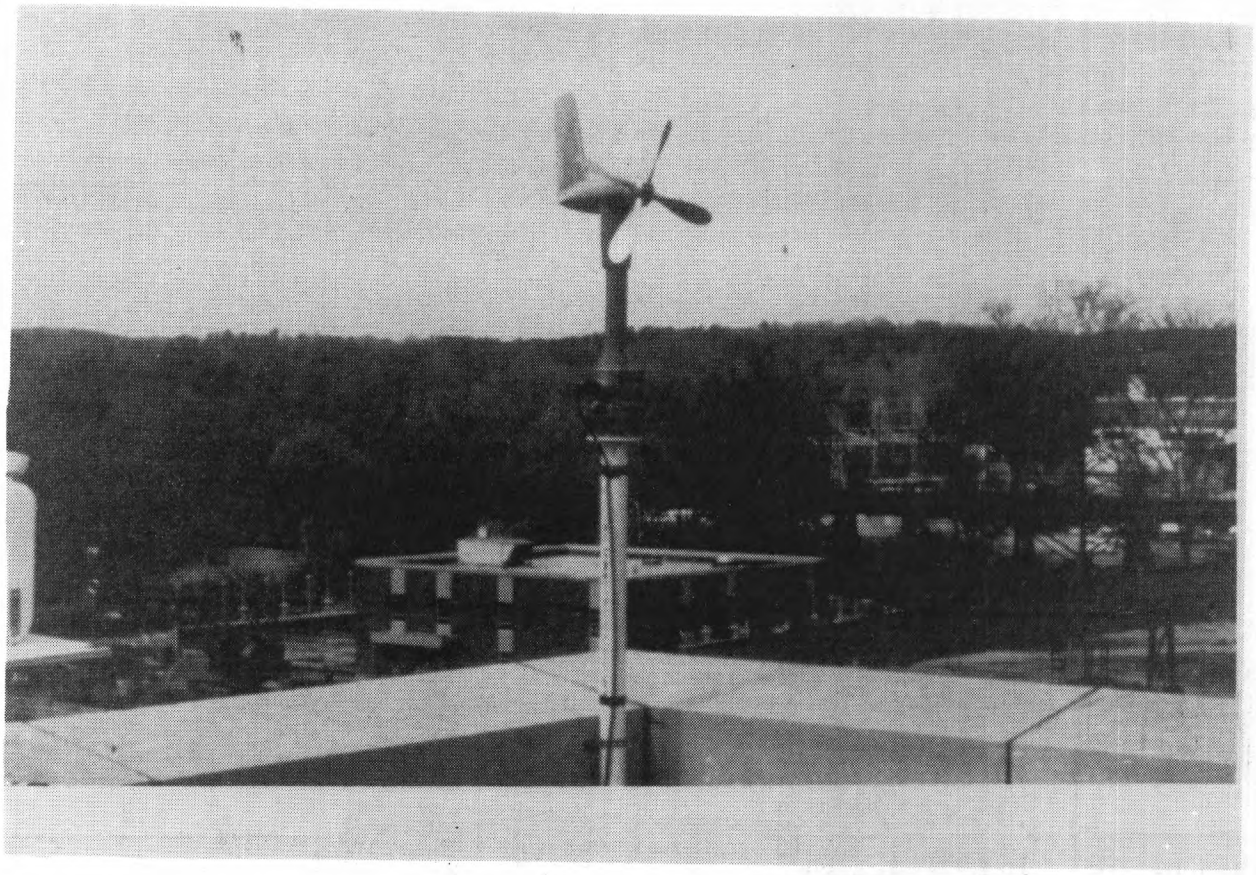

Figure 25.--Closeup of the anemometer showing the Chattahoochee River in the background.

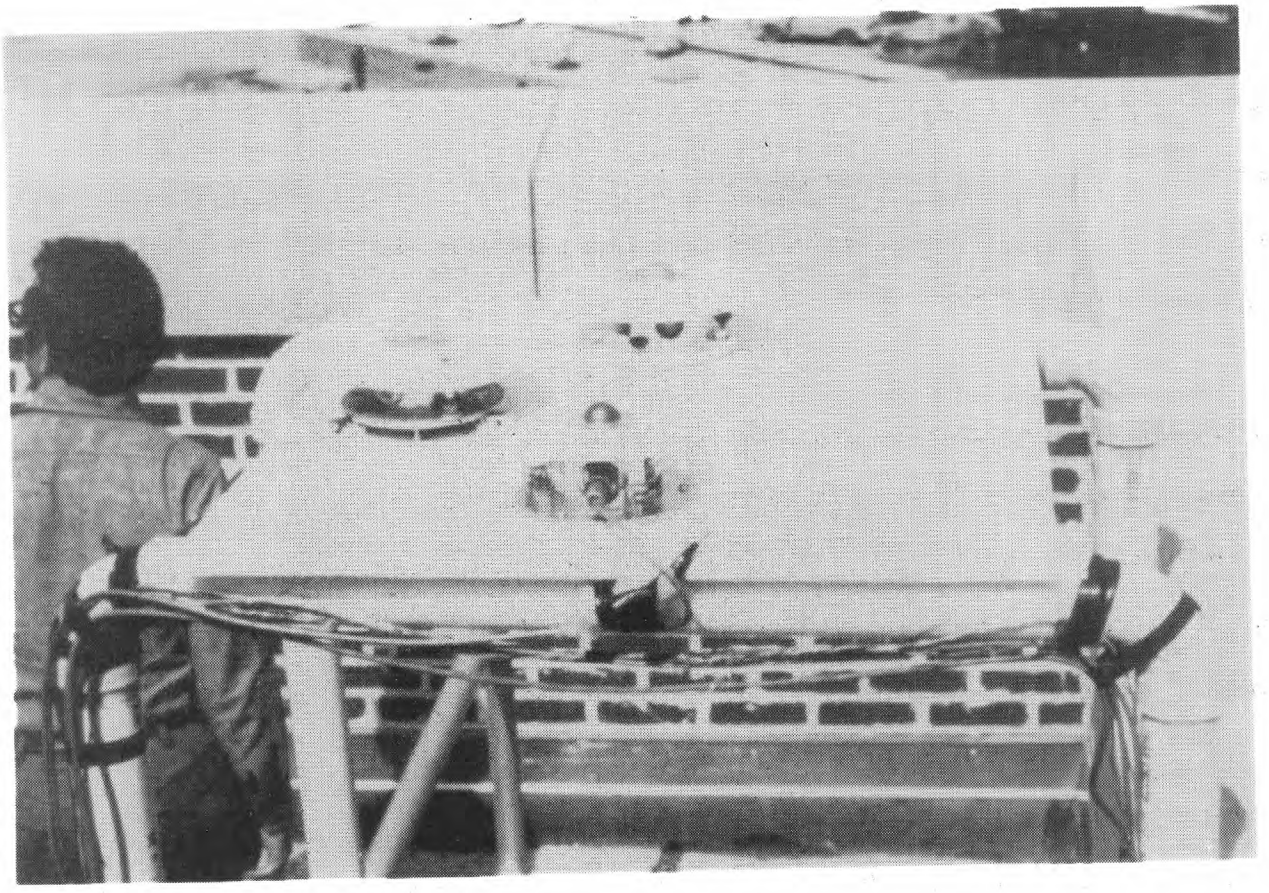

Figure 26.--Closeup of pyranometer and pyrgeometers at the R. M. Clayton Sewage Treatment Plant in Atlanta.

Two psychrometers were also used to determine the wet- and dry-bulb air temperatures. These can be seen projecting from the tower in figure 24. A closer view of the ventilated psychrometer is shown in figure 27. The temperatures in this instrument were sensed by use of platinum resistance temperature devices, and the wet-bulb probe was covered by a wick which was continually wetted by distilled water. The probes projected across a plastic tube which was shielded from radiation by a curved aluminum sheet and through which air was drawn at a speed of 4.5 m/s by a vane axial fan. A detailed description of this psychrometer has been given by Jobson and Sturrock (1976).

A closer view of the nonventilated psychrometer is shown in figure 28. This instrument was originally designed for use during the Lake Hefner studies and has been described in detail by Anderson and others (1950). This instrument is generally called a Top Hat psychrometer because of the shape of the radiation shield. Temperatures are sensed by copper-constant thermocouples which are housed above a distilled water reservoir and within a housing that facilitates natural ventilation. Rainfall was measured by a tipping bucket rain gage.

An Esterline Angus D2020 recorder was housed in the tower and used to record all meteorologic data. At a specified time interval, the time as well as the millivolt values of the 10 parameters were printed on a paper tape. No averaging of the readings was possible, so the recorded value represented only an instantaneous reading. A sampling of the 10 channels required about 5 seconds. The recording was at hourly intervals in October and at 5-minute intervals in March.

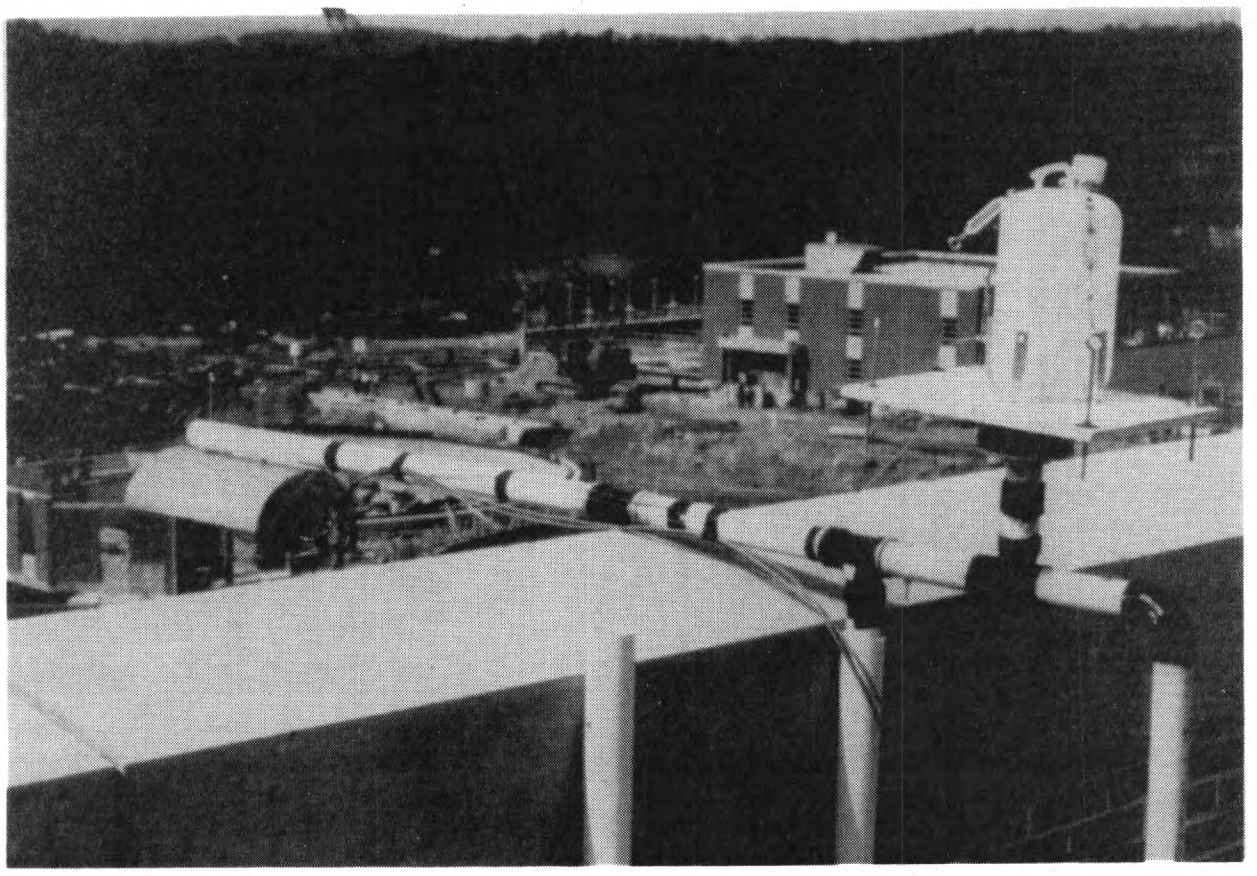

Figure 27.--Closeup of ventilated psychrometer at the R. M. Clayton Sewage Treatment Plant in Atlanta.

Figure 28.--Closeup of Top Hat psychrometer at the R. M. Clayton Sewage Treatment Plant in Atlanta.

No special processing of the windspeed and solar radiation data were required for the October period because the records were complete. October 20, 22, and 24 were essentially clear days and the radiation values indicated only a little cloudiness around noon on October 21 and 23. On October 25, it was partly cloudy. Daily average values of all meteorologic data are presented in table 4. The output of the two pyrgeometers agreed to within 3 percent, so their results were averaged for use in the model. Previous experience has indicated that the pyrgeometers indicate too much diurnal variation in the incoming atmospheric radiation, so daily average, rather than instantaneous values, were used in the model. No rainfall occurred during the October run.

Both psychrometers worked satisfactorily during the October run. It was believed, however, that the ventilated psychrometer was a little more accurate, so its readings were used throughout. Air temperature contained a typical diurnal swing of about 19°C and a gradual warming trend (table 4) occurred during the run.

Table 4.--Daily average values of meteorologic variables at the R. M. Clayton Sewage Treatment Plant in Atlanta

Date	Windspeed (m/s)	Solar radiation (Watts/m^2)	Atmospheric radiation (Watts/m^2)	Air temperature (°C)	Vapor pressure (kPa)
October 20, 1975	1.22	203	315	10.4	0.78
October 21, 1975	0.84	189	323	12.6	0.86
October 22, 1975	0.44	192	335	13.6	0.98
October 23, 1975	0.51	158	350	15.2	1.25
October 24, 1975	0.92	201	353	16.6	1.26
October 25, 1975	0.43	122	368	16.5	1.52
March 21, 1976	1.92	264	346	11.0	0.64
March 22, 1976	1.29	171	336	10.7	0.61
March 23, 1976	0.86	261	348	10.5	0.67
March 24, 1976	2.64	263	373	13.6	0.95

Data coverage during the March period was not as complete. No meteorologic data were available before 1140 hours on March 21. It was assumed that meteorologic conditions between midnight and 1140 hours on March 21 were identical to those which occurred between midnight and 1140 hours on March 23. Although rain is known to have occurred during this period, no record was available, so it was assumed to have been zero. After 1140 hours on the 21st, complete data were available for the wind-speed, solar radiation, and rainfall (which was zero). These values were used directly. The days of March 23 and 24, as well as the afternoon of March 21, were almost free of clouds. It was quite cloudy until about 1500 hours on March 22. The outputs of the two pyrgeometers differed by about 19 percent during the March run. The outputs of the two sensors were averaged, however, to give the values used in the model (table 4). The temperatures from the ventilated psychrometer were again used in the model except for an 8-hour period on March 24. During this period the values from the Top Hat psychrometer were used because the wick of the ventilated psychrometer was partly dry. During the March run the diurnal air temperature swing was about 15°C.

Like the temperature data, all meteorologic data were placed on punch cards, plotted, and edited. The hourly values, for the fall run, were then expanded to a 5-minute time base by straight line interpolation. The vapor pressures were then computed and the data sets stored on magnetic disk for use by the model.

The temperature model contains several physical constants and empirical coefficients. The usual modeling procedure is to select a calibration period during which one or several of the empirical coefficients are adjusted until a "good" fit occurs. The calibrated model should then be run with an independent set of data to verify that the coefficients, determined during the calibrating period, are "universally" applicable to the particular river reach.

In this case all model coefficients were assumed a priori on the basis of assumptions already given. Because no coefficients were adjusted to fit the measured temperatures, both the March and October data should be considered as verifications of the temperature model.

The measured and predicted water temperatures for the October verification are shown in figures 29, 30, 31, and 32. The observed temperatures at the Highway 20 Bridge, shown in figure 29, were used as the upstream boundary condition of the temperature model. The water temperature at the Highway 20 Bridge for times before 1130 hour on October 21 had to be assumed because no measured values were available. The assumption of these values of course invalidates any verification of the model during these first few hours, but it does allow the starting times of the flow and temperature model to be the same. Very few measured water temperatures were available at Littles Ferry Bridge (fig. 30) or Highway 120 (fig. 31). At Littles Ferry the data on October 22 consisted of three spot measurements which would appear to have been too high by 0.5 to 1°C. It is possible that these spot measurements were taken too near the bank or that poor procedures were used. The accuracy of periodic temperature-measuring techniques used by the U.S. Geological Survey has been estimated to be $\pm$0.8°C (Moore, 1969; Rawson, 1970; and Blodgett, 1971). On October 23 the spot field measurements are within 0.5°C of the computed values and the general shape of the computed and measured curves are alike. Except for the two points on October 23, the general shape and magnitude of the measured temperature distribution at the Highway 120 Bridge (fig. 31) agree closely with the predicted values. A complete temperature record was available at the Highway 141 Bridge, figure 32. The agreement between the computed and measured temperatures is very good. Ignoring the first 24 hours of record, the RMS (root-mean-square) difference between the measured and computed values is 0.32°C, and the mean difference is 0.21°C. The near perfect fit before noon on October 21 is of course the result of judicious estimates of the upstream temperature and should be disregarded in evaluating the verification of the model.

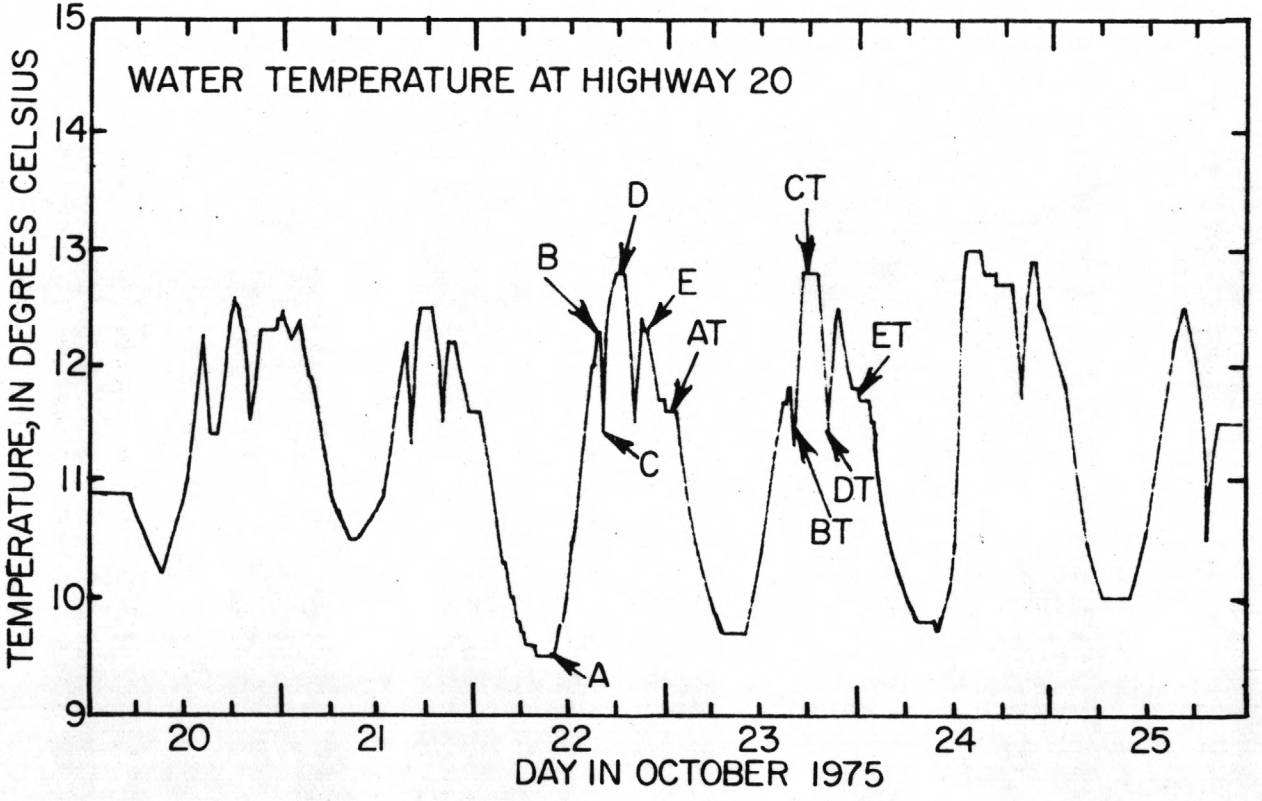

Figure 29.--Observed temperature in the Chattahoochee River at the Highway 20 Bridge during the October 1975 verification period. The symbols represent the time of arrival of specific water particles.

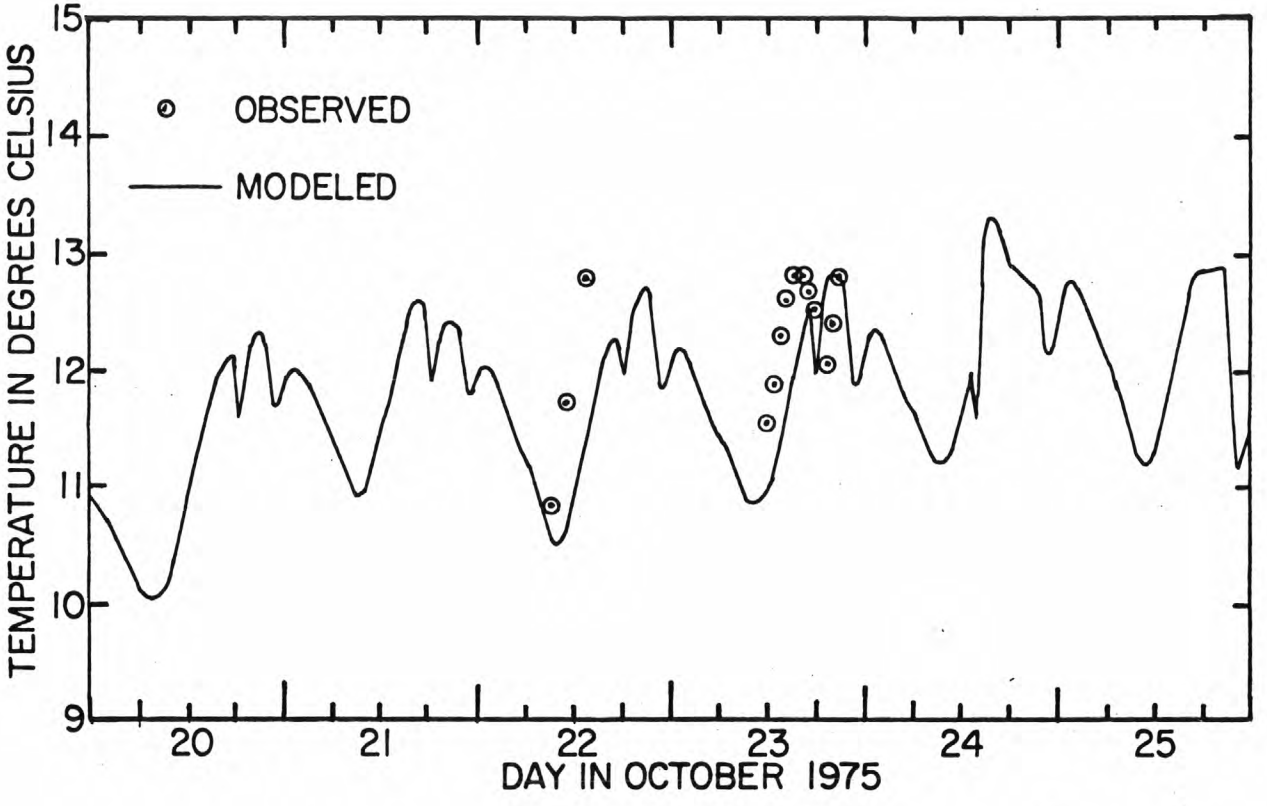

Figure 30.--Comparison of the observed and modeled temperatures at the Littles Ferry Bridge on the Chattahoochee River during the October 1975 verification period.

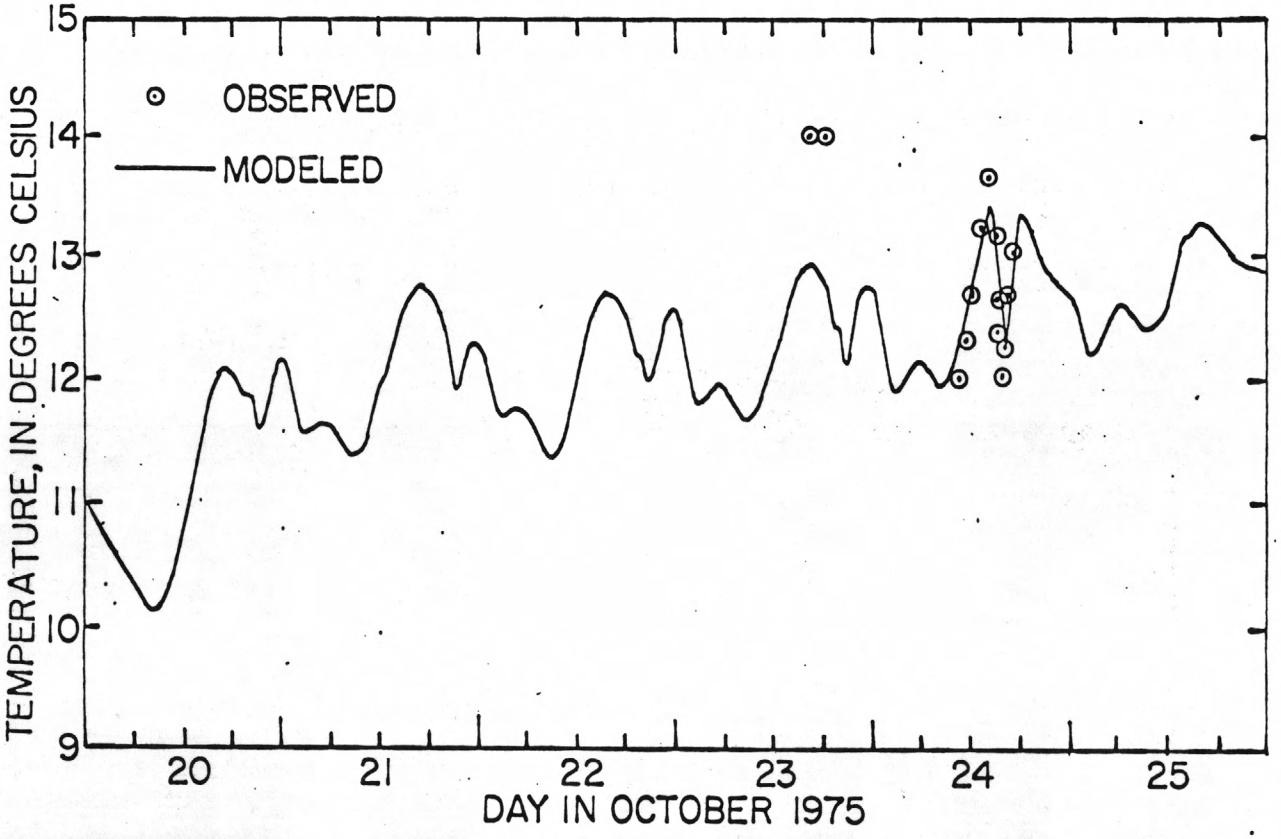

Figure 31.--Comparison of the observed and modeled temperatures at the Highway 120 Bridge on the Chattahoochee River during the October 1975 verification period.

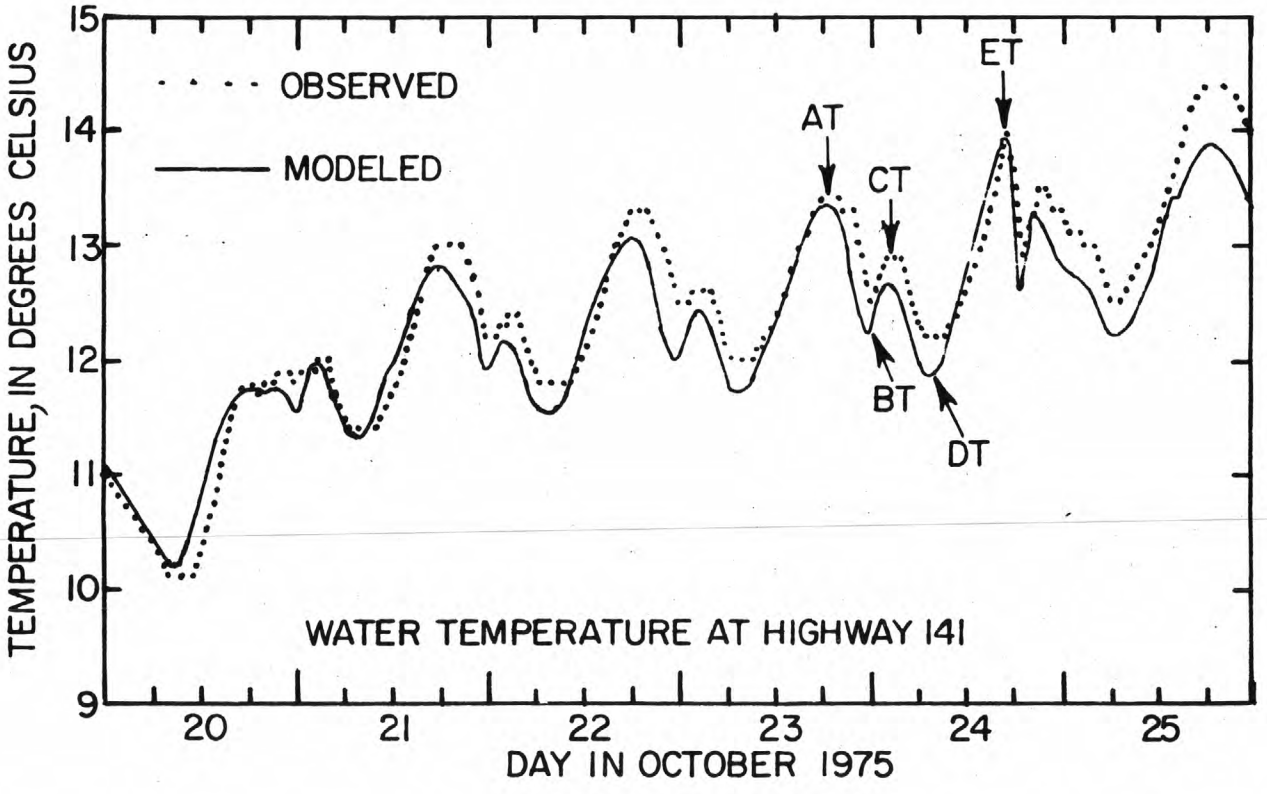

Figure 32.--Comparison of the observed and modeled temperatures at the Highway 141 Bridge on the Chattahoochee River during the October 1975 verification period. The symbols represent the time of arrival of specific water particles.

The measured and predicted temperatures for the spring verification are shown in figures 33, 34, 35, 36, and 37. It can be seen from figure 33 that the 113 m^3/s discharge pulse on March 23 increased the temperature by almost 2 degrees. The shapes of the modeled and observed temperature curves at Highway 20 (fig. 34) are very similar; however, the modeled temperatures appear to be about 1.5°C higher than the observed values. It is difficult to believe the model could be off this much since very little surface exchange can take place during the short traveltime between Buford Dam and Highway 20. This is particularly true during the high flow pulses around noon on March 22 and 23. At Littles Ferry Bridge the agreement between the modeled and observed temperatures is very good (fig. 35). The poorest agreement occurs between noon and 2100 hours on March 21. No meteorologic data were available before 1100 hours on this day, and a light rain had occurred during the night. In order to account for the heat input of the nontributary inflow caused by the rain, 150 $Watts/m^2$ was added to the incoming radiation term for the first 9 hours of March 21. At Highway 120 (fig. 36), the poorest fit occurred between 1500 and midnight on March 21 or about 3 hours later than at Littles Ferry. The errors at Highway 120 are also believed to be the result of the rainfall and lack of meteorologic data during the first part of March 21. Finally at Highway 141 (fig. 37) the region of poorest fit occurred between 1800 hours on March 21 and 0300 hours on March 22, again about 3 hours later than at Highway 120. It appears that the combination of rainfall and lack of data created an area of poor fit which shows up at each measurement point as the water is convected through the system. The RMS difference between the observed and computed temperatures at the Highway 141 Bridge was 0.20°C, and the mean difference was +0.09°C. These results are considered to be very good. Temperature occurring before 2315 hours on March 21 were not considered in these statistics because the time required for a particle to traverse the system was 23.24 hours on this day.

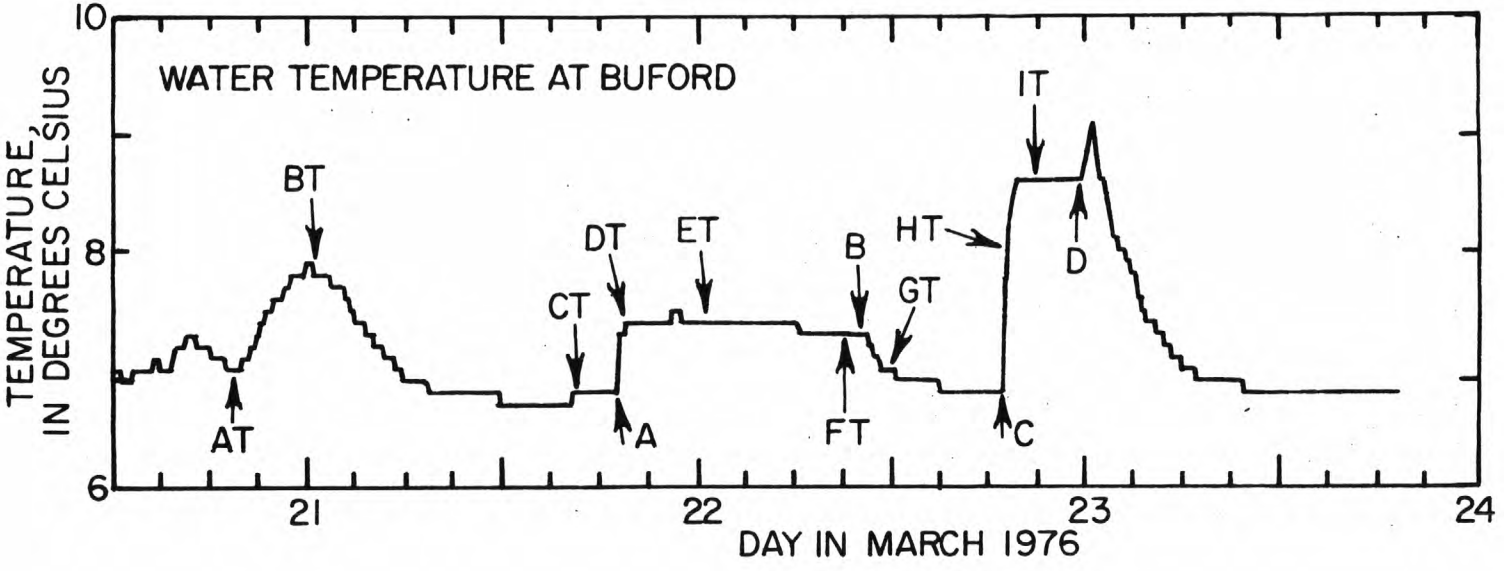

Figure 33.--Observed temperature in the Chattahoochee River below Buford Dam during the March 1976 verification period. The symbols represent the time of arrival of specific water particles.

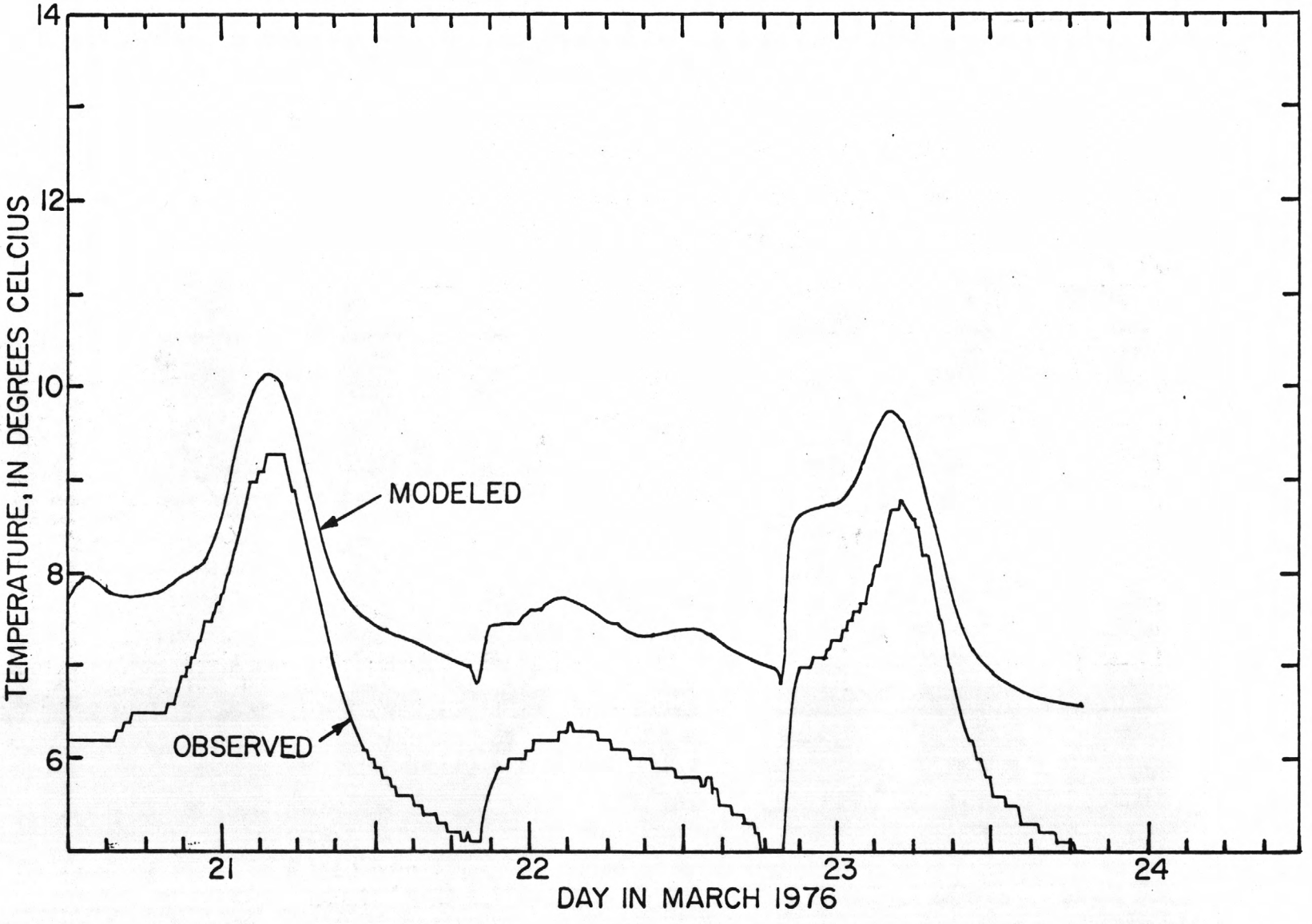

Figure 34.--Comparison of the observed and modeled temperatures at the Highway 20 Bridge on the Chattahoochee River during the March 1976 verification period.

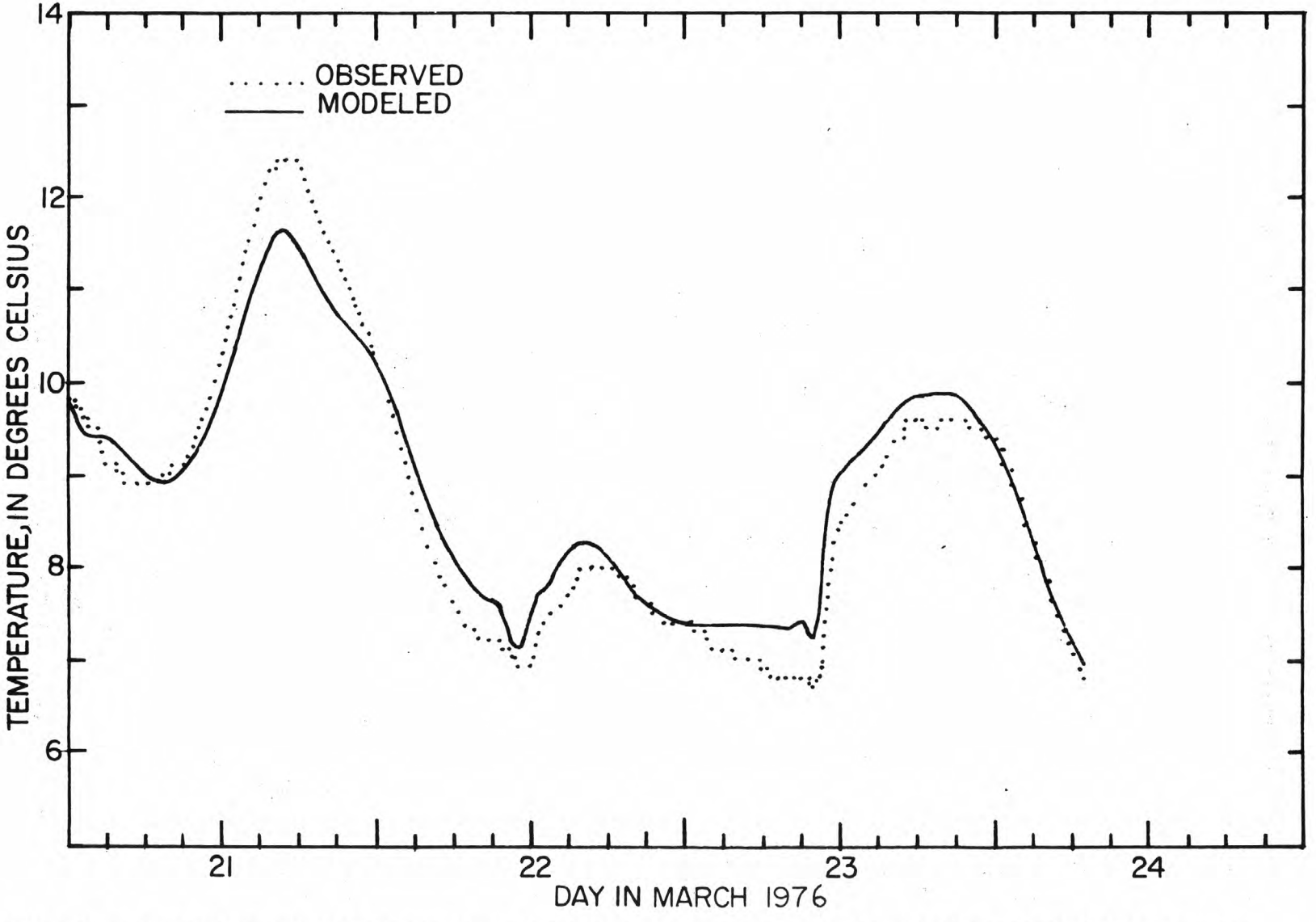

Figure 35.--Comparison of the observed and modeled temperatures at the Littles Ferry Bridge on the Chattahoochee River during the March 1976 verification period.

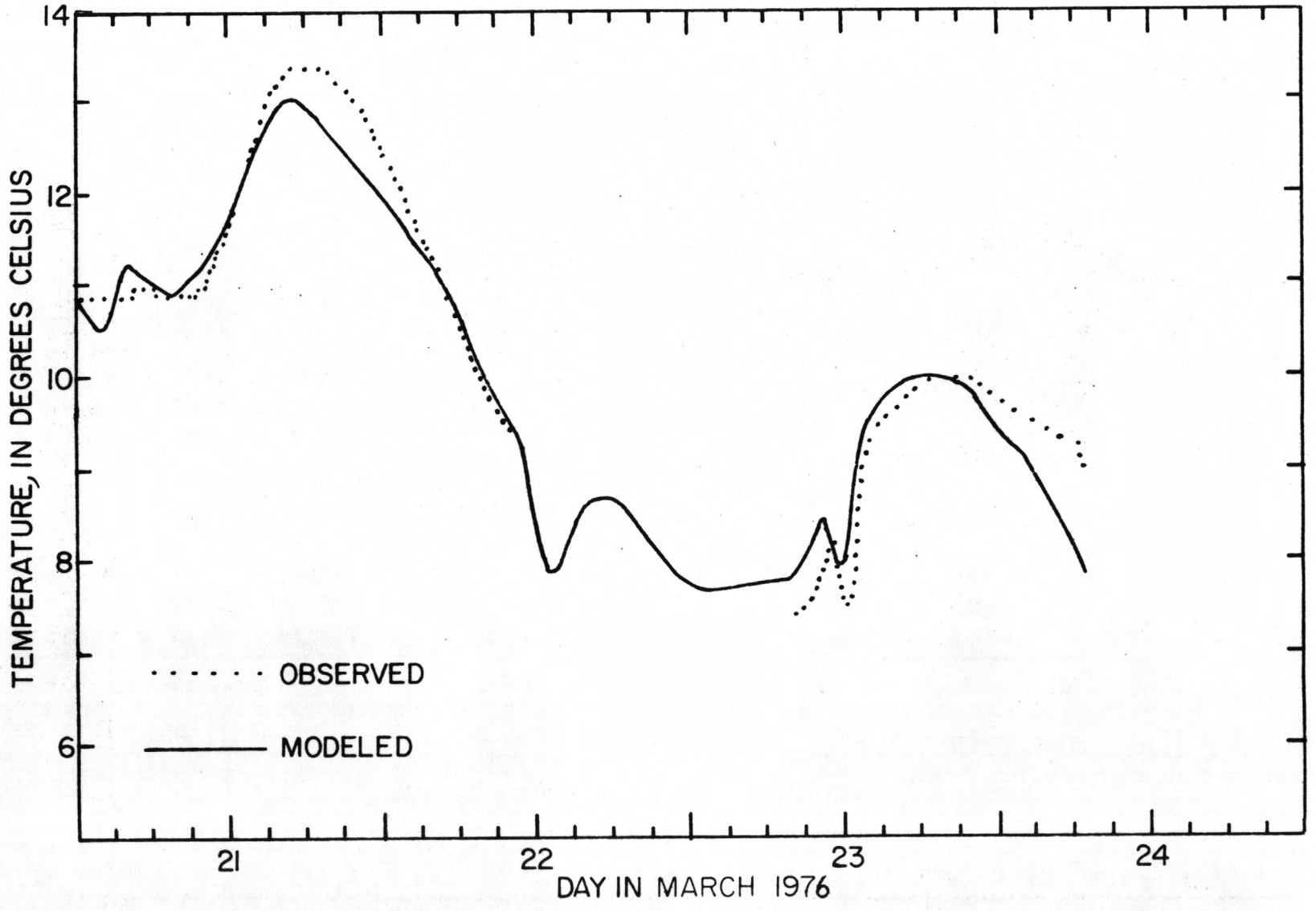

Figure 36.--Comparison of the observed and modeled temperatures at the Highway 120 Bridge on the Chattahoochee River during the March 1976 verification period.

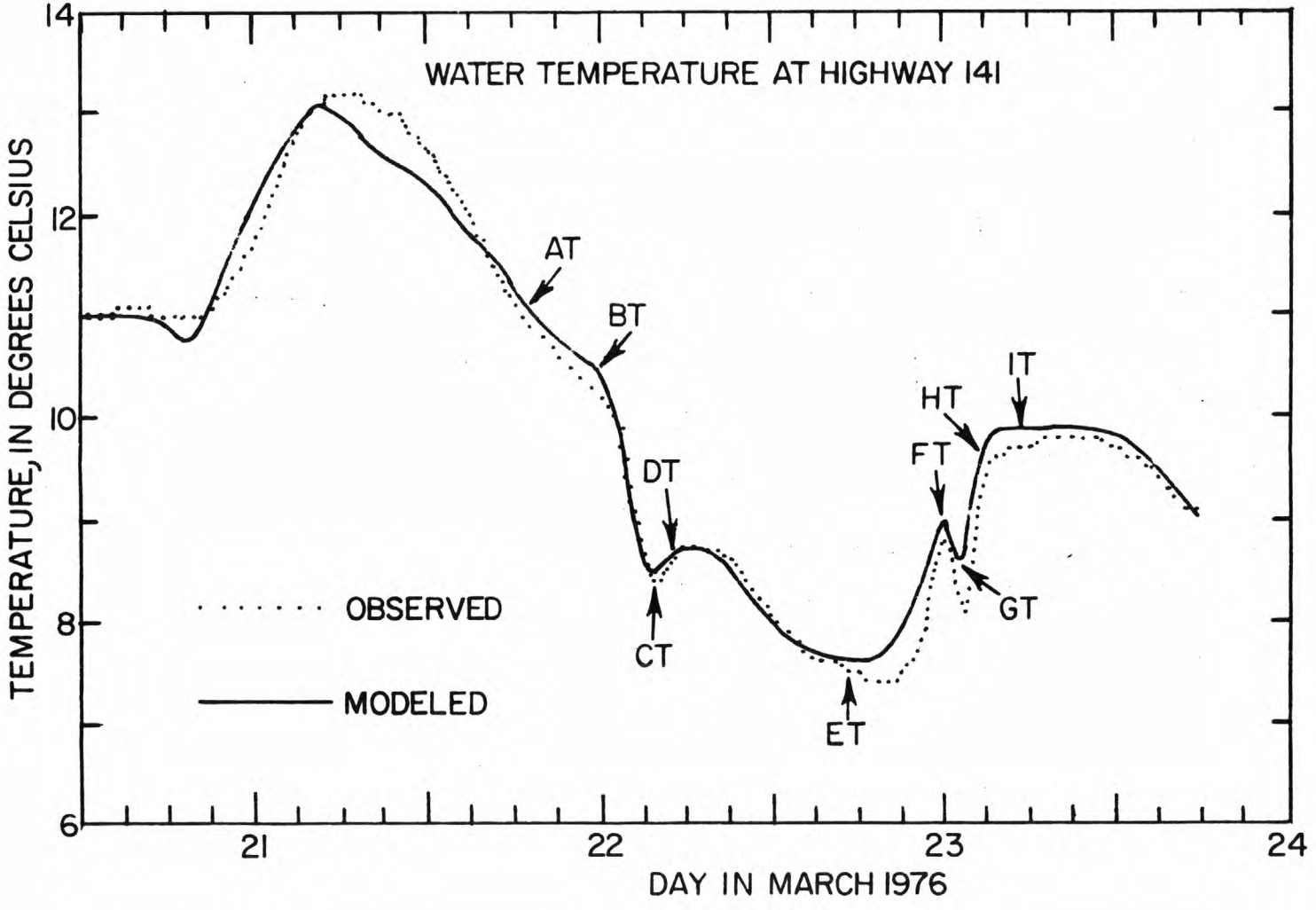

Figure 37.--Comparison of the observed and modeled temperatures at the Highway 141 Bridge on the Chattahoochee River during the March 1976 verification period. The symbols represent the time of arrival of specific water particles.

DISCUSSION OF RESULTS

Flow Dynamics

The results of the flow model may be summarized as follows. A linear, implicit finite-difference flow model was used to simulate the depth, velocity, and discharge at 48 points in a 27.9-km reach of the Chattahoochee River under highly unsteady flow conditions. The reach is fairly uniform in cross section but varies considerably in local slope, (fig. 8). Simulated results can be compared at all points for a single, steady low-flow condition and at 4 points during unsteady conditions. Generally the results of the flow model are considered to be very good. Visually the comparison of the measured and modeled stages (figs. 9 and 15) are excellent. In all cases the error in the modeled stage for the March calibration run was less than 0.16 m while for flows of less than 100 m^3/s the error remained less than 0.1 m.

The comparison of the modeled and observed discharge values (figs. 10-13), while not as good as the stage comparison, was considered good. Two types of differences between the observed and modeled discharges were apparent. These were differences in phasing and in peak discharge values. Differences in the peak discharge for the small pulse of March 22 were less than 5 percent, an excellent agreement, but differences as large as 20 percent occurred for the peak discharge of the large pulse of March 23. The percentage error generally seemed to increase in the downstream direction. Although the accuracy of the observed peak discharges, obtained under such highly unsteady conditions, may not be very good, they are consistently higher than the peak discharge computed by the model. Thus, it is apparent that the model underestimated the peak discharge.

The second type of difference appears in the timing, or phasing, of the discharge curves. The phasing difference appears to increase systematically in the downstream direction and the worst case appears to occur at the Highway 141 Bridge (fig. 13). Here the modeled and observed discharges agree very well on the rising limb of the hydrograph. The discharge computed by use of the rating table appears to be inadequate on the rising limb of the hydrograph. During a rising stage the hydraulic gradient in a river will be larger than under the steady state conditions upon which a rating curve is based, thus, the velocity and discharge will be larger than the rating table value. On the recession the reverse effect should occur although perhaps to a lesser extent. The observed and rating table values agree very closely on the recessions of figure 13, but the modeled values are much lower. The general phenomena discussed here is commonly known as a looped rating curve. The reasons this was not significant at the upstream end of the study reach has been discussed earlier under boundary conditions. The discharge results for the March run are plotted in figures 38 through 41 for the bridges at Highways 20, Littles Ferry, 120, and 141, respectively, in a form which demonstrates the looped ratings. Except at Highway 120, the model consistently predicts a more pronounced loop than was observed. Both the model and the observations indicate that the stage-discharge loop is affected by the magnitude of the pulse. The results shown in figures 38 through 41 probably present the model results in the worst possible light because for the modeled and observed curves to match, the model must simultaneously reproduce the correct stage, discharge, and rate of change of discharge with stage. The results at Littles Ferry and Highway 120 Bridges are considered very good. The model does appear to have some systematic

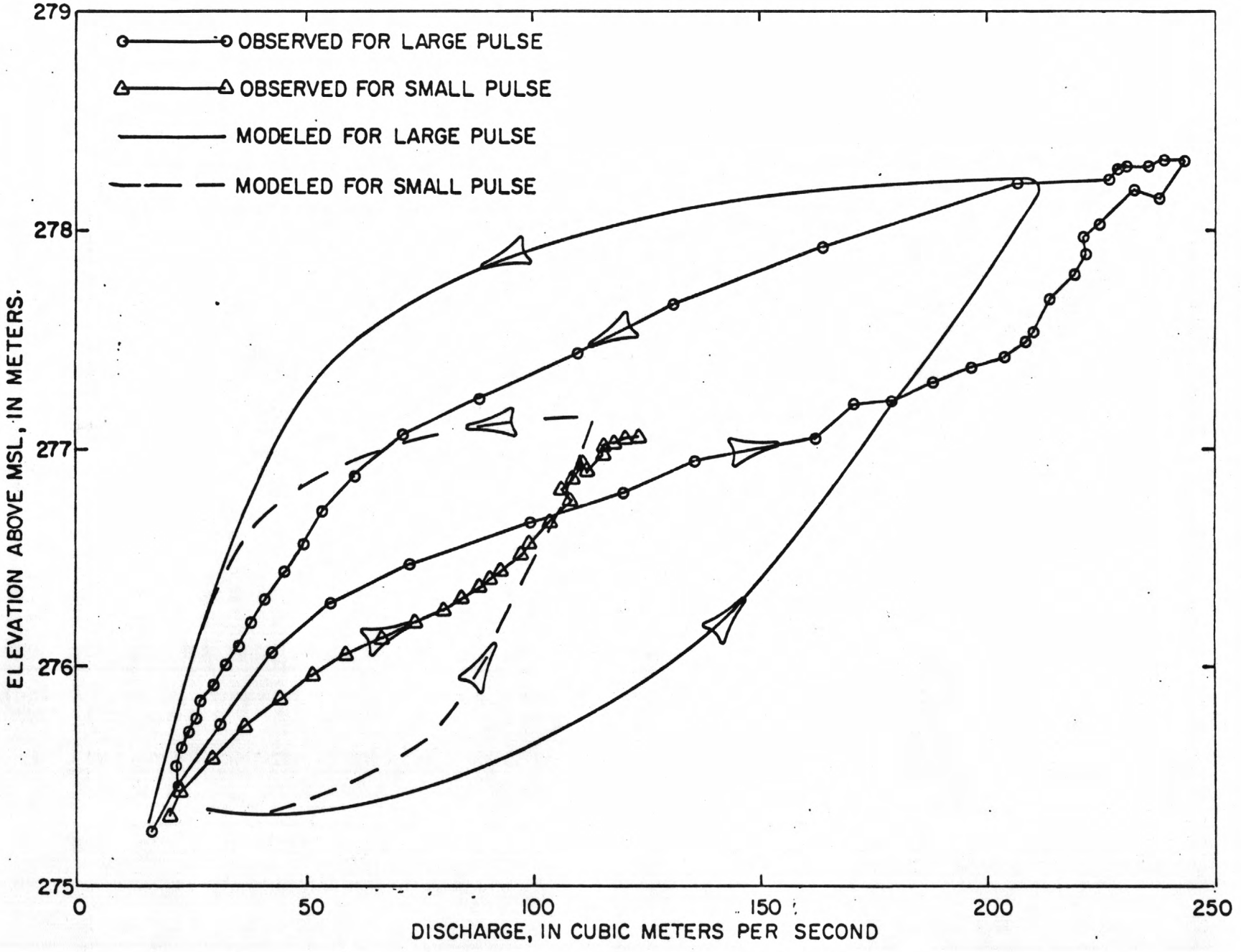

Figure 38.--Loop rating curves for the Chattahoochee River at the Highway 20 Bridge during the March 1976 calibration.

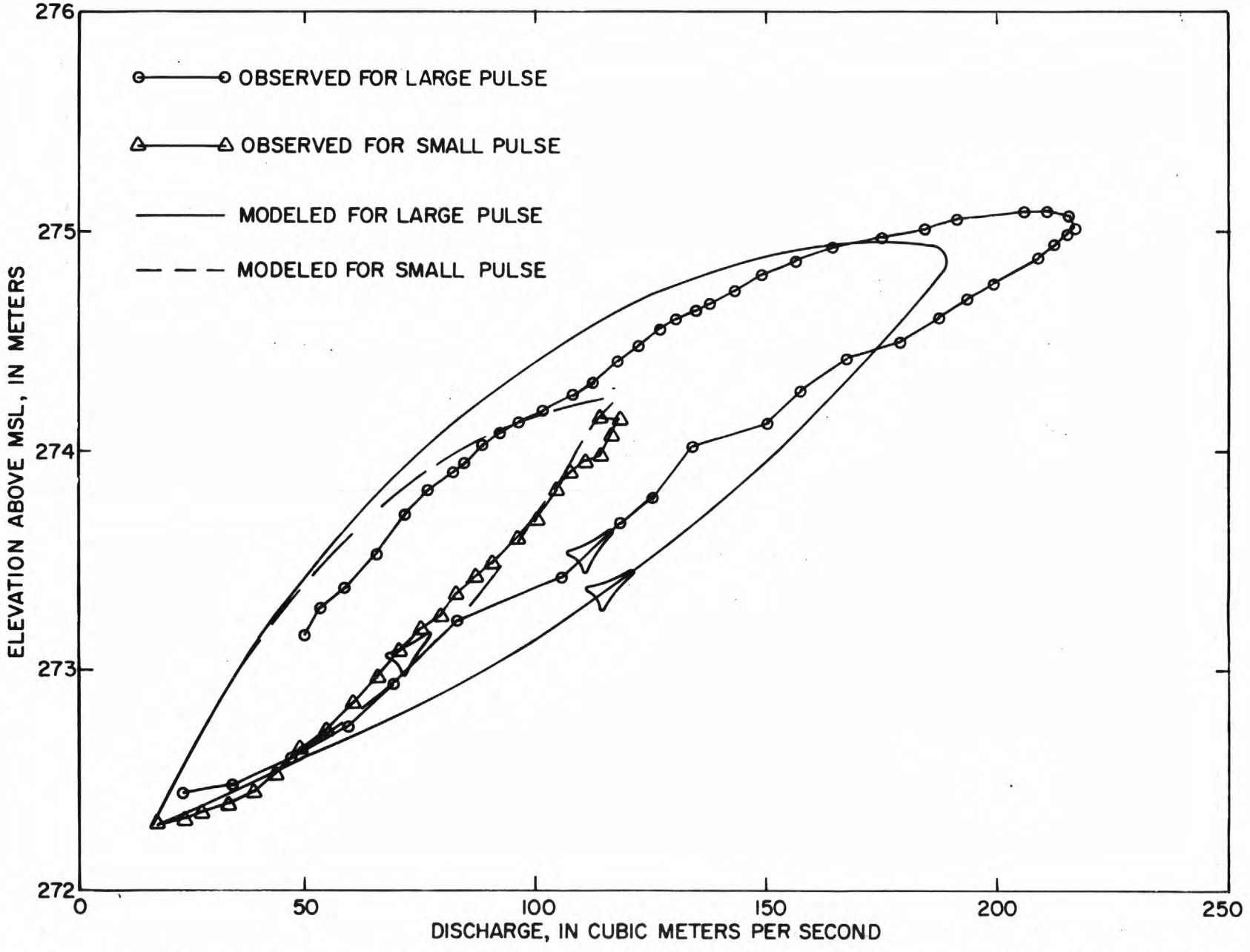

Figure 39.--Loop rating curves for the Chattahoochee River at the Littles Ferry Bridge during the March 1976 calibration.

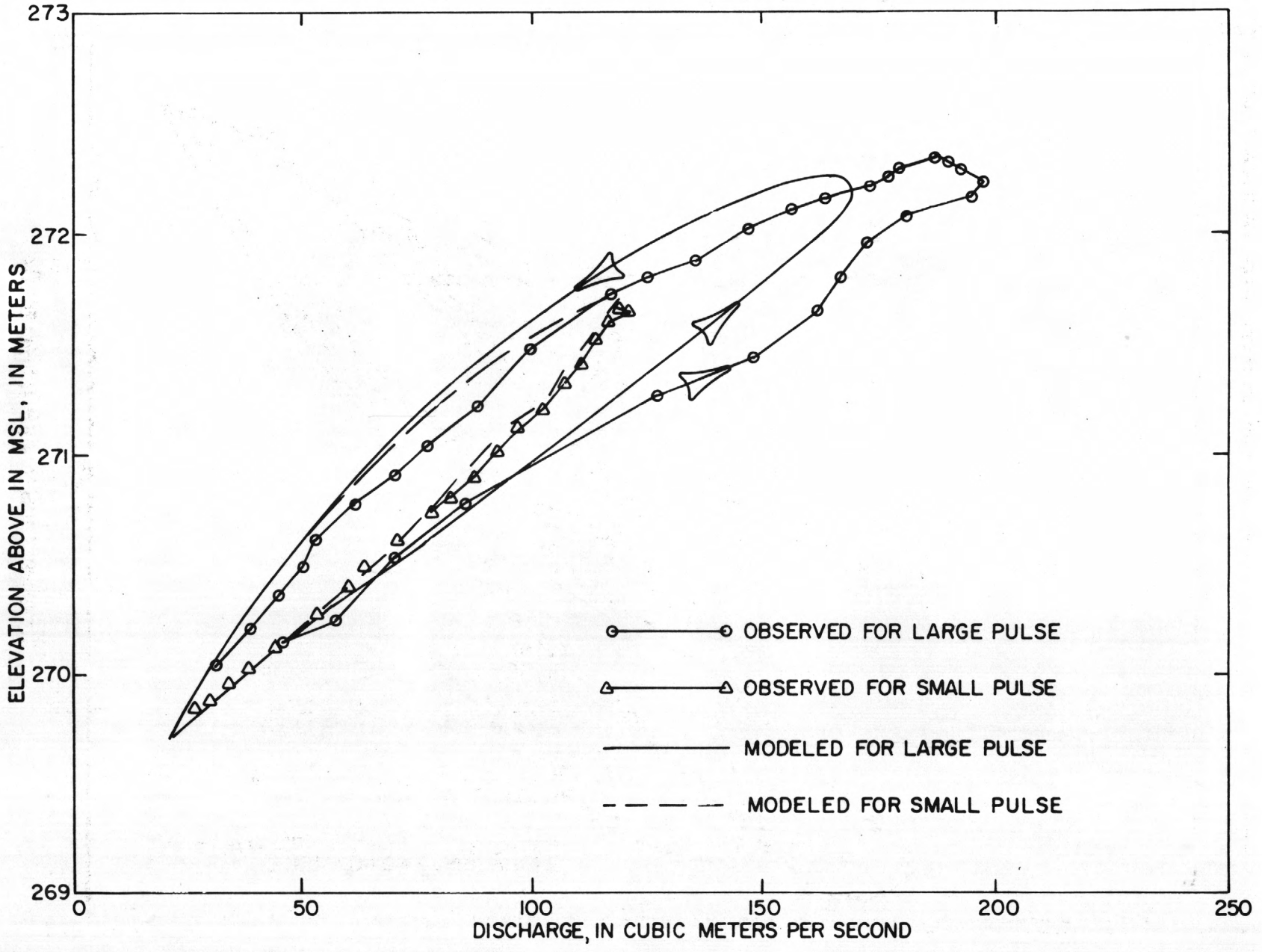

Figure 40.--Loop rating curves for the Chattahoochee River at the Highway 120 Bridge during the March 1976 calibration.

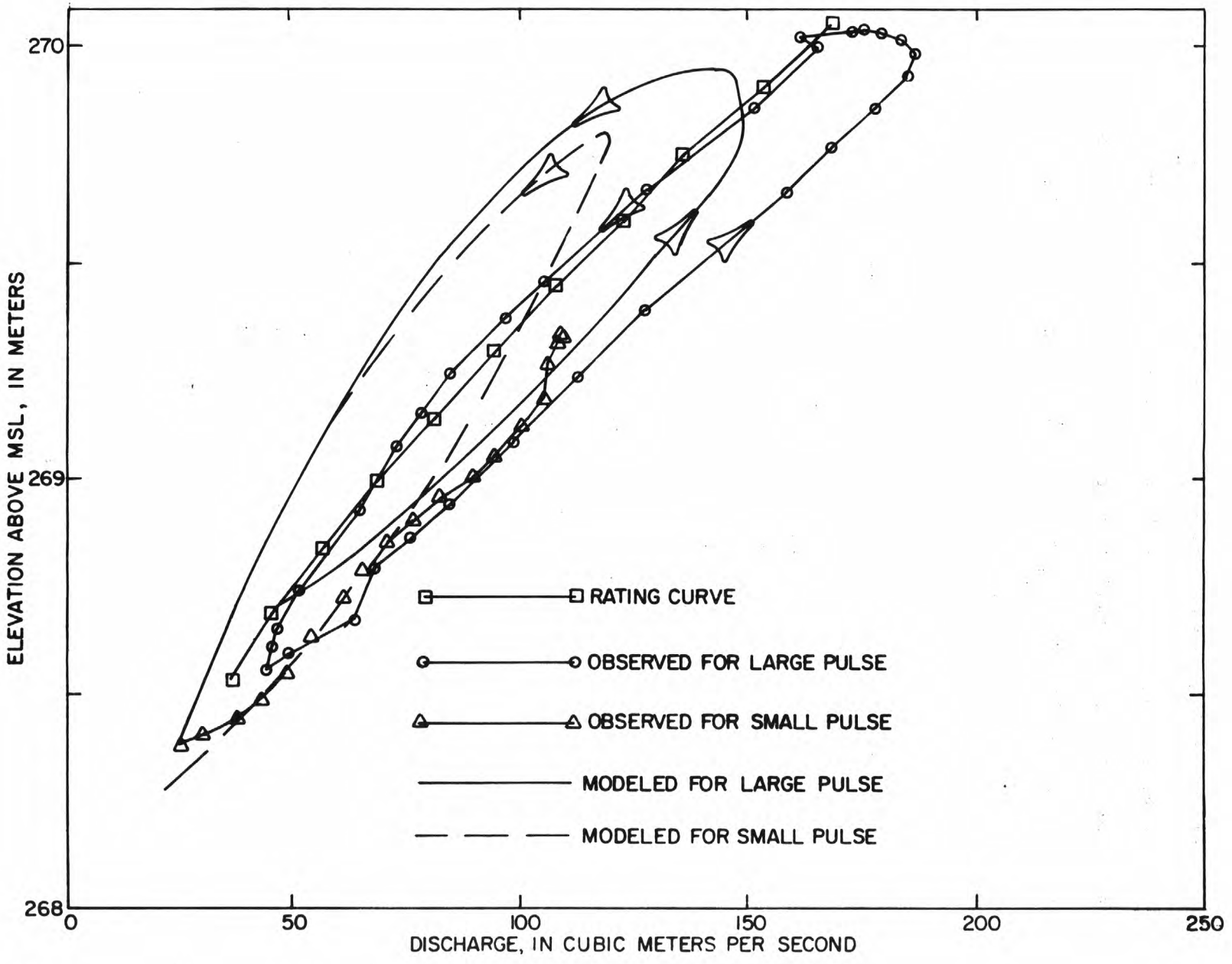

Figure 41.--Loop rating curves for the Chattahoochee River at the Highway 141 Bridge during the March 1976 calibration.

bias at Highway 141 which may be caused by some bias in the assumed channel characteristics downstream of the bridge, that is, the self-setting downstream boundary condition. The channel characteristics in the vicinity of the Highway 20 Bridge were believed to be less accurate than the values for other parts of the reach.

The major contribution of this study was to apply existing solution techniques, with certain minor improvements, to a very comprehensive data set in order to verify the existing technology of flow modeling. There are two questions that should be asked at this point. What can be done to improve the mathematical model, and what additions to the data base or calibration procedures could be incorporated to improve the results?

The first question is difficult to answer. In general, the linear-implicit technique is an entirely satisfactory method for routing flow. It is not perfect, however, and an uninitiated user will have problems. These problems will probably be related to boundary or initial conditions at first and later to schematization problems.

Contrary to the literature, the linear-implicit scheme is not unconditionally stable. Very good initial conditions are required, at least for models configured with nonuniform grid spacing and nonprismatic cross sections. For the Chattahoochee, a compatible backwater program which computed the initial velocities and depths was required. The use of the term compatible is intentional. The friction slope terms in the backwater program must be averaged in the same manner as in the dynamic model. To reduce programming difficulties in the dynamic model, a linear average was used in both the dynamic and backwater programs.

Instabilities can also result from boundary conditions. An unrealistic rating curve or a self-setting boundary condition based on discharge only can produce oscillations or waves at the upstream end. Each stream will have its own peculiarities, and experience is the only way to discover them.

Schematization problems not related to boundary conditions usually take the form of an anomalous grid point depth. For instance, the flow may proceed smoothly down a uniform slope through uniform sections and suddenly double in depth or produce some peculiar water-surface irregularity. The problem is not an instability, it just doesn't appear realistic. In the Chattahoochee model, two such places were encountered. The first occurred at river-kilometer 551.26 (fig. 8), and the other was at river-kilometer 541.24. These problems can usually be alleviated by adding an interpolated section to shorten the distance step. Apparently the friction and bed slopes are too different and extrapolating these slopes between grids give unrealistic conditions.

A compatible backwater program is very valuable for spotting and correcting problem areas. Experience with the Chattahoochee model indicates that any change in stage at a given steady discharge accomplished by changing the roughness coefficients or other parameters in the backwater program will produce an equal change in stage under unsteady discharge in the flow model. The backwater calculations can be performed quickly on a desk top calculator, so many trials can be evaluated quickly. Efforts which have gone into improving backwater programs, such as expansion loss coefficients, should now be incorporated into unsteady flow models.

Another area deserving further study is the method used to represent the cross-sectional shape. Aesthetic appeal is certainly important in some instances. The question can be raised as to whether equation 43 is an adequate representation of the cross-sectional shape, or should the actual measured shape be used for each section. Little research has been done on the question, and this study did not address the problem. It is the writers' opinion that computed results are not very sensitive to the actual cross-sectional shape as long as the correct areas are given as a function of stage.

In summary three areas should be investigated in order to improve the mathematical model. First, more needs to be known about the best way to handle boundary and initial conditions. Second, much of the existing knowledge used in sophisticated backwater programs should be incorporated into dynamic models. Finally, the question of how to best represent the cross-sectional shape should be studied.

The collection of necessary and sufficient field data as well as the intelligent use of these data appears to be more critical in the development of an accurate flow model than the selection of the particular solution technique. It was found that adequate cross-sectional information could be obtained quickly at high flow by use of a sonic-depth sounder and a boat. Top widths at the time of the traverse were obtained by stadia. Vertical control, between the bridges, while desirable, was not critical provided a depth profile at one steady flow condition is available. The depth profile, obtained at steady low flow was perhaps the most useful set of data available in calibrating the flow model. Furthermore these data were fairly easy to obtain. It would have been helpful to check the top widths when this profile was taken, however, so that cross-sectional areas could have been checked more closely.

Optimization is currently popular in the model field. Optimization in this case was obtained on a trial and error basis wherein the modeler selected each new trial on the basis of the results of his previous trials and engineering judgment. It would appear that a formalized optimization procedure which incorporates all factors that were considered in calibrating the Chattahoochee flow model would be extremely difficult to design. Furthermore, if all these factors are not considered, there exists a very real possibility that the resulting model would be far from realistic.

Transport

Many dye studies have been conducted in rivers of the United States. Virtually all of these, however, were performed as nearly as possible under conditions of steady flow and using an instantaneous slug injection. From these studies the steady flow traveltime and dispersion coefficients are inferred. Using the continuous injection procedure, the traveltime and dispersion characteristics can also be inferred from the timing and shape of the first rise in concentration under steady flow conditions. In addition, the response of the system to unsteady flow can also be determined. The continuous injection focuses the concentration changes in the regions of most interest, that is, in the regions where the flow is unsteady. The results in figures 19 and 20 or 21 and 22 indicate that the transport response of the system is being reproduced very well by either of the transport models.

Any differences in the modeled results in figures 19 and 21 or figures 20 and 22 are due to differences in the solution routines for the conservative and nonconservative forms of the transport equation. Although several significant differences existed in the solution schemes, there appears to be little difference in the results. As with the flow model, it appears that the key to successful modeling results is good data and calibration techniques and not the use of highly sophisticated solution schemes.

The anomalous rise in concentration on the leading edge of the power wave, shown in figures 19 and 21, is probably the most interesting result to be obtained from the dye study. The plateau concentration of 11 µg/L at Littles Ferry, which occurred between about 0600 and 1000 hours on March 22, is the value which would be computed by dividing the flow rate of dye by the river discharge at Littles Ferry. The observed peak concentration, which occurred about 1100 hours, on the other hand, is larger than the value which would be predicted by dividing the dye flow rate by the low flow discharge from Buford Dam. The cause of this anomaly served as the subject of many discussions and full agreement has not been reached. A plausable cause, however, appears to be the interaction of tributary inflow with the river stage. Stage variations in the Chattahoochee River are large and rapid, while considerable storage volume exists in the tributary channels (fig. 4). In fact, backflow up the tributaries was observed in the field during times of rapidly increasing stage. The reduced dilution which occurs as the water wave passes a tributary and reduces or stops the tributary inflow would certainly appear to be at least a partial explanation of the anomaly. Assuming complete mixing in the cross section, however, this phenomena should not raise the peak above 12.7 µg/L. Some of the anomaly may be due to inhibited transverse mixing which perhaps occurs on the leading edge of the power wave.

It can be noted that no negative anomaly occurs when the effect of the flow reduction passes Little Ferry bridge at about 0800 and 2200 hours on March 23. However, the effect of the tributaries at high flow would be expected to be much less. Furthermore, the water stored in the tributaries before the flow reduction probably contains about as much dye as the river water.

The flow and transport models were run for one hypothetical case in which the tributary inflow was set equal to zero, but the discharge at Buford Dam was the same as used in figures 18 through 22. An interesting, perhaps disturbing, result was that the anomaly, although reduced in size, remained.

Temperature

Both the October and the March runs are considered to be verifications of the temperature model because no calibration was involved. All physical parameters and coefficients were determined by deduction on the basis of other studies. In order to assess the sensitivity of the results to these determinations, however, the parameters were arbitrarily changed one at a time and the effect on the predicted temperatures determined. In the interest of economy and simplicity, the sensitivity analyses were restricted to the March data. The sensitivity to bed conduction, bank shading, and the two coefficients in the wind function were checked. In addition, the sensitivity of the computed temperatures to the measured values of top width and atmospheric radiation were determined. These two quantities were considered to be of somewhat questionable accuracy.

Rerunning the model assuming no heat transfer at the bed (no bed conduction) decreased the mean error in the computed temperature by 0.006°C, yet increased the RMS error by 7 percent. Visual changes in the predicted temperatures were subtle, but generally, bed conduction acts as a slight damper to the computed temperatures. The October data were also rerun with no bed conduction and again the RMS error increased even though the mean error decreased. Clearly, inclusion of the bed conduction term improved the model results.

The effect of shading by the banks and trees was thought to be a weakness in the temperature model. Estimates of the effective barrier heights were rather crude, so two cases were rerun. The first case eliminated shading entirely, and the second case reduced the effective barrier height by 20 percent. Completely eliminating the shading caused more damping of temperature swings at times and less at other times. It increased the mean error by 0.269°C and the RMS error by 86 percent. In general the changes were hard to characterize except that the computed temperatures with shading looked more like the measured values than did the temperatures computed without shading. Assuming that there was a tendency to overestimate the tree height in the field, the effective barrier heights were reduced 20 percent. This change increased the mean error by 0.073°C and the RMS error by 11 percent. The visual effect of this change was small.

The wind function (eq. 20) was developed from a thermal balance of the San Diego aqueduct which is in the arid region of southern California. Because of the sheltering due to trees and the humid climate in northern Georgia, the applicability of this wind function to the Chattahoochee River could be questioned. The constant term, 3.01, and the mass transfer coefficient, 1.13, were varied independently. Reducing the mass transfer coefficient by 25 percent increased the mean error by 0.053°C and the RMS error by 4 percent. Reducing the constant term by 50 percent increased the mean error by 0.118°C and the RMS error by 29 percent. Neither of these changes affected the visual fit significantly.

The cross-sectional area and flow velocity were believed to be fairly accurate because of the accuracy in timing of the transport model. The top width measurements, however, were subject to some doubt because of the dense brush and fallen trees along the banks (see fig. 2). Without changing the flow fields in terms of velocity and area, the top widths were increased by 10 percent and the model rerun. This change, which of course decreased the hydraulic depth by 10 percent, increased the mean error in the computed temperature by 0.055°C and the RMS error by 8 percent.

Reducing the atmospheric radiation by 10 percent lowered the mean temperature at the Highway 141 Bridge by 0.24°C and increased the RMS error by 42 percent.

In summary adjusting each coefficient or questionable measurement by an amount judged to be roughly equal to its maximum probable error always resulted in a poorer fit (in terms of the RMS) of the measured temperatures. Nevertheless, the fit could probably have been improved by adjusting more than one of the parameters simultaneously. For example, the mean error could have been forced to zero in any of several ways, by reducing the atmospheric radiation by 3 percent, by decreasing the top width by 13 percent, by increasing the effective barrier height by 20 percent, or by some combination of these. Some combination of adjustments could undoubtedly have been found which would have reduced the RMS error significantly. Furthermore, none of the adjustments would be large in comparison with the confidence limits of the original estimate or measurement. For example, a 3 percent error in the atmospheric radiation term seems to be reasonable when it is remembered that the measured atmospheric term represents the average output of two pyrgeometers which differed by 19 percent in March and were located about 30 km from the study reach. No juggling of the terms to improve the fit was attempted, however.

Within the limitations discussed above, the temperature model provides a powerful tool for determining the effect of hydropulsations on the temperature regime of the Chattahoochee. The effect on the temperature at the upstream end of the reach will be discussed first, and then the cause of some specific anomalies at the downstream end of the reach will be investigated. These investigations will also provide some insight into the effects of hydropulsations on other river-quality parameters.

Because of the simpler flow release pattern in March, these data will be discussed first. The data presented in figure 33 indicate that the Buford outlet temperature, during times of low flow, was constant at about 7°C. The small temperature rise, of about 0.25°C, occurring between 0300 and 0800 hours on March 21 is probably due to heating from inflow of the rainfall which occurred during the night. The solar heating, which occurred between 0900 and 1800 hours is obvious. It is perhaps surprising that for low flow near noon almost a 1°C temperature rise occurred over the short distance (0.48 km) between the dam and the recorder.

At 0700 hours on March 22 (point A in fig. 33), the turbines were started to provide the first flow pulse of 110 m^3/s. The river temperature increased by 0.6°C almost immediately. At 2200 hours on March 22 the flow was quickly reduced to 15.4 m^3/s (point B in fig. 33) and held constant until the start of the second pulse of 220 m^3/s which occurred at 0700 hours on March 23 (point C). At 1200 hours on March 23, point D, the flow was quickly returned to 15.4 m^3/s and remained constant at this value for the remainder of the study. The small amount of heating after 1200 hours on March 23 is probably due to solar radiation. A gradual decay in temperature occurs at the completion of each flow pulse. Considerable water is ponded between the dam and the temperature gage, and this gradual decay is probably the result of the rather slow flushing of this ponded water at low flow.

At high flow the traveltime and surface exchange between the dam and the temperature gage is negligible so the immediate temperature rises of 0.6°C and 1.8°C, respectively, for the small and large pulses indicate that the turbines withdraw mostly hypolimnion water at low flow but at least a mixture of hypolimnion and epilimnion water at high flow. The higher the flow the greater proportion of epilimnion water withdrawn. If any water-quality parameter has different values in the hypolimnion and epilimnion waters of the lake, the temporal variation of the parameter in the river could be easily predicted from the data in figure 33. At steady low flow, the river parameter will be close to the hypolimnion value, but with the starting of the turbines, the value will immediately shift toward the epilimnion value. The magnitude of the shift will be a function of the discharge. After the turbines are shut down, the river value will gradually shift back to the hypolimnion value.

During the October verification period, the upstream temperature distribution as well as the inflow hydrograph is much more complex. In addition, the first temperature measurements were at the Highway 20 Bridge, 4.2 km downstream of the dam. However, the steep gradient in this short reach (fig. 8) precludes much surface exchange, except at steady low flow. Consider October 22 which was a rather typical day. More specifically consider a water particle, which is labeled A in figure 29 and which passed the Highway 20 Bridge at 1000 hours. Since the traveltime for this water (from the upstream end of the model to Highway 20) was 2.75 hours, it had been released from the dam just before 0715 hours, and steady low flow had occurred during its entire passage (fig. 15). The model indicates that this particle cooled by only about 0.25°C during the passage, so the water released from the dam must have had a temperature of about 9.8°C during steady low flow.

The particle labeled B in figures 15 and 29 was released from the dam a little before 1240 hours and arrived at Highway 20 at 1520 hours, just after the turbines were started (fig. 15). The entry temperature of this particle would have been 9.8°C, therefore, and the 2.8°C temperature rise between points A and B in figure 29 resulted from surface exchange.

Between 1445 and 1500 hours on October 22, the power release at Buford began. Just before this power release started, the particle represented by point C in figures 15 and 29 entered the system with a temperature of about 9.8°C. It did not experience as much surface exchange as particle B, however, because the power pulse, which followed, flushed it through the system more rapidly than the particles which preceded or followed it. Its traveltime from the upstream end of the model was only 0.74 hours as compared to 2.75 hours for particles A and B or 1.01 hours for particle D. The reduction in temperature between points B and C, therefore, is the result of the flushing action of the power pulse.

The water particle presented by point D in figures 15 and 29 entered the system a little before 1700 hours which is about the time of the peak discharge in figure 15. Assuming that surface exchange was negligible for this particle because of the large depth, short traveltime, and the low solar radiation after 1700 hours, its entry temperature would have been 12.8°C. As in March the turbines appear to be withdrawing much more epilimnion water during high flow. A sudden temperature increase of 3°C (from 9.8 to 12.8°C) probably occurred at the upstream boundary when the turbines were started. Likewise, a sudden shift in values of other water-quality properties, which differ between the warm surface water and the cooler deep waters, probably occurs each time the turbines are started. Gerald Wiley, U.S. Army Corps of Engineers, (oral commun., 1977) has observed sudden shifts in the dissolved oxygen content of the discharge waters upon starting or stopping of the turbines at Buford.

Finally the particle of water labeled E left the dam a little before 2000 hours which corresponds to the second peak in discharge in figure 15. This water traversed the 3.7-km reach in 1.07 hours. The minimum temperature between points D and E in figure 29 undoubtedly is the result of a reduced release temperature during the reduced flow occurring at 1900 hours. The gradual flushing of the system after the flow shutdown is apparent in the gradual decay in temperature after point E just as in the March run.

In light of the above discussion, it is interesting to compare the observed temperatures at Highway 20 on October 24 to those of October 22. Meteorologic conditions were very similar on these two days so any temperature differences are primarily dependent on differences in flow scheduling. On Friday, October 24, the first power pulse began 3 hours earlier than on the 22d, figure 15. Moving the pulse ahead to 1200 hours increased the flow in the river before the solar heating had time to influence the river temperature. This eliminated the local minimum in temperature which occurred about 1600 hours (point C) on the other days.

In summary, hydropulsation had a significant effect on the water temperature below Buford Dam during both the March and October verification periods. At low flow the water temperature remained constant and low, but during the power releases, it almost immediately rose by between 0.6°C and 1.8°C in March and by as much as 3°C in October. Furthermore, the flushing action, illustrated by the temperature changes between points B and D in figure 29, helps accentuate these temperature changes and carry them downstream.

At the lower end of the reach, the effects of hydropulsation are still present although somewhat damped. As before, consider the March data first. Before 0700 hours on March 22 (point AT in fig. 37) a steady low flow of 15.4 m^3/s existed throughout the reach. The diurnal swing occurring before this time should, therefore, be fairly typical of steady low flow conditions. A light rain occurred during the early morning hours of March 21, and although its exact influence is not known, it is believed to have increased the river temperature by as much as 1.2°C at 0900 hours on March 21 and to have increased the peak temperature that day by as much as 0.6°C. The influence of this warming is not completely dissipated until 0700 hours on March 22. Nevertheless, water particles released from the dam just after midnight on March 21 with a temperature of 7.0°C gained 5.8°C during their 23.25-hour traveltime and arrived at Highway 141 at 2315 hours with a temperature of 12.8°C.

The thermal effect of the first power wave is first observed at Highway 141 about 1200 hours on March 22, just 5 hours after the turbines were started. The traveltime of the particles passing the 141 Bridge at 1200 hours on March 22 (labeled BT in figs. 9, 33, and 37) was reduced to 23.16 hours meaning that the flushing had just began.

For reference, the times at which particles left Buford Dam and arrived at Highway 141 are also indicated in figure 9 and figure 33.

Stream temperatures decreased rapidly after 1200 hours on March 22 due to the flushing action and obtained minimum values at 1630 hours (labeled CT in figs. 9, 33, and 37) on March 22. This water entered the reach only 11.5 hours earlier, at 0500 hours on March 22, 2 hours before the turbines were started (figs. 9 and 33). Even though this water was in the river during the entire heating part of the day (0500-1630 hours), the short traveltime and relatively large depth (1.7 m) during transit prevented much warming from surface exchange. The water-temperature increase during transit was 1.6°C, and surface exchange accounted for only 1.0°C of this change. The 0.6°C occurred due to mixing with the warm water which was both upstream and downstream of the slug. Flushing action decreased the water temperature at Highway 141 by 1.9°C in 4.5 hours.

The water particles that traversed the reach most rapidly (9.75 hours) passed the Highway 141 Bridge at 1730 hours (DT in figs. 9, 33, and 37) on March 22. This water entered the system at 0745 hours, 45 minutes after the turbines were started, with a temperature of 7.4°C. The warming from CT to DT in figure 37 is the result of the arrival of the warm epilimnion water withdrawn by the turbines at high flow. The epilimnion water warmed only 1.2°C during transit, because of the shorter traveltime and higher initial temperature, compared to a warming of 1.6°C for the hypolimnion water represented by CT.

Some warming occurred even at night indicating the natural river temperature is higher than the release temperature, even at high flow. Consider the water passing Highway 141 at 0600 hours on March 23 (labeled ET in figs. 9, 33, and 37). This water entered the system at 1845 hours on March 22 with a temperature of 7.3°C (fig. 33). Even though it traversed the system during the cool part of the night, it warmed by 0.3°C during the transit.

The warming of the river between points ET and FT in figure 37 at Highway 141 is caused by natural heating due to surface exchange and longer transit times due to low flow. The water particles represented by point FT had the longest traveltime of any water to traverse the system between the two flow pulses (15.75 hours). This water entered the system, during the high flow, on March 22 at 2130 hours (figs. 9 and 33) with nearly the same temperature as the water represented by ET, but it absorbed the morning solar radiation.

The drop in temperature from point FT to GT in figure 37 is partly due to flushing action, but it is mainly due to the reduction in the upstream temperature which occurred during the low flow between power pulses. The flushing action on March 23 had little effect on the temperature because the river was already cold, whereas, it had been warm on March 22 when the flushing action began. The traveltime of the water labeled GT was 14.0 hours indicating it entered the system at midnight with a temperature of 7.0°C, figure 33.

The water particles with shortest traveltime on March 23 (labeled HT) rode the rising stage like the particles labeled DT on March 22. This water entered the system at 0730 hours with a temperature of 8.0°C.

Finally the water leaving the system at 1800 hours on March 23 (IT) traversed the reach at approximately a high steady flow of 225 m^3/s. This water experienced a traveltime of 8.9 hours, a depth of 2.75 m, and a temperature rise of 1.2°C. Most of the temperature rise was due to absorbed solar radiation.

The effects of hydropulsation during the October verification can be illustrated in the same manner. Consider the temperature variations observed to occur at Highway 141 between 1900 hours on October 23 and 2400 hours on October 24. The flow release schedule and meteorologic conditions were similar during most other days. As before the times for which the temperature are discussed are labeled in figures 15, 29, and 32. Consider first the water particles that passed the Highway 141 Bridge at 1900 hours on October 23. This water, labeled AT, passed the Highway 20 Bridge at midnight with a relatively high temperature of 11.6°C. It traversed the reach during relatively low and receding flow, figure 15, and was in the river during all of the daylight hours. The water temperature increased by about 1.8°C during its transit. Radiant exchange should have increased its temperature by 1.72°C, so evaporative cooling and other exchange processes nearly balanced one another.

Next consider the minimum temperature on October 23 which occurs at Highway 141 at about midnight, point BT. This water that left the dam just before the turbines were started was from the hypolimnion and had a low temperature of about 9.8°C. Furthermore, it was flushed through the system very quickly, and it entered the stream about sunset so surface exchange was also minimal. The model indicates that surface exchange accounted for only 0.1°C of the 1°C temperature rise actually measured. The remaining 0.9°C temperature rise was the result of dispersive mixing with the warm water ahead and behind it in the river. In summary, three factors combined to give the local temperature minimum at point BT in figure 32. These were, flushing, low initial temperature, and small surface exchange because of the nighttime passage.

The water passing Highway 141 at 0200 hours on October 24 is labeled CT in the figures. The traveltime of this water was only a little longer than that represented by BT (8.9 versus 8.0 hours), but it entered the system after the turbines were started (fig. 15) and therefore, at a higher temperature (fig. 29). The increase in temperature from BT to CT in figure 32 represents the arrival of the warmer epilimnion water being withdrawn at high flow. The net surface exchange for this water was less than 0.1°C and in fact, the total temperature change of the water as it traversed the reach was less than 0.1°C.

The minimum temperature at Highway 141 on October 24 occurred at 0715 hours and is labeled DT in figures 15, 29, and 32. This water entered the reach at 2000 hours on March 23 between the high flow pulses (fig. 15) with a low temperature of 11.4°C (fig. 29). Because of nighttime passage and relatively rapid transit speed, little surface exchange occurred. Most of the 0.5°C temperature rise of the water was the result of dispersive mixing with the warm water ahead of and immediately behind it in the river.

Meteorologic conditions on October 24 were similar to those of the other days, however, the flow release was started about 3 hours earlier. This change in the flow schedule had a significant effect on the temperature of the river. Consider the maximum temperature at Highway 141 on October 24, point ET. The water represented by this point was released from Buford Dam about 2100 hours on October 23 (fig. 15) passing Highway 20 about midnight (fig. 29). This water started out warm (fig. 29), slowly traversed the reach under low-flow condition (fig. 15), and was in the river during the entire warm part of the day. As a result it absorbed enough radiation to warm it by 2.10°C while evaporative cooling lowered its temperature by 0.3°C. It is interesting that the temperature minimum which occurs at Highway 20 between points AT and BT as well as the temperature maximum which occurs between DT and ET have been completely dissipated by the time the water reaches the Highway 141 Bridge.

By tracing the route of a few individual water particles through the river reach, the effects of hydropulsation on the thermal regime of the river have been illustrated. These effects are complicated, however, in that they depend on several factors such as the timing of the release in relation to the time of day and of earlier releases. Rapid temperature rises of as much as 3°C are common at the upper end of the reach. At the lower end of the reach, these effects are still significant although they are somewhat damped. Rapid temperature decreases caused by flushing are more likely at the lower end of the reach. By studying the traveltimes and flow release schedules, it is possible to predict the origin of the river water (epilimnic or hypolimnic) for any particular time. This could be important if water-quality parameters vary significantly between hypolimnetic and epilimnionic waters.

One way to view the effect of the reservoir on the river temperature is to consider an excess temperature, either positive or negative, as the difference between the observed water temperature and the temperature which would have occurred had the reservoir not been present. The question can then be ask: How fast does this excess temperature decay in the downstream direction?

To illustrate the rate of decay of a temperature perturbation downstream of the reservoir, the thermal model was rerun with all conditions identical to those in figures 32 and 37 except that the upstream temperature was increased by 1°C. The difference between the two predicted temperatures is then a direct measure of the percentage of the excess temperature (or effect of the reservoir) which has been dissipated within the reach. Figure 42 is a plot of the excess temperature remaining at Highway 141 for the March run. To facilitate analysis the letters AT through IT shown in the previous figures are also included. Under steady low flow conditions, before point BT, at least 65 percent of any thermal effect caused by Buford Dam should be dissipated by the time the water reaches the Highway 141 Bridge. At a steady flow of about 100 m^3/s, points DT to ET, only a little more than 10 percent of the perturbation is dissipated, and at a steady flow of about 200 m^3/s, points HT to IT, less than 10 percent of any excess heat would be dissipated by the time the water reaches Highway 141. The percentage of the excess heat to be dissipated within the reach is very dependent on the traveltime.

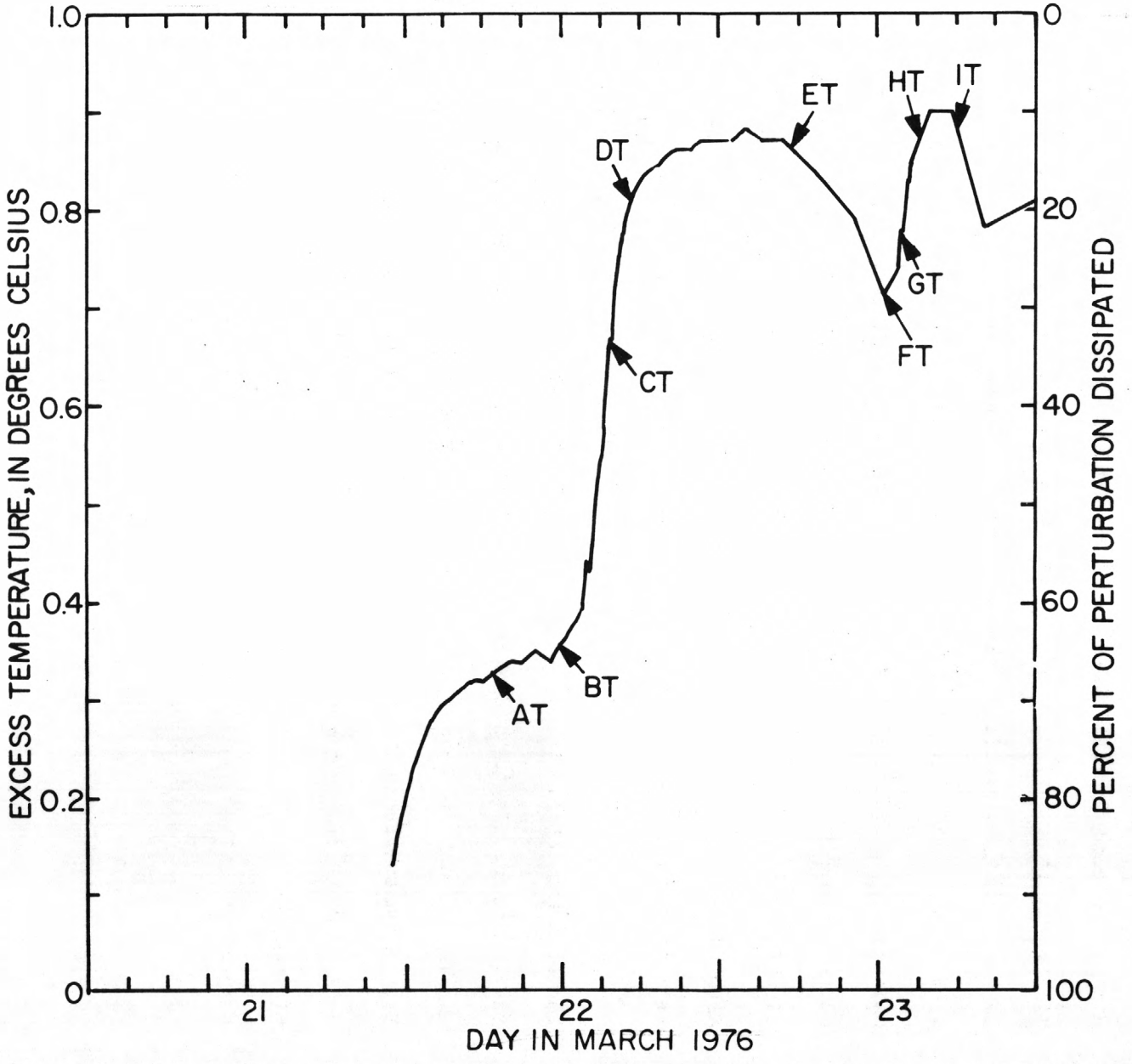

Figure 42.--Excess temperature at the Highway 141 Bridge during the March run due to an excess temperature of one degree at Buford.

The excess temperatures at the Highway 141 Bridge during the October run are illustrated in figure 43 and again specific points are labeled. In general it appears that a smaller percentage of the excess heat is dissipated during the October run. At high flow, points BT to CT, only about 5 percent is dissipated and at low flow, AT, only slightly over 30 percent is dissipated. There are a number of reasons for the apparent decrease in the rate of return to natural temperature for the October run. First, the traveltime at low flow in October, point AT, is only 19 hours compared to 23.2 hours in March. The frequent power releases in October never allowed the river to reach steady low flow. The release schedule was also different between the two runs. In October the low flow water, AT, spent most of its time in the river at night when meteorologic conditions are not optimal for rapid decay.

At high flow the March and October results are in better agreement. The minimum traveltimes in October and March were 8.8 and 7.7 hours, respectively. In March the fast moving water, DT, ET, traversed the reach during the daylight hours while in October the fast moving water, points BT, CT, traversed the reach at night.

It thus appears that the results of the two runs are fairly consistent. At high flow as little as 5 to 10 percent of the excess temperature is dissipated before reaching Highway 141. Unless low flow is maintained for more than 18 hours, seldom would more than 40 percent of the excess temperature be dissipated before reaching Highway 141.

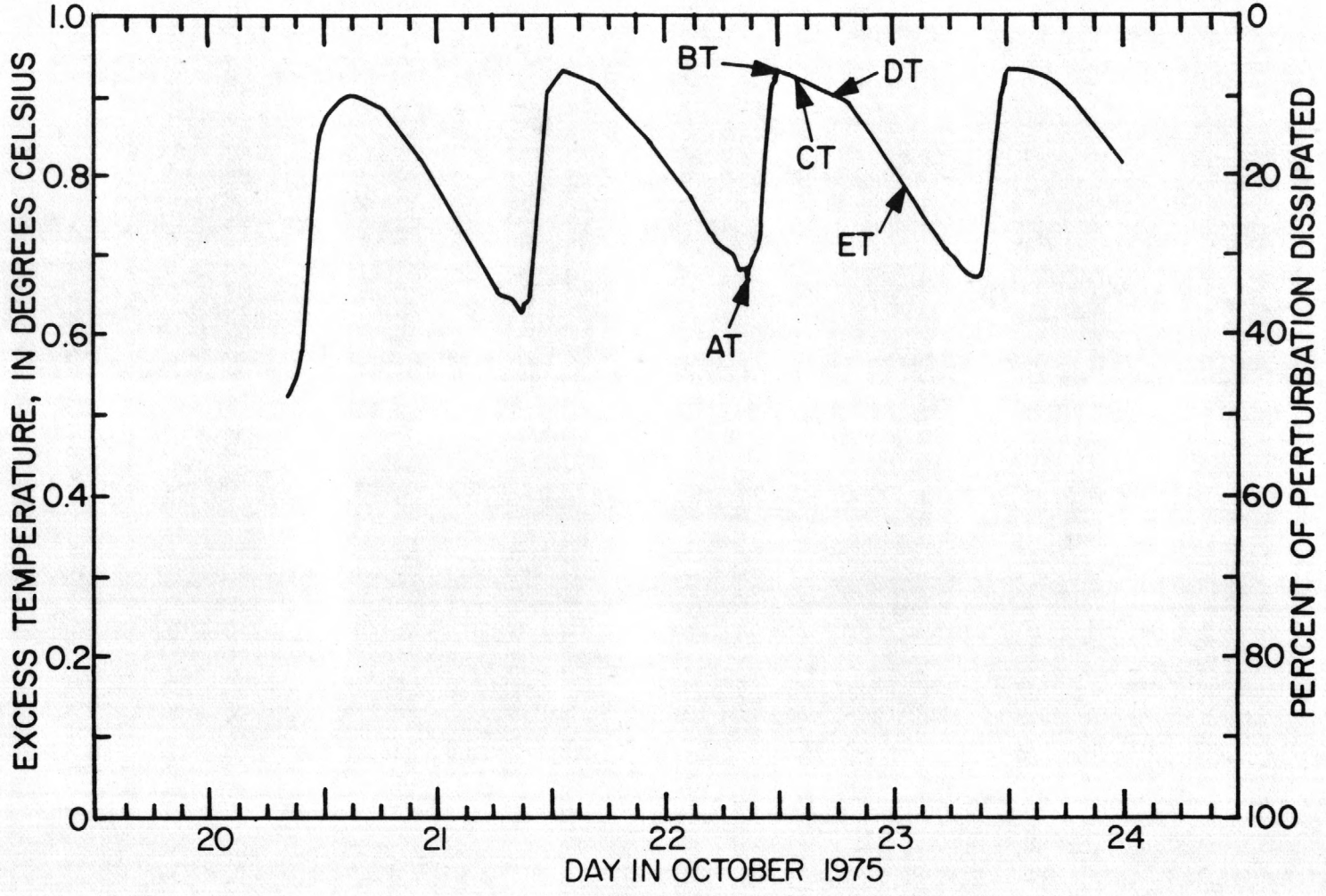

Figure 43.--Excess temperature at the Highway 141 Bridge during the October run due to an excess temperature of one degree at Buford.

SUMMARY AND CONCLUSIONS

A coupled flow-temperature model has been developed and verified with data collected on a 27.9-km reach of the Chattahoochee River between Buford and Norcross, Ga. A major contribution of this study has been to apply existing solution techniques, with minor improvements, to a very comprehensive data set in order to verify the existing technology of modeling flow and transport under highly unsteady flow conditions. The modeling analysis has identified transport phenomena unique to unsteady flow.

A linear, implicit finite-difference flow model was coupled with implicit, finite-difference transport and temperature models. Both the conservative and nonconservative forms of the transport equation were solved, and the difference in the predicted concentrations of dye were found to be insignificant. The temperature model, therefore, was based on the simpler nonconservative form of the transport equation.

Two extensive data sets were available for calibration and verification of the models under conditions of extremely unsteady flow. Continuous flow, temperature, and meteorologic data were available for the periods of October 20-26, 1975, and March 21-24, 1976. In addition, rhodamine-WT dye was injected to the flow at the upstream end of the reach at a constant rate during the March run, and frequent samples were obtained near the center and at the downstream end of the reach. The dye concentrations were used to verify the transport models.

The flow model was calibrated using the depth profile obtained at steady low flow and dynamic stage data collected in March 1976. A comparison of the modeled and observed stages at four points in the reach indicated that timing errors were generally less than 15 minutes, and errors in absolute stage were generally less than 0.15 m. Agreement of the modeled and observed discharges for flows less than 100 m^3/s was excellent, the difference being less than 5 percent. At higher flows the model generally predicted a peak discharge which was about 20 percent less than the observed value.

The flow model was verified by use of the data collected during October 1975. The modeled values of the stage were generally within 0.15 m of the observed values and timing errors were generally less than 30 minutes. The verification results were considered to be very good.

Numerical solution of either the conservative or nonconservative form of the transport equation did an excellent job of simulating the observed concentrations of dye in the river under highly unsteady flow conditions. Timing errors generally appeared to be less than 15 minutes. The agreement between the observed and modeled dye concentrations was considered to be an excellent verification of the transport models.

Both the October and March runs were considered as verifications of the temperature model because no calibration was involved. Results were considered to be very good. Temperature change as large as 5.8°C occurred as the water traversed the reach. The model was able to predict the downstream temperature with a RMS error of 0.32°C in October and 0.20°C in March.

Hydropulsation has a significant effect on the water temperature below Buford Dam. At low flow the release temperature is low and constant. At the beginning of a power release, the water temperature increased by as much as 3°C almost instantaneously because the turbines withdraw warm epilimnetic water at high flow. Any water-quality property which differs markedly between the epilimnetic and metilimnetic waters of the reservoir are likely to experience similar sudden changes in the river. The flushing action of the power release often causes a rapid temperature reduction to occur prior to the arrival of the warm epilimnetic water. The effects of hydropulsation are somewhat damped at the lower end of the reach. The thermal effects of hydropulsation are complicated because they are dependent on the timing of the releases with respect to both the time of day and past releases.

At least during the March run, the temperature of the water released from the dam was lower than the natural river temperature, even at high flow. Unless the river is held at steady low flow for longer than 18 hours, at least 60 percent of the thermal effect caused by Buford Dam will remain at the Georgia Highway 141 Bridge.

By use of both the Lagrangian and Eulerian forms of the transport equation, it was usually possible to predict the origin of the water in the river, whether from the epilimnion or hypolimnion. This ability could be very helpful in predicting water quality, if the parameter of interest differs significantly between the epilimnetic and hypolimnetic waters of the reservoir.

REFERENCES

Amein, M. M., and Fang, C. S., 1970, Implicit flood routing in natural channels: American Society of Civil Engineers Proceedings, Journal of the Hydraulics Division, v. 96, no. HY12, p. 2481-2500.

Anderson, L. F., 1954, Instrumentation for mass-transfer and energy budget studies, in Water-loss investigation: Lake Hefner studies, technical report: U.S. Geological Survey Professional Paper 269, p. 35-45.

Anderson, E. R., Anderson, L. J., and Marciano, J. J., 1950, A review of evaporation theory and development of instrumentation, Lake Mead water loss investigation: Navy Electronics Laboratory, Interim Report 159, February 1.

Bendat, Julius S., and Piersol, Allan G., 1966, Measurement and analysis of random data: John Wiley and Sons, Inc., New York, 387 p.

Blodgett, J. C., 1971, Water temperatures of California streams, Sacramento Basin Subregion: U.S. Geological Survey open-file report, 29 p.

Braslavskii, A. P., and Vikulina, Z. A., 1963, Evaporation norms from water reservoirs: Translated from Russian by Israel Program for Scientific Translations, Jerusalem, p. 85.

Brown, G. W., 1969, Predicting temperatures of small streams: Water Resources Research, v. 5, no. 1, p. 68-75.

Brutsaert, W., and Yeh, Gour-Tsyh, 1970, Implication of a type of empirical evaporation formula for lakes and pans: Water Resources Research, v. 6, no. 4, p. 1202-1208.

Carslaw, H. S., and Jaeger, J. C., 1959, Conduction of heat in solids: 2d ed., Oxford University Press, New York, p. 68-75.

Fischer, Hugo B., 1973, Longitudinal dispersion and turbulent mixing in open channel flow: Annual Review of Fluid Mechanics, p. 57-98.

Fread, D. L., 1974, Numerical properties of implicit four-point finite difference equations of unsteady flow: U.S. Department of Commerce, National Oceanic and Atmospheric Administration, March, Technical Memorandum NWS HYDRO-18, 38 p.

Garrison, J. M., Granju, J. P., and Price, J. T., 1969, Unsteady flow simulation in rivers and reservoirs: American Society of Civil Engineers Proceedings, Journal of the Hydraulics Division, v. 95, no. HY5, p. 1559-1576.

Jobson, Harvey E., 1973, The dissipation of excess heat from water systems: American Society of Civil Engineers Proceedings, Journal of the Power Division, v. 99, no. PO1, p. 89-103.

_____1976, Thermal modeling and its relation to canal evaporation: National Conference on Complete WateReuse Proceedings, 3d, American Institute of Chemical Eengineers, Cincinnati, p. 370-379.

_____1977, Thermal model for evaporation from open channels: Congress of the International Association for Hydraulic Research Proceedings, 17th, Baden Baden, Germany, v. 2, p. 95-102.

Jobson, Harvey E., and Sturrock, Jr., Alex M., 1976, Comprehensive monitoring of meteorology, hydraulics and thermal regime of the San Diego aqueduct, California: U.S. Geological Survey Open-File Report 76-628, 102 p.

Lai, C., 1967, Computation of transient flows in rivers and estuaries by the multiple reach method of characteristics: U.S. Geological Survey Professional Paper 575-D, p. D273-D280.

Messenger, Harry, 1963, Dissipation of heat from a thermally loaded system: U.S. Geological Survey Professional Paper 475-C, p. C175-C178.

Moore, A. M., 1969, Correlation and analysis of water-temperature data for Oregon streams: U.S. Geological Survey Water-Supply Paper 1819-K, p. 8-14.

Pluhowski, E. J., 1970, Urbanization and its effects on the temperature of the streams on Long Island, New York: U.S. Geological Survey Professional Paper 627-D, p. 110.

Price, H. S., Cavendish, J. C., and Varga, R. S., 1968, Numerical methods of higher-order accuracy for diffusion-convection equations: Society of Petroleum Engineers Journal, American Institute of Mechanical Engineers, v. 8, September, p. 298-303.

Rawson, J., 1970, Reconnaissance of water temperature of selected streams in southeastern Texas: U.S. Geological Survey in cooperation with the Texas Water Development Board, p. 2-4.

Roache, Patrick J., 1972, Computational fluid dynamics: Hermosa Publishers, Albuquerque, 434 p.

Ryan, P. J., and Stolzenbach, K. D., 1972, Chapter I of engineering aspects of heat disposal from power generation: Environmental Heat Transfer, MIT Summer Session, June 26-30, Ralph M. Parsons Laboratory for Water Resources and Hydrodynamics, Cambridge, Mass., 75 p.

Sayre, W. W., and Chang, F. M., 1968, A laboratory investigation of open-channel dispersion for dissolved suspended, and floating dispersants: U.S. Geological Survey Professional Paper 433-E, 71 p.

Stone, H. L., and Brian, P. L. T., 1963, Numerical solution of convective transport problems: American Institute of Chemical Engineers Journal, v. 9, no. 5, p. 681-688.

Tennessee Valley Authority, 1972, Heat and mass transfer between a water surface and the atmosphere: Water Resources Research Laboratory Report No. 14, Norris, Tenn., April, p. 4.20.

Von Rosenberg, D. W., 1969, Methods for the numerical solution of partial differential equations: Elsevier, New York, 128 p.

Wylie, E. Benjamin, 1970, Unsteady free-surface flow computations: American Society of Civil Engineers Proceedings, Journal of the Hydraulics Division, v. 96, no. HY11, p. 2241-2251.

Yevjevich, V., and Barnes, H. H., 1970, Flood routing through storm drains, Part 1, Solution of problems of unsteady free surface flow in storm drains: Fort Collins, Colorado State University Hydrology Paper No. 43, 108 p.